REVEALING THE BIOGEOCHEMISTRY AND HYDRODYNAMIC EXCHANGE PROCESSES OF FLOCCULENT SEDIMENTS IN SHALLOW FRESHWATERS

By

Dustin William Kincaid

A DISSERTATION

Submitted to
Michigan State University
in partial fulfillment of the requirements
for the degree of

Integrative Biology—Doctor of Philosophy
Ecology, Evolutionary Biology and Behavior— Dual Major

2018

ABSTRACT

REVEALING THE BIOGEOCHEMISTRY AND HYDRODYNAMIC EXCHANGE PROCESSES OF FLOCCULENT SEDIMENTS IN SHALLOW FRESHWATERS

By

Dustin William Kincaid

Although often small in area, shallow freshwaters are abundant in many landscapes, and their roles in watershed biogeochemical cycles are increasingly appreciated. However, shallow waterbodies have been far less studied than larger lakes and rivers. To understand the aggregate role of small waterbodies at watershed scales, their distinctive features need more investigation.

Biogeochemical processes in waterbodies are strongly influenced by sediment-water interactions, which influence aquatic ecosystem metabolism and productivity, fluxes of nutrients to downstream ecosystems, and atmospheric greenhouse gas exchanges. The influence of the sediment-water interface (SWI) is especially great in smaller waterbodies because of their shallow depths and high biological productivity, and because they often receive high inputs of groundwater, nutrients, and detrital organic matter.

Thick accumulations of flocculent sediments, or floc, are common in many shallow freshwaters that have productive aquatic and/or riparian vegetation and lack strong current or wave action. Loosely structured floc layers form a transitional zone that is potentially more connected to overlying water than relatively consolidated sediments, and are subject to dynamic variation in physical structure, thermal stratification, and reduction-oxidation (redox) status. Despite the prevalence of floc, its biogeochemical importance has been little studied. These sediments represent a potentially reactive SWI that can be considered an ecotone between overlying water, sediment porewater, and deeper groundwater. As with other better studied SWIs (e.g., deep lacustrine and marine waters, river hyporheic zones), floc sediments may play an

important role in the biogeochemical cycles of freshwater ecosystems, and their distribution in shallow waters may be very extensive.

In this dissertation I employ a broad array of approaches to reveal the biogeochemical importance of floc in shallow freshwaters. In Chapter 1, I describe the physicochemical properties of floc and examine which environmental features serve as predictors of floc thickness across a diverse set of shallow waterbodies in southwestern Michigan. In Chapter 2, I investigate organic matter decomposition rates in floc and quantify the temperature-sensitivity of this process. In Chapter 3, I consider the potential for floc to remove nitrate from overlying waters and compare nitrate removal rates for floc to rates reported in the literature for other common sediment types. Finally, in Chapter 4, I evaluate two physical exchange processes, diffusion and buoyancy-induced flow, using heat transport modeling and direct observation of flow to determine the drivers of solute exchanges between overlying waters and floc porewaters.

This research confirms that floc is abundant in shallow freshwaters and reveals that floc can be distinguished by high organic matter percentages, low bulk densities, and high volumes of occluded gas bubbles compared with other organic sediments. Floc layers are active sites for decomposition despite persistent anoxia, and results suggest floc accumulations are sustained by particularly high rates of organic matter input rather than slow decomposition. Further, decomposition rates could increase 12-56% with a 1-4°C increase in water temperatures—a likely scenario for this region in the next 100 years. Third, floc has the potential to remove nitrate from overlying waters, but the limitations of our approach hinder our ability to conclude that removal rates are much greater than those measured with other sediments. Lastly, buoyancy-induced mixing of overlying water and floc porewaters is an important mechanism driving the exchange of heat and fluid across the SWI in shallow waterbodies, at least seasonally.

This dissertation is dedicated to my late mother,
who always supported and believed in me
even though I became the wrong kind of doctor

ACKNOWLEDGEMENTS

I am forever grateful for the support I received during my doctoral program. First and foremost, I would like to thank my advisor, Steve Hamilton. As a scientist and mentor, Steve both challenged and supported me. He demonstrated that a scientist can be all-of-the-things(!), including passionate, fastidious, productive, and innovative, while still being kind and compassionate. Steve helped me navigate one of the most academically rigorous and personally tumultuous periods of my life, and I leave his lab a better scientist and more humble and grateful individual.

I would also like to thank the other members of my committee, Sarah Evans, Mantha "Phani" Phanikumar, and Jay Zarnetske. I appreciate all of the time and energy they put into helping me develop my dissertation research and improve it along the way. I am especially grateful to Phani; his enthusiasm and time made learning about the physics of my study systems a joy. He even helped me become slightly less mathematically illiterate along the way.

I am incredibly thankful for all of my mentors outside of MSU and my colleagues and family in the Society for Freshwater Science, especially Emily Stanley, Emma Rosi, Stuart Findlay, Colden Baxter, Amy Marcarelli, and Heather Bechtold. I fell in love with limnology because of the opportunities they provided me and I am incredibly thankful for their continued friendship and support. I can't wait to collaborate with them in the future.

Much of this research would not have been possible without the many individuals that helped me in the field and laboratory. Thank you to David Weed for managing a productive and organized lab and being so forgiving of my clutter and mistakes. To my labmate and colleague, Bonnie McGill, your work ethic, creativity, and passion are inspirational; I am forever grateful

for your friendship and support. To all of my mentees, your time, energy, and enthusiasm made working in the muck fun and productive. Natalie Harnsakunatai, Bradley Dawson, Andrew Copsey, Adamaris Muñiz Tirado, Jezreel Wallace, and Nicolas Lara—thank you, thank you, thank you. Gretchen Allison, a dedicated and incredibly giving KBS volunteer, thank you for all of the time you put into preparing the cotton strips for my decomposition studies.

Chad Zirbel, a gentleman, scholar, and master of structural equation models. His generous gifts of time and knowledge helped me become more proficient in R and SEM.

I am so grateful to have been a part of the community at the Kellogg Biological Station. I would especially like to thank the director, Kay Gross, for all of the support she provided me during my PhD program. Jenny Smith and Andy Fogiel make doing research at KBS so much easier and enjoyable and I thank them for all of their help and kind words along the way. And lastly, to all of my friends at KBS, thank you for all of the support, commiseration, conversations, dance parties, carpool sing-a-longs, and kindness. I feel extremely fortunate to have been at KBS at the same time as them and I know many of our friendships will be life-long.

A very special thanks to Austin Ashley, the most amazing partner. He supported me in countless ways the last few years. I am so lucky and fortunate to have you in my life. I love you.

I have the most wonderful family anyone could ask for and I greatly appreciate their lifelong love and support.

Lastly, I would like to thank my funding sources: the National Science Foundation, the KBS LTER program, the KBS GK-12 program, KBS summer and science outreach fellowships, the MSU Graduate School, Department of Integrative Biology, and Ecology, Evolutionary Biology, and Behavior program, CUASHI, and the Society for Freshwater Science.

TABLE OF CONTENTS

LIST OF TABLES x

LIST OF FIGURES xii

CHAPTER 1: PHYSICOCHEMICAL PROPERTIES AND PREVALENCE OF FLOCCULENT ORGANIC SEDIMENT IN SHALLOW FRESHWATERS 17
ABSTRACT 17
INTRODUCTION 18
METHODS 19
Site selection 19
Surveys of flocculent sediments 20
Porewater sampling 24
Floc chlorophyll a profiles 26
Water and gas analyses 27
Sediment analyses 28
Data analysis 28
RESULTS 30
Physical properties and organic content of floc 30
Algal biomass 31
Porewater chemistry 32
Occluded gas volume and chemistry 34
Floc thickness 36
DISCUSSION 39
Organic carbon and floc sediment structure 39
Algal biomass 43
Solute chemistry in floc 44
Occluded gas 47
Floc thickness 48
CONCLUSIONS 51
APPENDIX 52
LITERATURE CITED 57

CHAPTER 2: DECOMPOSITION IN FLOCCULENT SEDIMENTS OF SHALLOW FRESHWATERS 67
ABSTRACT 67
INTRODUCTION 68
METHODS 71
Site selection 71
Cotton strip decomposition assays 72
Tensile strength loss determination 74
Temperature measurements and water chemistry 74
Fungal biomass 76

Data analysis 76
RESULTS 81
Seasonal variation in cellulosic decomposition 81
Differences in cellulosic decomposition rates between overlying water and the floc layer . 83
Differences in fungal biomass on cotton strips in October 85
Predictors of cellulosic decomposition rates in the floc layer 85
Apparent temperature sensitivity of cellulosic decomposition in floc 87
DISCUSSION 89
Decomposition rates in flocculent sediments 89
Why are decomposition rates greater in floc layers than in overlying water? 89
Predictors of decomposition in floc layers 93
Apparent temperature sensitivity of decomposition in floc 96
CONCLUSIONS 97
APPENDIX 100
LITERATURE CITED 107

CHAPTER 3: NITRATE REMOVAL BY FLOCCULENT SEDIMENTS IN SHALLOW FRESHWATERS 115
ABSTRACT 115
INTRODUCTION 116
METHODS 119
Site selection 119
Nitrate removal assays 120
Surface water sampling and analyses 123
Sediment sampling and analyses 124
Compilation of NO_3^- removal rates from the literature 124
Data analysis 125
RESULTS 125
Sediment characteristics 125
Water column characteristics 126
Nitrate removal rates 126
Response of NH_4^+, SO_4^{2-}, and SRP to enrichment 129
DISCUSSION 129
Nitrate removal rates for floc relative to other sediment types 132
CONCLUSIONS 135
APPENDIX 137
LITERATURE CITED 148

CHAPTER 4: TRANSPORT MECHANISMS DRIVING EXCHANGE BETWEEN FLOCCULENT SEDIMENT AND OVERLYING WATER IN SHALLOW FRESHWATERS 155
ABSTRACT 155
INTRODUCTION 156
METHODS 159
Site selection 159
Measuring temperature profiles 160

Measuring high-resolution water current velocity profiles 160
Sediment sampling and analyses 161
Two-dimensional heat transport modeling 162
RESULTS AND DISCUSSION 169
ADCP: direct observations of fluid movement 169
Two-dimensional heat transport modeling 171
CONCLUSIONS 177
APPENDIX 178
LITERATURE CITED 181

LIST OF TABLES

Table A1.1. Names, descriptions, and locations of waterbodies sampled. 53

Table A2.1. Results of Kruskal-Wallis rank sum tests and Conover-Iman test of multiple comparisons using rank sums to test for differences in tensile strength loss rates between seasons. 101

Table A2.2. Results of Wilcox signed rank tests to compare differences in tensile strength loss rates (TSL day^{-1}, % per day; TSL degree day^{-1}, % per degree day) between those measured in the overlying water and those measured in each subsequent depth in the floc, by season. These comparisons were only made following the rejection of a Friedman test ($\alpha = 0.05$). The Benjamini-Hochberg procedure was used to adjust *p*-values to control the false discovery rate. 102

Table A2.3. Results of generalized least squares modeling to select the best predictors of temperature-adjusted tensile strength loss (TSL degree day^{-1}, % degree day^{-1}) ratios using surface water chemistry variables. 103

Table A2.4. Results of Wilcox signed rank tests to compare differences in ergosterol concentrations (ng g $AFDM^{-1}$) between those measured in the overlying water (depth +1.4) and those measured in each subsequent depth in the floc (depths -1.4, -7.1, and -15.6). These comparisons were only made following the rejection of a Friedman test ($\alpha = 0.05$). The Benjamini-Hochberg procedure was used to adjust *p*-values to control the false discovery rate. 104

Table A2.5. Results of linear mixed effects modeling to select the best predictors of temperature-adjusted tensile strength loss (TSL $degday^{-1}$, % degree day^{-1}) rates using floc porewater chemistry variables. 105

Table A2.6. Results of linear mixed effects modeling to predict tensile strength loss rates (ln TSL day^{-1}, % per day) and estimate the apparent activation energy..... 106

Table 3.1. Physical and chemical characteristics of sediments and overlying waters in the mesocosms used for *in situ* NO_3^- removal experiments. Surface water temperatures and dissolved oxygen (DO) concentrations represent averages from both pre-and post-enrichment periods. Nutrient concentrations are averages from samples collected during the pre-enrichment period only. 121

Table 3.2. Nitrate removal rates for each site. Negative values denote removal (presumably mainly due to fluxes from the water column to the sediment). 127

Table A3.1. Nitrate flux values (mmol N m^{-2} hr^{-1}) reported in the literature for major sediment types in freshwater and marine systems. Measurements made in different locations within a

water body are maintained as discrete observations, but repeated measurements made over time in each water body were averaged. Negative fluxes indicate movement of nitrate from the water column to the sediment. Citations listed below table 138

Table A3.2. Response of NH_4^+, SO_4^{2-}, and SRP to nitrate enrichment in the overlying water columns. Slopes represent the slope of the linear relationship between log transformed solute to bromide (Br^-) ratios and time lapsed (days). Negative fluxes indicate movement of the solute from the water column to the sediment..... 146

Table A3.3. Results of Kruskal-Wallis rank sum tests and post-hoc pairwise comparisons using Dunn's test to test for differences in nitrate removal rates among sediment types without and with consideration of nitrate enrichment. 147

Table 4.1. Parameter values for the buoyancy-induced flow model..... 169

LIST OF FIGURES

Figure 1.1. Sediment coring device used to collect intact (undisturbed) cores of flocculent sediment. The corer was modeled after a design by Gardner et al. (2009) and consists of a check-valve coring head with a release valve and an exchangeable transparent acrylic coring tube. Here small holes drilled into the coring tube to facilitate porewater sampling are covered with lengths of vinyl electrical tape. Also pictured is an example of the round end cap used to seal the coring tube during transport. 22

Figure 1.2. Customized sliding plate sampler for sampling porewater in flocculent sediments at multiple depths with Rhizon samplers. The photo on the left depicts the sampling setup before deployment and the photo on the right depicts the sampler deployed in flocculent sediment. 26

Figure 1.3. Histograms showing the distributions of (**A**) water content, (**B**) dry bulk density, (**C**) porosity, (**D**) organic matter content estimated as loss-on-ignition, (**E**) organic carbon content, and (**F**) C:N molar ratios of the upper 20 cm of flocculent sediment in shallow waterbodies in southwestern Michigan, USA. The vertical dashed lines represent the median. 31

Figure 1.4. Vertical profiles of chlorophyll *a* content (per sediment dry weight, DW) in flocculent sediments in 10 different shallow waterbodies in southwestern Michigan, USA. Open circles represent measured concentrations and the lines represent a LOESS curve fit to each profile. Zero on the depth axis represents the interface between flocculent sediment and overlying water. 32

Figure 1.5. Surface water (SW) and flocculent sediment porewater (PW) concentrations of (**A**) dissolved organic carbon (DOC), (**B**) soluble reactive phosphorus (SRP), (**C**) ammonium (NH_4^+), (**D**) nitrate (NO_3^-), and (**E**) sulfate (SO_4^{2-}) in shallow waterbodies in southwestern Michigan, USA. Porewater concentrations represent the mean concentration of each solute in the upper 10 cm of the floc layer. Lines in the scatterplots represent the 1:1 ratio. 33

Figure 1.6. Vertical profiles of flocculent sediment porewater concentrations of (**A**) dissolved ferrous iron (Fe^{2+}), (**B**) dissolved free sulfide (ΣH_2S), (**C**) sulfate (SO_4^{2-}), (**D**) soluble reactive phosphorus (SRP), (**E**) ammonium (NH_4^+), (**F**) nitrate (NO_3^-), (**G**) dissolved carbon dioxide (CO_2), and (**H**) dissolved methane (CH_4) from shallow waterbodies in southwestern Michigan, USA. Profiles were collected from intact cores of flocculent sediment and in situ sampling events. Open circles represent measured concentrations and the lines represent a LOESS curve fit to each profile. Zero on the depth axis represents the interface between flocculent sediment and overlying water. 34

Figure 1.7. Histograms showing the distributions of (**A**) volume, (**B**) percent methane (CH_4), and (**C**) percent nitrogen gas (N_2) of occluded (trapped) gas in flocculent sediments in shallow waterbodies of southwestern Michigan, USA. The vertical dashed lines represent the median. (**D**) shows the sum of the percent CH_4 and N_2 in each sample of occluded gas arranged in order of decreasing percent CH_4. 35

Figure 1.8. Relationships between (**A**, **D**, **G**) floc thickness, flocculent sediment temperature (**B**, **E**, **H**), or (**C**, **F**, **I**) emergent vegetation cover (includes the sum of emergent and floating vegetation cover) and (**A**, **B**, **C**) the volume, (**D**, **E**, **F**) percent methane (CH_4), and (**G**, **H**, **I**) percent nitrogen gas (N_2) of occluded (trapped) gas in flocculent sediments of shallow waterbodies in southwestern Michigan, USA. Shown are measured values (open circles) and linear relationships ($p < 0.05$; black lines). 37

Figure 1.9. Thickness of flocculent sediments in the littoral margins (from the shore to water no more than approximately 2 m in depth) of 13 shallow waterbodies in southwestern Michigan, USA. The vertical dashed line represents the median. 38

Figure 1.10. Structural equation model of predictors of floc thickness in shallow lentic ecosystems in southwestern Michigan, USA. Black paths represent significant relationships ($p < 0.05$, piecewise SEM). Gray paths represent non-significant relationships. The path labeled d-sep. was added to improve model fit based on a test of *d-separation*. Solid lines represent positive relationships and dashed lines negative relationships. Paths are weighted by standardized path coefficients. Values inside of the box are the pseudo-R^2 values for that response variable. Overall fit of piecewise SEM was evaluated using Shipley's test of *d-separation*: Fisher's *C* statistic (if $p > 0.05$, then the model is a good fit), Akaike information criterion (AIC), and AIC corrected for small sample sizes (AICc). 39

Figure 1.11. (**A**) Relationship between dry bulk density (DBD) and organic carbon (OC) for flocculent sediments from shallow waterbodies in southwestern Michigan, USA. (**B**) Relationship between water content and OC for flocculent sediments. Data in all plots are from the 2014 intact core survey (all core slices in the upper 20 cm) and the 2015 survey of floc abundance (average of upper 20 cm of the floc layer). 43

Figure A1.1. Meta-model representing the relationships between waterbody characteristics (depth to bottom, catchment slope), aquatic vegetation cover (surface vegetation and submerged vegetation cover), water and flocculent sediment temperatures, and floc thickness. 56

Figure 2.1. (**A**) Illustration of a cotton strip array in the lab (numbers are depths relative to the floc-water interface when deployed in the field) and (**B**) two replicate arrays deployed in the field. 73

Figure 2.2. (**A**) Mean temperatures, (**B**) non-adjusted tensile strength loss (TSL), and (**C**) temperature-adjusted TSL across all sites for cotton strips in the overlying water and in floc layer. Data used in each plot are site means. Error bars in (**A**) represent ± standard error of the mean. Violin plots in (**B** & **C**) show the density distribution of TSL rates. Boxplots within the violin plots represent the median and interquartile range. Values above brackets in plots (**B** & **C**) are *p*-values for pairwise comparisons; (*) indicates significant *p*-values (Appendix Table A2.1). Values in parentheses in plots (**B** & **C**) are the number of measurements. 82

Figure 2.3. (**A**) Non-adjusted tensile strength loss (TSL) and (**B**) temperature-adjusted TSL at each depth above (1.4 cm) and below (-1.4 to -18.4 cm) the floc-water interface (depicted as dashed horizontal line) for all sites. (*) indicates that rates at these depths are significantly

different than those above the floc-water interface for that season according to post hoc comparisons (Appendix Table A2.2). 83

Figure 2.4. The relative difference in tensile strength loss (TSL) rates measured in the water versus those measured in the floc layer at each site. Each ratio is the mean TSL rate measured in the water at that site divided by the mean TSL rate measured in the floc layer. (**A**) includes ratios for non-adjusted TSL rates (% per day) and (**B**) includes ratios for temperature-adjusted TSL rates (% per degree day). Open circles are the ratios at each site and the ◆ is the mean of for all sites and seasons. 84

Figure 2.5. Fungal biomass estimated as ergosterol concentrations on cotton strips deployed above (1.4 cm) and below (-1.4, -7.1, and -15.6 cm) the floc-water interface (depicted by dashed horizontal line) for all sites in October. (*) indicates that concentrations at that depth are significantly different than those in the overlying water (1.4 cm) according to post hoc comparisons (Appendix Table A2.4). 85

Figure 2.6. Linear relationship between non-adjusted tensile strength loss rates (TSL, % per day) and mean temperature in the floc layers for all seasons and depths. A line of best fit (solid black line) and 95% confidence intervals (gray area) are overlain. 86

Figure 2.7. (**A**) The apparent activation energy (E_a, eV) of non-adjusted tensile strength loss rates (TSL, % per day) of cotton strips deployed in flocculent sediment. The x-axis is the inverse absolute temperature (T) in Kelvin (K) multiplied by the Boltzmann constant (k_B, 8.62×10^{-5} eV K^{-1}) and normalized by a standard water temperature (T_0), 291.15 K or 18°C. The slope approximates the inverse of E_a. (**B**) The apparent activation energy of TSL at each depth in the floc layer. Bars represent the 95% confidence intervals. 88

Figure 2.8. Linear relationships for each season between temperature-adjusted tensile strength loss rates (TSL, % per degree day) in floc and the natural log of the molar ratio of NH_4-N to SRP concentrations in the floc porewaters. The data are limited to cotton strips with TSL between 25-75%. Linear regressions were significant ($p < 0.05$) for June and October, but not for August. The vertical line shows the 16:1 molar N:P ratio. 95

Figure 3.1. Examples of NO_3^- removal in the mesocosms at three sites including Loosestrife, a case where NO_3^- concentrations became depleted and hence only early measurements were used to generate comparable estimates. 123

Figure 3.2. Relationships between NO_3^- removal rates and (**A**) minimum surface water dissolved oxygen concentration, (**B**) mean surface water temperature, (**C**) surface water depth, and (**D**) floc organic matter content measured as loss-on-ignition. The rate from Turkey Marsh (TM) was an outlier and was excluded from regression fits in **B**-**D**. Lines in **B** and **C** indicate relationships between NO_3^- removal rates and the covariate including (bold) the rate from Wintergreen Lake Outlet (WLO) and excluding WLO (dashed). 128

Figure 3.3. (**A**) Nitrate removal rates reported in the literature for major sediment types in freshwater and marine environments. Negative values imply net removal from the water column.

For clarity purposes, rates more negative than -2 mmol N m^{-2} h^{-1} are not shown. (**B**) I further distinguish between measurements made by adding additional NO_3^- of any amount to the water column (enriched) versus those made at ambient nutrient conditions (no enrichment). Three of the floc measurements are from the literature (Svensson et al. 2001; O'Brien et al. 2012a; McCarthy et al. 2016); the remaining 14 values are from this study. Measurements were made using different methods (i.e., *in situ* mesocosms and benthic chambers and in the lab using sediment cores; Table S1. Asterisks (*) indicate that rates for these sediment types are significantly different ($P < 0.05$; Table S3) than those for floc (**A**) and significantly different than those for floc measured by enriching the overlying water with NO_3^- (enriched, **B**). 133

Figure 4.1. Aerial photo of the LTER Kettle Pond. The star denotes the location of the vertical temperature array (temp. array). 159

Figure 4.2. Modeling domain for buoyancy-induced flow simulations in the LTER Kettle Pond. The vertical dashed lines indicate the locations of the acoustic Doppler current profiler (ADCP) and the vertical temperature array..... 163

Figure 4.3. (Upper) Temperature times series measured 54 cm above and 18 cm below the floc surface during the 24-hour deployment of the HR-ADCP in the LTER Kettle Pond. (Lower) vertical profiles of the velocity magnitude (speed) of fluid flow at various times throughout the measurement period. The dashed vertical gray lines in the upper plot show at what time point each vertical profile was captured..... 171

Figure 4.4. Temperature time series from the LTER Kettle Pond during the 8-day modeling period. Observed temperatures are plotted for 54 cm above (solid blue line) and 18 cm below (solid brown line) the floc surface. Eight-day temperature means for those depths are plotted as dashed lines. The first 4 days of temperatures were used for the unsteady or transient solution for the buoyancy-induced flow model, but I only use results from the final 4 days of this temperature series for comparisons. Also shown is the period when the HR-ADCP was deployed in the pond (gray rectangle). 172

Figure 4.5. Time series of (**a**) observed temperatures, (**b**) simulated temperatures with buoyancy-induced flow, and (**c**) simulated temperatures with diffusion only in the water column and within the floc layer for the 4-day period of comparison shown in Figure 4.4. The y-axis represents the vertical distance between the top and bottom of the model domain (0.72 m) normalized by the thickness of the floc layer (0.18 m). Consequently, the surface of the floc layer is at a depth of 1. Because time was normalized by a characteristic time scale of a half day in the model, the dimensionless time τ (x-axis) for the 4-day period is 8. 174

Figure 4.6. Comparison of observed temperatures and simulated temperatures at selected depths, including (**a**) 0.02 m above the floc surface, (**b**) at the floc-water interface, and (**c**) 0.04 m and (**d**) 0.08 m below the floc surface. Depths shown above subplots are relative to the bottom of the floc layer and model domain. Depth = 0.18 m is at the floc-water interface. Time on the y-axis is model time and represents the 4-day period of comparison shown in Figure 4.4. 175

Figure 4.7. Simulated velocity profiles in the floc layer and the overlying water column at selected times. The y-axis represents the vertical distance between the top and bottom of the model domain (0.72 m) normalized by the thickness of the floc layer (0.18 m). Consequently, the surface of the floc layer is at a depth of 1. High velocities were generally associated with large temperature differences in the system and occurred at the interface between the floc layer and the overlying water, a feature also noted in our ADCP observations. 176

CHAPTER 1

PHYSICOCHEMICAL PROPERTIES AND PREVALENCE OF FLOCCULENT ORGANIC SEDIMENT IN SHALLOW FRESHWATERS

ABSTRACT

Shallow freshwater ecosystems often disproportionately contribute to nutrient cycling and carbon storage relative to deeper waterbodies, yet have not received as much study. Shallow waters are often highly productive and their biogeochemical processes are strongly influenced by sediment-water interactions. I surveyed a rarely investigated sediment type found in many shallow waterbodies—flocculent organic sediment (floc)—that represents a potentially reactive sediment-water interface (SWI) that may modulate biogeochemical fluxes and carbon storage in shallow freshwaters. Here I describe the physicochemical properties of floc, compare these to the properties of organic sediments from other freshwaters, and examine which environmental features serve as predictors of the thickness of floc layers in a variety of shallow freshwaters in southwestern Michigan. Thick accumulations (>10 cm) of floc were abundant in most of the shallow waters I surveyed. The physicochemical properties of floc do not differ much from other organic sediments found in freshwaters, with the exception of their relatively high OC concentrations, low bulk densities, and high volumes of occluded gas bubbles. However, these distinctive features may have consequences for the exchange of solutes across the SWI and carbon burial, especially given the prevalence of floc in shallow waters. I suggest that a greater focus on exchange processes and resulting biogeochemical rates at the floc-water interface would enhance our understanding of biogeochemical processes in shallow waterbodies.

INTRODUCTION

Although often small in area, shallow aquatic ecosystems are recognized as being abundant in many landscapes, and their cumulative roles in global biogeochemical cycles (including carbon sequestration and nitrogen retention) are increasingly appreciated (Downing et al. 2008; Harrison et al. 2009; Tranvik et al. 2009; Cheng and Basu 2017). However, shallow waters have been far less studied than larger and deeper lakes and rivers (Smith et al. 2002; Harrison et al. 2009; Downing 2010; Raymond et al. 2013). To understand the aggregate role of shallow waters at watershed scales, their distinctive features need more investigation. And to scale results to watersheds, it is necessary to relate those features to waterbody characteristics, vegetation, and abiotic factors like temperature.

Biogeochemical processes in waterbodies are strongly influenced by sediment-water interactions (McClain et al. 2003; Abbott et al. 2016; Bernhardt et al. 2017), which influence aquatic ecosystem metabolism and productivity, fluxes of nutrients to downstream ecosystems, and atmospheric greenhouse gas exchanges (Grimm and Fisher 1984; Golterman 2004; Megonigal et al. 2004). The influence of the sediment-water interface (SWI) is especially great in smaller waterbodies because of their shallow depths and high biological productivity, and because they often have high watershed inputs of groundwater, nutrients and organic matter (Wetzel 1992; Alexander et al. 2000; Beaulieu et al. 2011; Helton et al. 2011).

Thick accumulations of flocculent organic sediments, or floc, are common in many shallow freshwater ecosystems that have productive aquatic and/or riparian vegetation and lack strong current or wave action. Loosely structured floc layers, often exceeding 10 cm depth, form a transitional zone that is potentially more connected to overlying water than relatively consolidated sediments, and are subject to dynamic variation in physical structure, thermal

stratification, and reduction-oxidation (redox) status. Despite the very common occurrence of these sediments in a diversity of shallow waterbodies, their biogeochemical and ecological importance has been little studied, and they are often incorrectly sampled using core methods developed for relatively consolidated sediments, or simply avoided in sediment studies. These floc sediments represent a potentially reactive SWI that can be considered an ecotone continuum between the water column and the sediment porewater and deeper groundwater. As with other better studied SWIs (e.g., deep lacustrine and marine waters, river hyporheic zones), floc sediments may play an important role in the biogeochemical cycles of freshwater ecosystems, and their distribution in shallow waters may be very extensive.

Here I present the results of multiple surveys of flocculent sediments in shallow waterbodies of southwestern Michigan, USA. My primary objectives were to (1) describe the physicochemical properties of particulate floc and the floc layer, (2) compare these to the properties of organic sediments from other freshwaters, and (3) examine which environmental features serve as predictors of floc abundance—measured as thickness of the floc layer—in shallow freshwaters. I used a structural equation modeling approach to infer the relative importance of waterbody characteristics, aquatic vegetation, and temperature to predict the thickness of floc sediment in shallow wetlands and lake littoral zones.

METHODS

Site selection

I conducted multiple surveys of flocculent sediments in a variety of shallow freshwater ecosystems near the Kellogg Biological Station in Barry and Kalamazoo Counties, Michigan, USA (see Appendix Table A1.1 for site information). These sites included the littoral zones of

lakes, shallow through-flow wetlands, submarine deltas where streams entered lakes, and depositional zones on the margins of stream channels. Waterbodies in this region are embedded in a heterogeneous rural landscape consisting mostly of agricultural land and unmanaged terrestrial uplands (primarily secondary deciduous forest and successional old fields). Many of the lakes and wetlands in this area occupy glacial depressions (kettles) and submersed and floating aquatic vegetation communities tend to be abundant in waters less than about 2.5 m deep during the summer. Dominant aquatic vegetation species include *Myriophyllum* spp., *Potamogeton* spp., *Chara* spp., *Nuphar advena*, *Nymphaea odorata*, and *Brasenia schreberi*. Streams draining the glacial terrain often originate or pass through lakes and wetlands and are commonly fringed by riparian fen wetlands. Because there is a high degree of linkage between surface water and groundwater in the area and surface runoff is low, most surface waters are heavily influenced by groundwater discharge and many have relatively stable water levels as a result (Grannemann et al. 2000; Hamilton 2015).

Surveys of flocculent sediments

Intact flocculent sediment core survey—I collected intact (undisturbed) cores of flocculent sediment from a variety of shallow (<1 m depth) freshwater ecosystems in July and August 2014. I targeted locations largely devoid of vascular plant growth, though often these were small open patches surrounded by dense aquatic vegetation. The coring device I used (Figure 1.1) was modeled after a corer designed by Gardner et al. (2009), which was developed to collect intact cores of soft sediments in marine environments. To minimize compaction of the floc sediment during collection, I used a wide transparent acrylic coring tube (15.2 cm outer diameter, 14.6 cm inner diameter, varying lengths to suit site needs, Delvie's Plastics, Salt Lake City, Utah) with a

beveled edge at the bottom to create a sharp edge. I then fitted the coring tube with a check-valve coring head, which allowed air and water to pass through the top of the coring tube during deployment, but closed during retrieval of the core (Gardner et al. 2009). The coring head consisted of a plumbing check-valve (5.1 cm [2 in.] inlet and outlet inner diameter) connected to a 10.2 cm (4 in.) to 15.2 cm (6 in.) rubber plumbing adapter using a 10.2 cm (4 in.) to 5.1 (2 in.) pipe reducer bushing. To facilitate sampling of porewater directly from the sediment core, I also drilled a series of small holes (2.5 mm diameter) into the coring tube every 1 cm along the entire length of the tube on four sides. Prior to deployment, I sealed the holes with continuous lengths of vinyl electrical tape. I collected the cores by carefully inserting the coring device into the floc layer while rotating it until the coring tube reached the consolidated sediment below the floc. If substantial ebullition (release of trapped gas bubbles) occurred during core retrieval or I observed disturbance of the sediment through the core liner, I discarded the core and collected a new one. I then capped both ends of the coring tube with a pipe end cap made of flexible PVC (16 cm inner diameter, Fernco Inc., Davison, Michigan) leaving enough overlying water in the core to completely fill the space between the top of the floc layer and the top of the coring tube (i.e., no headspace). Cores were processed after careful transport back to the lab.

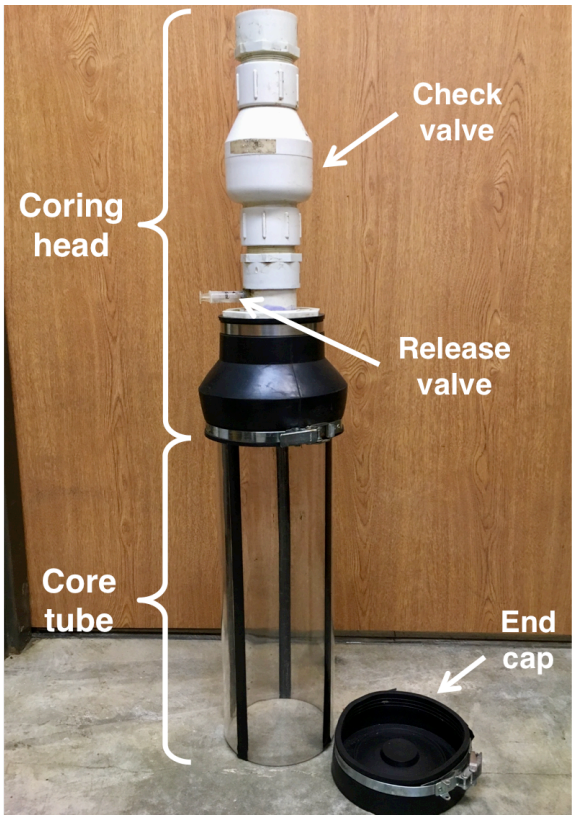

Figure 1.1. Sediment coring device used to collect intact (undisturbed) cores of flocculent sediment. The corer was modeled after a design by Gardner et al. (2009) and consists of a check-valve coring head with a release valve and an exchangeable transparent acrylic coring tube. Here small holes drilled into the coring tube to facilitate porewater sampling are covered with lengths of vinyl electrical tape. Also pictured is an example of the round end cap used to seal the coring tube during transport.

Following porewater sampling in the laboratory (see below), I removed the water overlying the floc and sectioned the cores into 1-5 cm depth intervals by extruding the sediment out of the top of the core. If the water content of the floc was too high (often the case in the upper several centimeters), I scooped the section out of the core.

Before collecting the intact core, I sampled the water overlying the floc. I did this by collecting approximately 250 mL of overlying water and immediately filtering it through Supor polyethersulfone membrane filters (0.45 µm pore-size; Pall Corp., Port Washington, New York). Samples were stored at 4°C until analysis within 5 days of sample collection.

Survey of floc abundance and physicochemical characteristics—I surveyed flocculent sediments along the littoral margin (from the shore to water no more than approximately 2 m in depth) of 13 waterbodies in June and early July 2015. I made measurements at approximately 10 sites in each waterbody representing the dominant habitat types in each ecosystem (e.g., open water versus vegetated, confluence of flowing waters with non-flowing waters). At each site, I measured the depth of the water column and the thickness of the floc layer. I partitioned the sediments into floc and underlying consolidated layers and other types of organic-rich deposits (e.g., peat) by adopting an operational definition of the floc layer depth based on the depth to which a 0.33-kg, 0.64-cm diameter cylinder sank on its own weight or I could no longer freely swirl the cylinder without feeling resistance. I also measured water temperature, floc temperature, and estimated percent cover of emergent, floating, and submerged vegetation.

At a subset of sites, I collected additional samples to characterize the physicochemical characteristics of floc. At these sites, I collected samples of the upper 15-20 cm of the floc layer using a smaller coring tube (coring tube inner diameter, 5.4 or 6.2 cm). I also measured the bulk volume of occluded (trapped) gas in the floc layer in an undisturbed area of floc near the core selection site. To do this I submersed a bowl (inner diameter, 23 or 38 cm) in the water column to remove all of the air and then inverted the bowl in the water column above the floc layer. While holding the inverted bowl in a constant location, I used a canoe paddle to disturb the floc layer beneath the bowl and captured the released gas bubbles in the bowl. I then estimated the volume of gas in the bowl and collected a subsample in a 60-mL syringe with a 3-way valve by piercing a rubber septum embedded in the bowl. Gas volumes are expressed per area ($L\ m^{-2}$) or per volume of floc ($L\ m^{-3}$) by multiplying the area of the sampling bowl by the thickness of the floc layer. I quantified the percent composition of nitrogen (N_2) and methane (CH_4), which

comprised most of the gas in these samples, via gas chromatography within 24 hours. At the same subset of locations, I sampled the water overlying the floc. I did this by collecting approximately 250 mL of overlying water and immediately filtering it through Supor polyethersulfone membrane filters (0.45 μm pore-size; Pall Corp., Port Washington, New York). I stored samples at 4°C until analysis within 5 days of sample collection.

Porewater sampling

Intact cores—I collected samples of porewater directly from the intact cores to measure dissolved gas and solute concentrations at multiple depths throughout the vertical profile of the floc core. I began sampling at approximately 1 cm below the floc-water interface and then collected samples every 1 cm for the first 5 cm and then every 2-3 cm for the remaining depths. Each sample was collected from a different side of the core than the previous one to ensure I sampled undisturbed porewater. To extract the porewater from the core, I pierced the vinyl electrical tape and carefully inserted a 10 cm long Rhizon sampler (0.15 μm mean pore-size; cat. no. 19.21.21, Rhizosphere Research Products, Wageningen, The Netherlands) horizontally into the floc. I minimized water loss and held the Rhizon samplers in place using additional vinyl electrical tape to secure the samplers on the outside of the core. I slowly extracted an initial 2 mL of pore water using a spring-loaded 30-mL syringe connected to the Rhizon via a 3-way syringe valve with a standard Luer lock. After discarding this initial volume, I collected another 3 mL of pore water for determination of dissolved gas concentrations. I then attached a new syringe and 3-way valve to the Rhizon sampler, extracted an additional 14 mL of porewater, and immediately added subsamples of the filtered porewater into reagents to produce stable colorimetric complexes with dissolved Fe^{2+} and ΣH_2S (i.e., $H_2S + S^{2-}$). Finally, I extracted an additional 5 mL

of pore water and stored this filtered sample at 4°C until analysis within 5 days of sample collection. Once all samples were collected, I extracted the dissolved gases from the porewater sample into a gaseous headspace (ambient lab air) using a static headspace equilibration (Ioffe and Vitenberg 1984) and stored the headspace sample in a glass vial sealed with a septum. I determined the concentration of carbon dioxide (CO_2) and CH_4 via gas chromatography within 30 days.

In situ sampling—I collected samples of porewater in situ using two methods. In mid-September and early October 2015, I collected porewater samples at multiple depths (intervals, ≥ 1 cm) of the floc layer in 6 different waterbodies at locations with water columns <1 m deep. To facilitate collection of undisturbed porewater samples at known depths, I attached 10-cm long Rhizon samplers to a customized sliding plate device (Figure 1.2) carefully inserted the device into the floc, and slid the samplers horizontally into undisturbed floc adjacent to the sliding plate sampler. I extracted 15 mL of porewater from each depth using a spring-loaded 30-mL syringe connected to the Rhizon via Tygon PVC tubing. In 2016, I collected a depth-integrated porewater sample from the upper 10 cm of floc at a variety of shallow (<1 m) freshwater ecosystems in July, August, and October. Instead of using the sliding plate sampler method, I inserted a 10-cm long Rhizon sampler vertically into the floc layer and slowly extracted 20 mL of porewater using a spring-loaded 30-mL syringe connected to the Rhizon via Tygon PVC tubing. For both sampling approaches, I added subsamples of the filtered porewater into reagents in the field to produce stable colorimetric complexes with dissolved Fe^{2+} and ΣH_2S. The remaining filtered portion stayed cold on ice until return to the laboratory. I stored all filtered samples at 4°C until analysis within 5 days of sample collection.

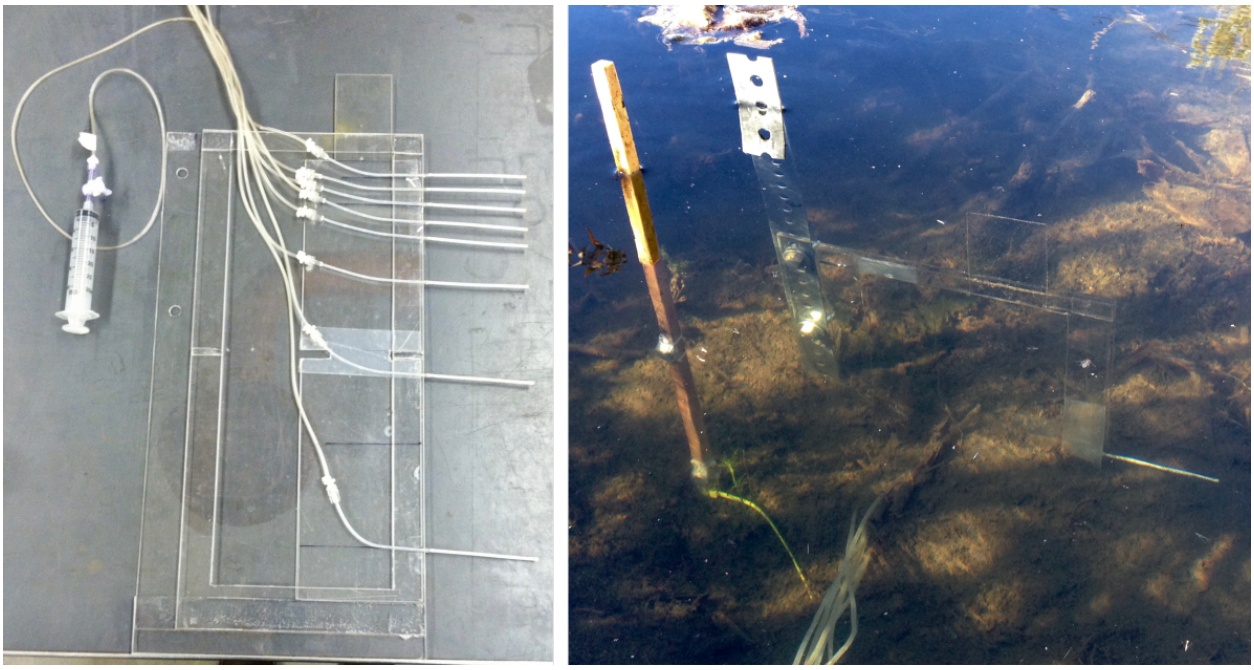

Figure 1.2. Customized sliding plate sampler for sampling porewater in flocculent sediments at multiple depths with Rhizon samplers. The photo on the left depicts the sampling setup before deployment and the photo on the right depicts the sampler deployed in flocculent sediment.

Floc chlorophyll a profiles

In late June and early July 2016, I collected intact cores of flocculent sediment from 10 waterbodies to measure chlorophyll *a* (chl *a*) concentrations throughout the floc profile. Once again, I targeted locations with water columns <1 m deep that were also largely devoid of vascular plant growth. I collected floc cores using a transparent coring tube (inner diameter, 7.2 cm) and then transported them back to the lab for processing. The cores were sectioned into 1-5 cm depth intervals by extruding the sediment out of the top of the core. If the water content of the floc was too high, I scooped the section out of the core. I collected a homogenized 0.3 mL subsample of floc from each core slice using a cutoff 3-mL syringe. To dewater the floc, I centrifuged the subsample in a 15-mL centrifuge tube at 4000 rpm for 3 min. and then removed the liquid layer from the top using a pipette. Samples were capped and frozen until extraction. To

determine chl *a* concentrations, I extracted pigments from the sediment in 90% acetone for 24 hours at 4°C, followed by measurement of chl *a* concentrations on filtered subsamples using a calibrated Turner Designs fluorometer (TD-700, Turner Designs, Sunnyvale, CA, USA). Data are expressed both gravimetrically (μg per sediment dry weight, DW, μg g^{-1} DW) and volumetrically (μg per volume of sediment, μg cm^{-3}).

Water and gas analyses

I determined the concentrations of solutes in overlying water and porewater using the following analytical methods. I measured concentrations of major ions using Dionex membrane-suppression ion chromatography. Analysis of NH_4^+ differed for overlying water and porewater samples: I determined NH_4^+ concentrations in porewater samples using ion chromatography and in overlying water colorimetrically using the phenylhypochlorite technique (Aminot et al. 1997). I measured soluble reactive phosphorus (SRP) concentrations colorimetrically using the molybdate blue method and long-path-length spectrophotometry (Murphy and Riley 1962) and dissolved organic carbon (DOC) using the non-purgeable organic carbon (NPOC) method on a Shimadzu carbon analyzer equipped for high-temperature, Pt-catalyzed combustion and gas chromatographic measurement of the resultant CO_2. I measured dissolved Fe^{2+} in porewater colorimetrically using a ferrozine reaction method modified from (Lovley and Phillips 1987) and (Stookey 1970), in which I added filtered porewater to a solution of 50 mM 4-(2-hydroxethyl)-1-piperazineethanesulfonic acid buffer containing ferrozine (1 g l^{-1}). I measured ΣH_2S in porewaters using the methylene blue spectrophotometric method (Golterman and Clymo 1969).

I determined the concentrations and percent composition of gases using the following analytical methods. To determine the partial pressures of CO_2 and CH_4 in the extracted gas

samples from the intact core survey, I used an Agilent 7890 gas chromatograph equipped with a flame ionization detector for CH_4 and Licor 820 infrared gas analyzer for CO_2. To measure the percent composition of N_2 and CH_4 in the occluded gas bubbles, I used gas chromatography equipped with a flame ionization detector (CH_4) and a thermal conductivity detector (CO_2).

Sediment analyses

I analyzed sediment samples for water and organic matter content, dry bulk density, porosity, and total particulate carbon and nitrogen content using the following methods. I determined the water content (% of wet weight) by drying homogenized subsamples in the oven at 60°C. After weighing the dried subsamples, I determined organic matter content (% of dry weight) by loss on ignition (LOI) upon combusting the subsamples at 550°C for two hours. I calculated the dry bulk density and porosity of each depth layer assuming a sediment particle density of 1.25 and 2.65 g cm^{-3} for organic particles and inorganic particles, respectively (Avnimelech et al. 2001). I also determined total carbon and nitrogen content of the particulate fraction of floc by combusting dried and finely ground subsamples in a Costech CHN automated combustion analyzer. Prior to analysis in the CHN analyzer, I removed inorganic C from the samples via HCl fumigation (Harris et al. 2001). I performed the previous analyses on subsamples of the bulk core samples from the floc abundance survey and on subsamples from the individual depth intervals for the intact cores and chl *a* samples.

Data analysis

I used a structural equation modeling (SEM) approach to infer the relative importance of waterbody characteristics (catchment slope and depth to consolidated bottom [depth to bottom]),

aquatic vegetation cover (combined emergent and floating cover [surface vegetation] and submerged vegetation cover), and temperature (water column and floc sediment) to the thickness of floc in shallow wetlands and the littoral zones of lakes. The SEM allowed me to evaluate the nature and magnitude of direct and indirect effects of a hypothesized network of causal relationships that together influence the thickness of floc in shallow waters. In lieu of the traditional variance covariance-based SEM, I fit a piecewise SEM (Shipley 2009; Lefcheck 2016) using the 'piecewiseSEM' package in R (Lefcheck 2016). This approach is able to (1) piece together multiple generalized linear models fit to different distributions to a single causal network, (2) account for hierarchy by nesting variables in a mixed model framework, and (3) use Shipley's test of *direct separation* (*d-separation*) to examine missing paths in the model and overall model fit (Shipley 2013; Lefcheck 2016).

I constructed the piecewise SEM based on a meta-model depicting the hypothesized potential relationships (Appendix Figure A1.1). The data I used for this analysis were from waterbodies with low flow measured during the 2015 survey of floc abundance (not including measurements from Morrow Lake, a run-of-river reservoir in the Kalamazoo River). I fit each component model of the piecewise SEM as linear models fit to a negative binomial distribution for floc thickness, binomial distributions for vegetation cover proportion data, and normal distributions for water column and floc sediment temperatures. To properly model the overdispersion in the vegetation cover proportion data, I included an observation-level random effect in both of those models (Harrison 2014; Harrison 2015). I included site (waterbody) as a random effect in all models to account for between-site variation and correlations between measurements made in the same site while assessing the independent variables. I evaluated overall fit of the piecewise SEM using Shipley's test of *d-separation*: Fisher's *C* statistic

(Shipley 2009), the Akaike information criterion (AIC), and AIC corrected for small sample sizes (AICc) (Shipley 2013). I added missing paths that would significantly improve model fit as indicated by the test of *d-separation* ($p < 0.05$) if they were also ecologically relevant. The pseudo-R^2 values for each component model were estimated using the Nakagawa and Schielzeth approach (Nakagawa and Schielzeth 2012) in the 'piecewiseSEM' and 'r2glmm' packages (Jaeger 2017) in R. All statistical analyses were completed in R v.3.4.3 (R Core Team 2017) using RStudio v.1.1.383 (RStudio Team 2017).

RESULTS

Physical properties and organic content of floc

The upper 20 cm of floc sediments in shallow waterbodies of southwestern Michigan have high water contents (Figure 1.3A, median = 88%) and are loosely consolidated with a median dry bulk density of 0.13 g cm^{-3} (Figure 1.3B) and a median porosity of 0.94 (Figure 1.3C). Organic matter and organic carbon concentration ranged widely (Figure 1.3D, E), with median values of 40% and 20% by dry weight, respectively. The median C:N molar ratio of particulate floc was 11.7 (Figure 1.3F).

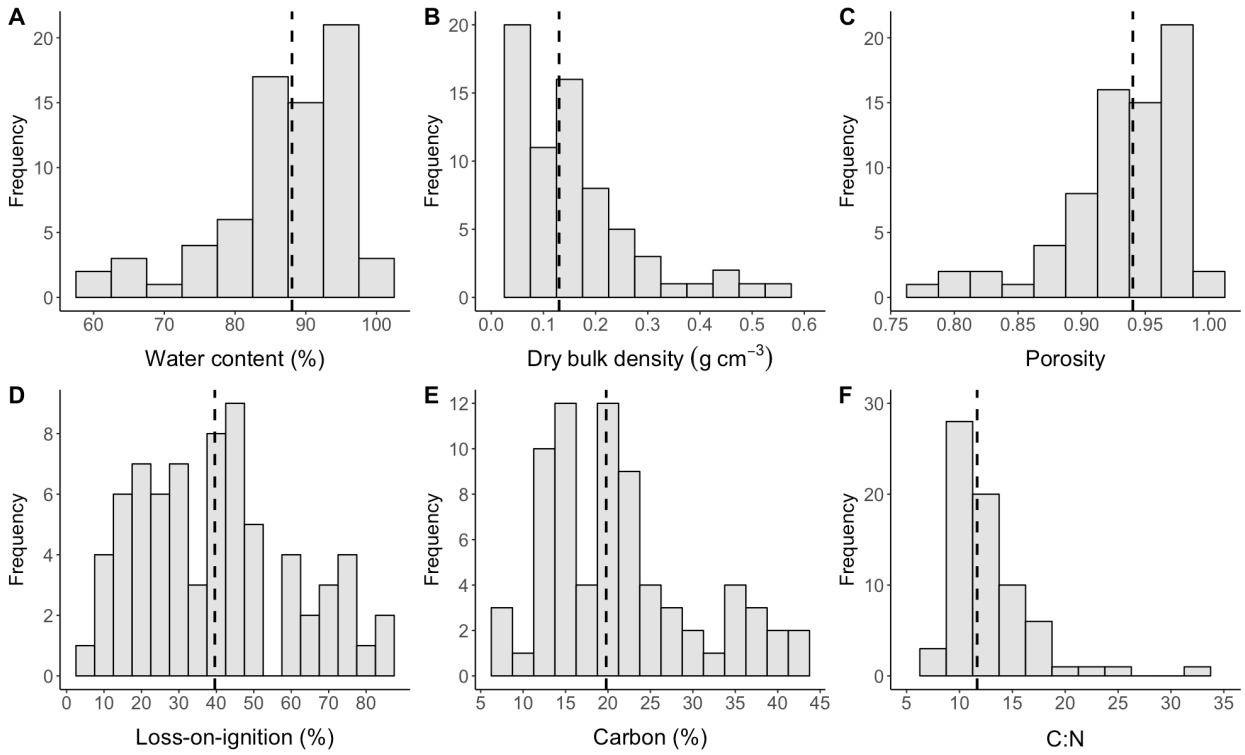

Figure 1.3. Histograms showing the distributions of (**A**) water content, (**B**) dry bulk density, (**C**) porosity, (**D**) organic matter content estimated as loss-on-ignition, (**E**) organic carbon content, and (**F**) C:N molar ratios of the upper 20 cm of flocculent sediment in shallow waterbodies in southwestern Michigan, USA. The vertical dashed lines represent the median.

Algal biomass

Chlorophyll *a* concentrations varied widely in the upper 5 cm of floc sediments (9.3-266.1 µg g^{-1} DW or 1.2-26.3 µg cm^{-3}) and decreased with depth (Figure 1.4). Detectable levels of chl *a* often remained at depths of more than 20 cm below the floc-water interface. I did not seek to identify the algae present in the floc sediment cores, but I observed filamentous algae in many of the cores, and at one site, the duckweed *Wolffia* sp. was present throughout the depth of the core.

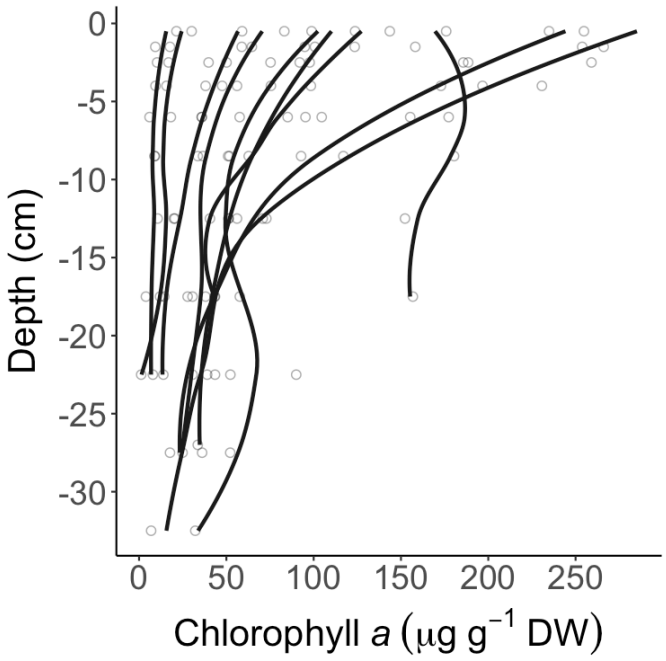

Figure 1.4. Vertical profiles of chlorophyll *a* content (per sediment dry weight, DW) in flocculent sediments in 10 different shallow waterbodies in southwestern Michigan, USA. Open circles represent measured concentrations and the lines represent a LOESS curve fit to each profile. Zero on the depth axis represents the interface between flocculent sediment and overlying water.

Porewater chemistry

Concentrations of DOC, SRP, and NH_4^+ in the upper 10 cm of the floc layer typically exceeded concentrations in overlying waters by factors ranging from approximately 2 to 6, 0 to 600, and 7 to 2100, respectively (Figure 1.5A-C). Conversely, floc porewater concentrations of NO_3^- and SO_4^{2-} were typically less than concentrations in overlying waters (Figure 1.5D, E). Dissolved nutrient concentrations in the upper 10 cm of the floc layer were found at detectable levels in most samples, with the exception of NO_3-N, which was near or below the analytical detection limit (~15 μg L^{-1}) for most porewater samples.

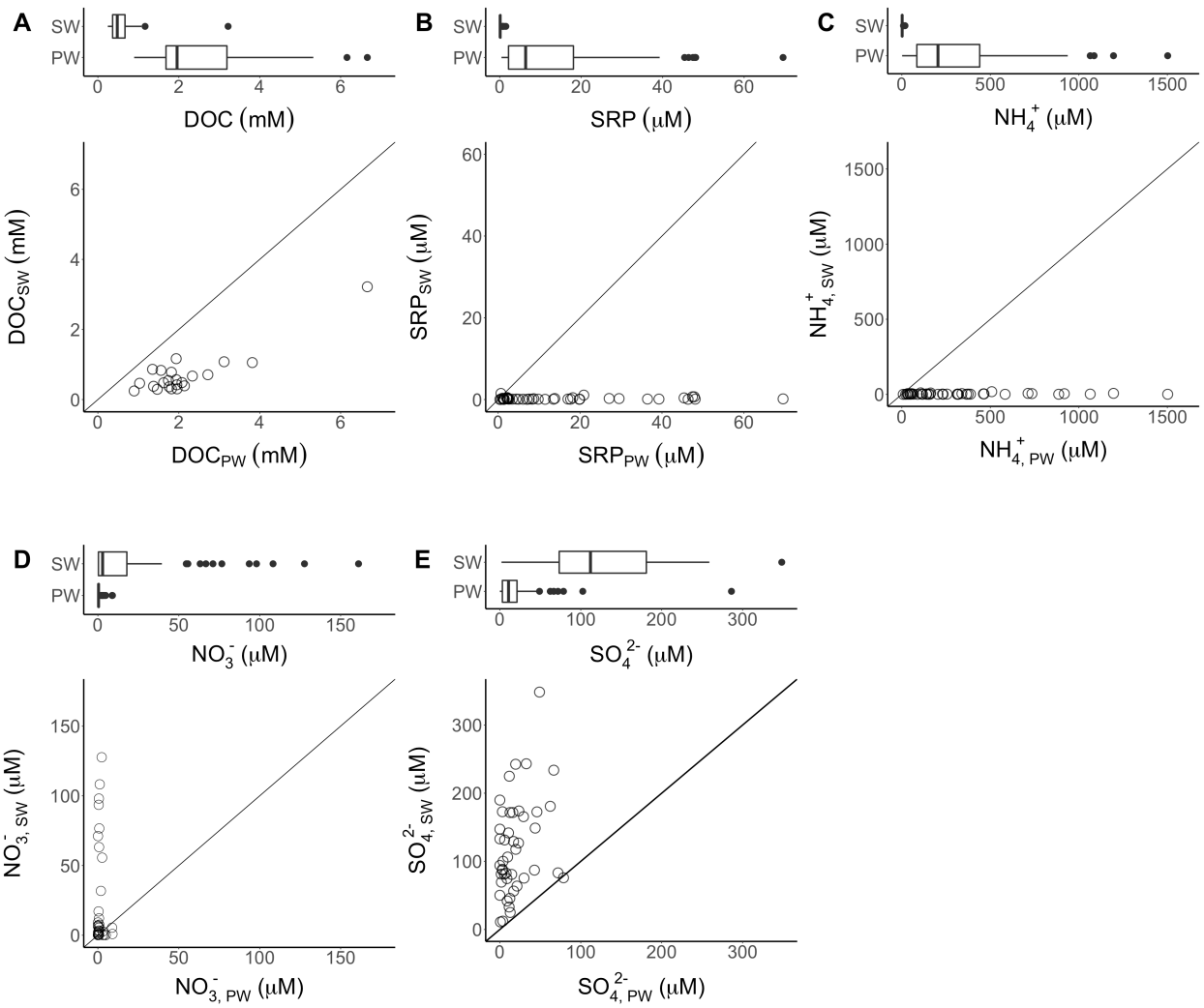

Figure 1.5. Surface water (SW) and flocculent sediment porewater (PW) concentrations of (**A**) dissolved organic carbon (DOC), (**B**) soluble reactive phosphorus (SRP), (**C**) ammonium (NH_4^+), (**D**) nitrate (NO_3^-), and (**E**) sulfate (SO_4^{2-}) in shallow waterbodies in southwestern Michigan, USA. Porewater concentrations represent the mean concentration of each solute in the upper 10 cm of the floc layer. Lines in the scatterplots represent the 1:1 ratio.

The shape of vertical porewater profiles through the floc layer, which reflects net production or consumption of solutes, was dependent on the solute. The profiles for Fe^{2+}, ΣH_2S, SRP, NH_4^+, CO_2, and CH_4 (Figure 1.6A, B, D, E, G, H) were typically concave implying net production of these solutes within the floc sediment layer (Lerman 1979; Berner 1980). Conversely, the profiles of SO_4^{2-} and NO_3^- (Figure 1.6C, F) were typically convex implying net

removal of these solutes in the floc sediment layer, though there was one site where NO_3^- increased with depth. Zones of production or consumption based on visual inspection of the profile curves seemed to occur in the upper 15-20 cm of the floc layer, with the exception of NO_3^-, which was nearly undetectable in most profiles below upper 1 cm of the floc layer.

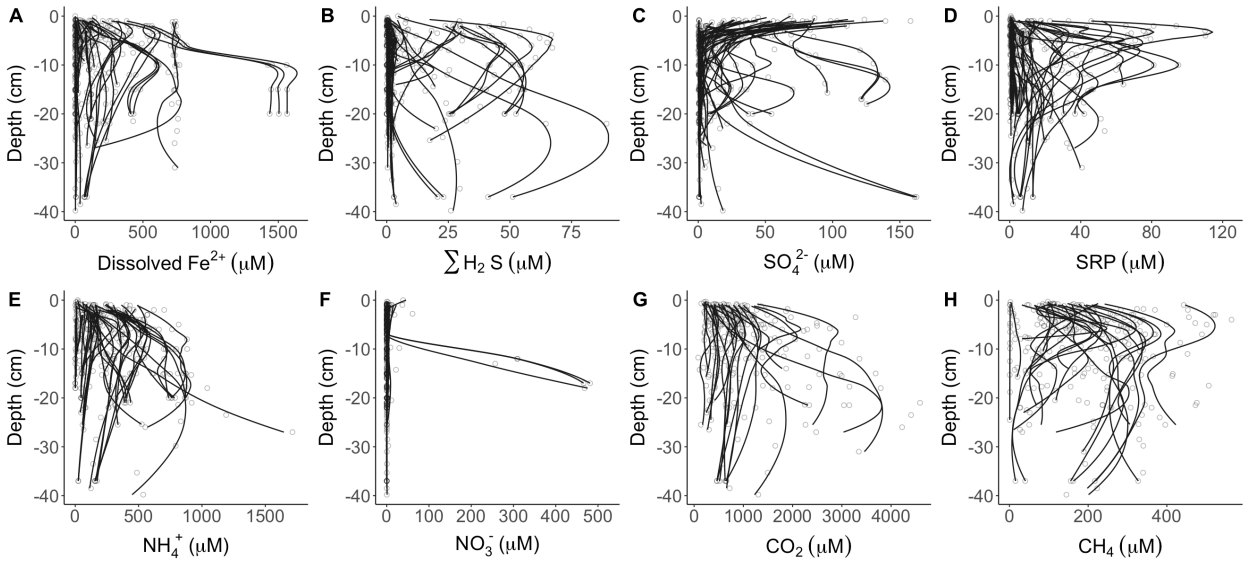

Figure 1.6. Vertical profiles of flocculent sediment porewater concentrations of (**A**) dissolved ferrous iron (Fe^{2+}), (**B**) dissolved free sulfide (ΣH_2S), (**C**) sulfate (SO_4^{2-}), (**D**) soluble reactive phosphorus (SRP), (**E**) ammonium (NH_4^+), (**F**) nitrate (NO_3^-), (**G**) dissolved carbon dioxide (CO_2), and (**H**) dissolved methane (CH_4) from shallow waterbodies in southwestern Michigan, USA. Profiles were collected from intact cores of flocculent sediment and in situ sampling events. Open circles represent measured concentrations and the lines represent a LOESS curve fit to each profile. Zero on the depth axis represents the interface between flocculent sediment and overlying water.

Occluded gas volume and chemistry

The total volume of occluded gas in flocculent sediments ranged from 0.2 to 10.6 L m^{-2} with a median volume of 2.4 L m^{-2} (Figure 1.7A). Gas volume expressed per volume of floc ranged from 2.2 to 80.2 L m^{-3} with a median volume of 7.6 L m^{-3}. The composition of occluded gas was predominantly CH_4 and N_2; together these two gases composed between 86 and 95% of the total occluded gas volume (Figure 1.7D). I did not quantify the composition of the balance of

occluded gas. Methane in the occluded gas ranged from 0.1 to 76%, with a median value of 47% (Figure 1.7B). Nitrogen gas ranged from 16 and 95%, with a median value of 42% (Figure 1.7C).

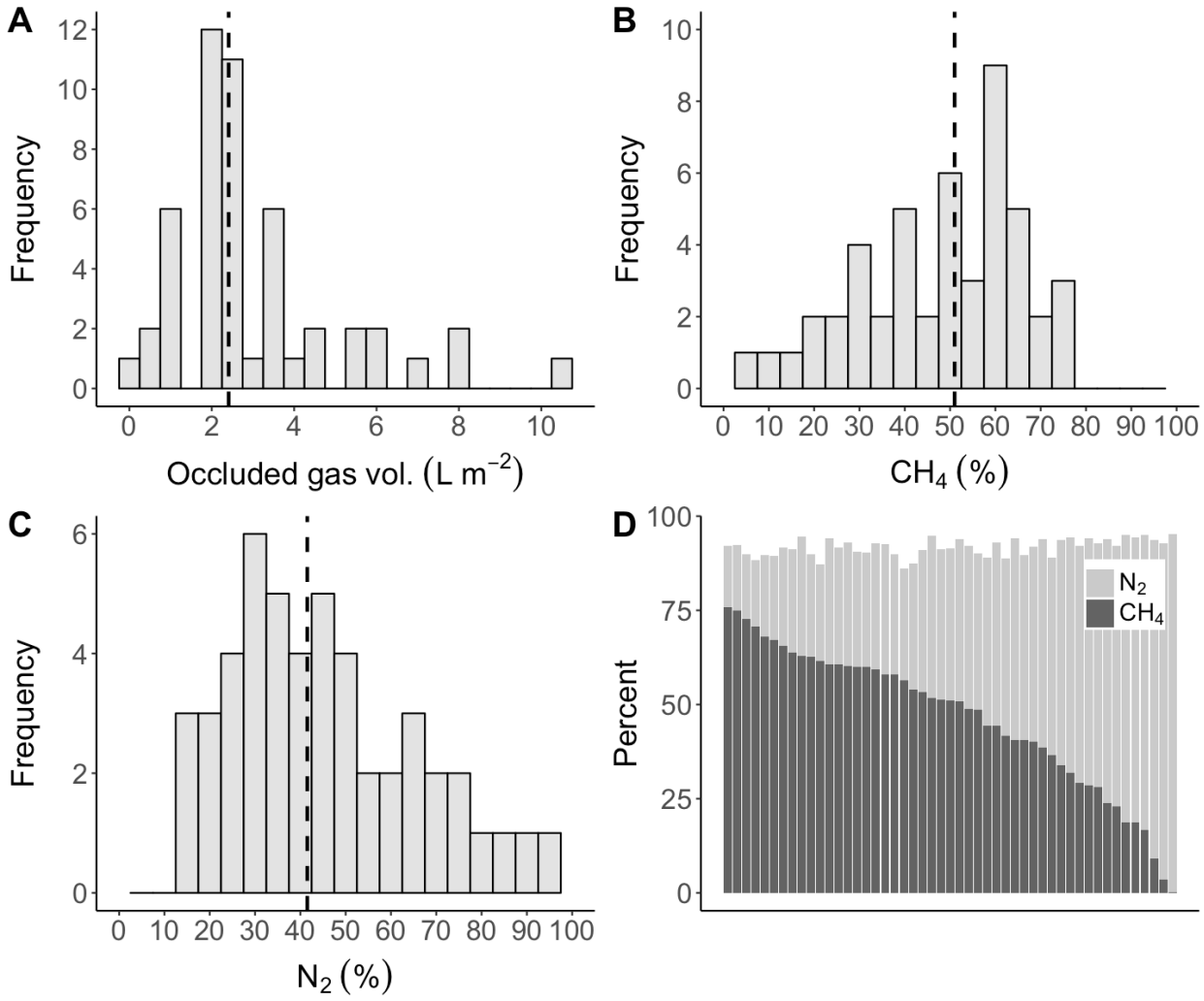

Figure 1.7. Histograms showing the distributions of (**A**) volume, (**B**) percent methane (CH_4), and (**C**) percent nitrogen gas (N_2) of occluded (trapped) gas in flocculent sediments in shallow waterbodies of southwestern Michigan, USA. The vertical dashed lines represent the median. (**D**) shows the sum of the percent CH_4 and N_2 in each sample of occluded gas arranged in order of decreasing percent CH_4.

Occluded gas volume, CH_4 content, and CH_4 to N_2 ratios were correlated with various environmental variables (Figure 1.8), but not to measures of organic matter content (LOI or OC content, $p > 0.05$), N content of particulate floc (C:N molar ratio, $p > 0.05$), or sediment structure

(dry bulk density or water content, $p > 0.05$). The volume of occluded gas was positively correlated with floc thickness (Figure 1.8A, $p < 0.001$, $R^2 = 0.29$, slope = 0.034, standard error [SE] = 0.008), but not floc sediment temperature (Figure 1.8B) or emergent vegetation cover (includes both emergent and floating vegetation cover; Figure 1.8C). Percent CH_4 was positively correlated with floc thickness (Figure 1.8D, $p = 0.006$, $R^2 = 0.15$, slope = 0.23, SE = 0.08) and floc sediment temperature (Figure 1.8E, $p = 0.004$, $R^2 = 0.17$, slope = 2.90, SE = 0.96), but negatively correlated with emergent vegetation cover (Figure 1.8F, p 0.014, $R^2 = 0.12$, slope = -0.25, SE = 0.10). The ratio of CH_4 to N_2 (by % volume) in occluded gas was positively correlated with floc thickness (Figure 1.8G, $p = 0.001$, $R^2 = 0.21$, slope = 0.02, SE = 0.005) and negatively correlated with emergent vegetation cover (Figure 1.8I, $p = 0.024$, $R^2 = 0.10$, slope = -0.01, SE = 0.006). With the exception of percent CH_4, which was negatively correlated with organic matter contents ($p = 0.037$, $R^2 = 0.09$, slope = -0.24, SE = 0.11), the volume of occluded gas and its composition were not significantly correlated with percent organic matter, percent organic C, or C to N ratios of particulate floc.

Floc thickness

Floc sediments along the littoral margins of shallow waterbodies ranged from 1 to 190 cm in thickness (Figure 1.9, median = 30 cm).

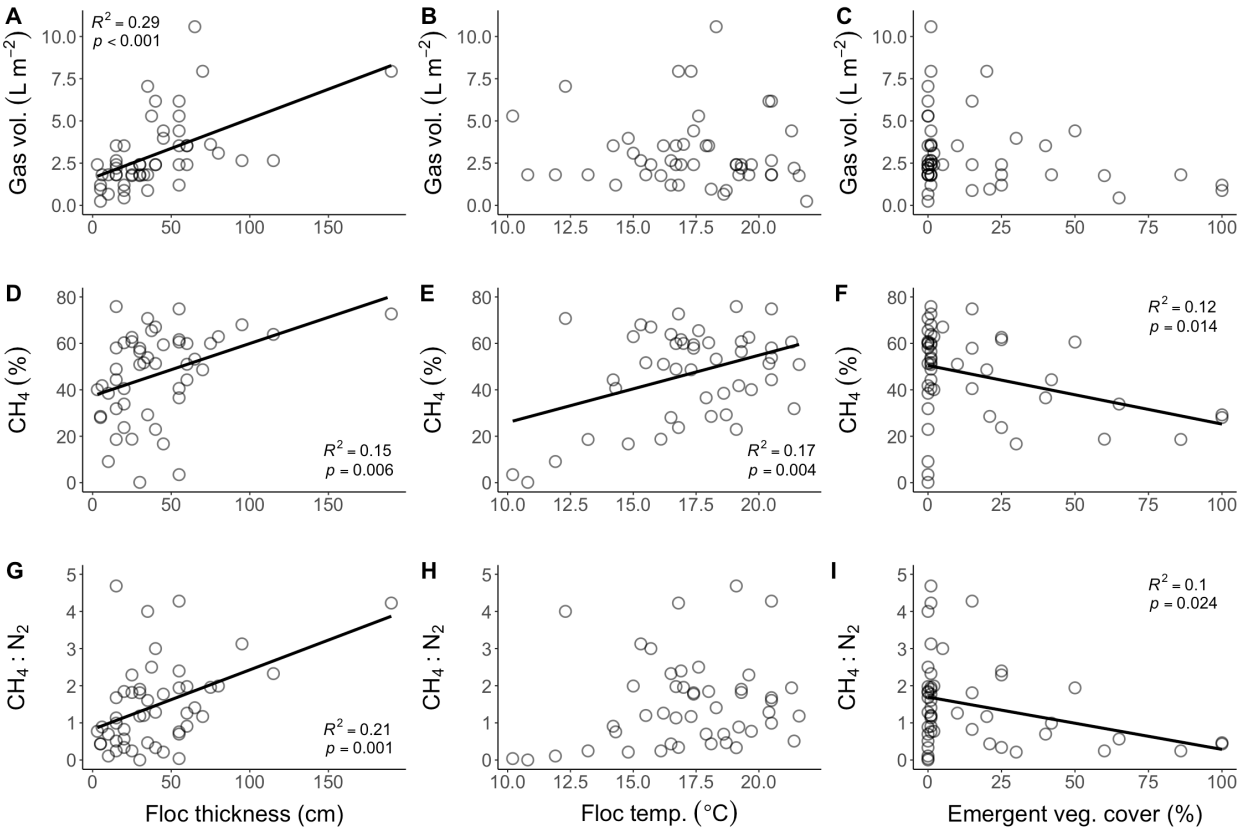

Figure 1.8. Relationships between (**A**, **D**, **G**) floc thickness, flocculent sediment temperature (**B**, **E**, **H**), or (**C**, **F**, **I**) emergent vegetation cover (includes the sum of emergent and floating vegetation cover) and (**A**, **B**, **C**) the volume, (**D**, **E**, **F**) percent methane (CH_4), and (**G**, **H**, **I**) percent nitrogen gas (N_2) of occluded (trapped) gas in flocculent sediments of shallow waterbodies in southwestern Michigan, USA. Shown are measured values (open circles) and linear relationships ($p < 0.05$; black lines).

The piecewise SEM fit the data well ($p = 0.56$ for Fisher's C statistic; $p > 0.05$ indicates good fit; Shipley 2009) and explained a substantial amount of variation in floc thickness (pseudo-$R^2 = 0.60$). Waterbody characteristics and temperature, but not vegetation cover, were most important to explaining floc thickness (Figure 1.10). Depth to the consolidated bottom directly affected floc thickness (standardized coefficient [β] = 0.43, $p < 0.001$). Catchment slope impacted floc thickness directly ($\beta = 0.14$, $p = 0.009$) and indirectly through surface water temperature ($\beta = -0.22$, $p = 0.04$). Floc sediment temperature had a direct effect on floc thickness

where warmer temperatures resulted in less accumulation of floc (β = -0.30, $p < 0.001$). Surface water temperature indirectly affected floc thickness through floc sediment temperature (β = 0.63, $p < 0.001$). Neither class of vegetation cover had a significant relationship in the piecewise SEM.

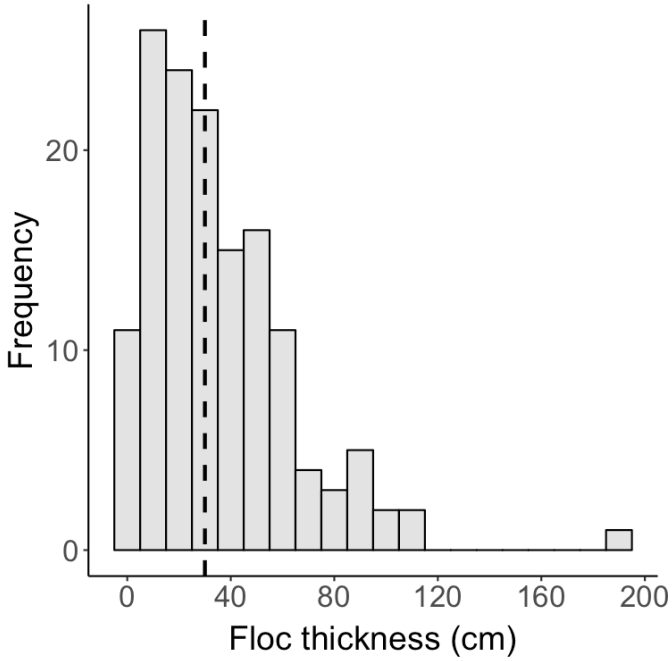

Figure 1.9. Thickness of flocculent sediments in the littoral margins (from the shore to water no more than approximately 2 m in depth) of 13 shallow waterbodies in southwestern Michigan, USA. The vertical dashed line represents the median.

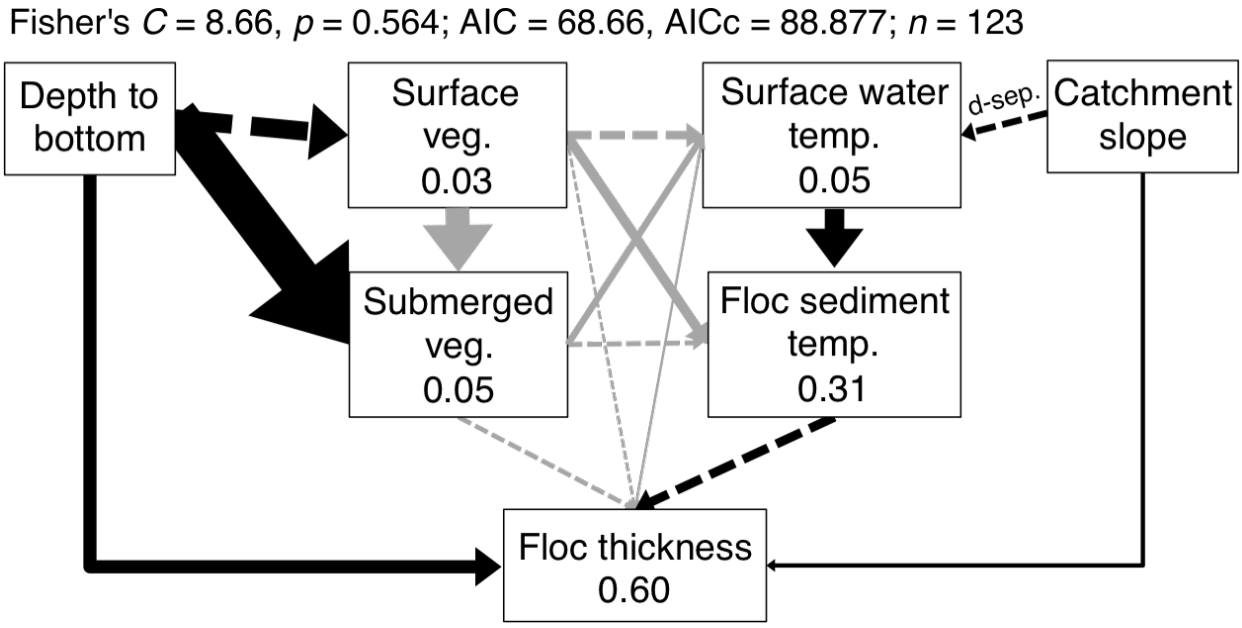

Figure 1.10. Structural equation model of predictors of floc thickness in shallow lentic ecosystems in southwestern Michigan, USA. Black paths represent significant relationships ($p < 0.05$, piecewise SEM). Gray paths represent non-significant relationships. The path labeled d-sep. was added to improve model fit based on a test of *d-separation*. Solid lines represent positive relationships and dashed lines negative relationships. Paths are weighted by standardized path coefficients. Values inside of the box are the pseudo-R^2 values for that response variable. Overall fit of piecewise SEM was evaluated using Shipley's test of *d-separation*: Fisher's *C* statistic (if $p > 0.05$, then the model is a good fit), Akaike information criterion (AIC), and AIC corrected for small sample sizes (AICc).

DISCUSSION

Organic carbon and floc sediment structure

The median OC concentration of floc sediments (20%; range, 7-43%) is greater than or equivalent to the OC concentration of surficial sediments in most lakes of glaciated regions in the Northern Hemisphere. Dean and Gorham (1998) reported that English lakes had the lowest average OC concentration (7%; range, 4-13%), followed by lakes in Wisconsin, USA (11%) and Minnesota, USA (12%; range, 3-29%). Conversely, OC concentration in floc sediments were nearly identical to the average concentration in lakes in the Experimental Lakes Area in

northwestern Ontario, Canada (20%; range 13-27%)(Dean and Gorham 1998), though the range for flocculent sediments in this study was greater.

While these observations of OC concentrations in floc are on the high end of ranges reported for lakes in similar regions, they are not outside the range reported for sediments in other regions and particularly when organic sediments are specifically targeted. For example, in a northern Everglades marsh, Florida, USA, average C concentrations were 45-49% in the floc layer (defined as the unconsolidated material above the layer researchers visually classified as soil) (Corstanje et al. 2006). Wetland soils in Louisiana, USA marshes had OC concentrations ranging <4-43% (Gosselink et al. 1984) very similar to floc in this study. In arctic lakes in Alaska, USA, organic matter concentrations in sediments ranged from 9 to 81% (Whalen et al. 2013; Bretz and Whalen 2014; Fortino et al. 2016); converting OM to OC using a standard correction factor (0.469)(Dean 1974) gives a range of OC concentrations in arctic lakes (4-38%) similar to floc sediments in this study. Similarly, in a study focused on organic sediments in Danish lakes, Hansen (1959) found that OC concentrations ranged from 2 to 48% (mean, 16%). And in organic-rich (muck) sediments of a stream in northern Wisconsin, USA, organic matter concentrations ranged from 12 to 81% (Crawford et al. 2014), corresponding to OC concentrations in these sediments ranging from approximately 5 to 38%.

The elevated OC concentration of flocculent sediments in this study likely results from several factors. The first factor is the balance of OM versus inorganic sediment inputs to waterbodies in the study landscape. In the watersheds of the study area in southwestern Michigan, infiltration rates in upland soils are high and surface runoff is low (Hamilton 2015) and thus, delivery of inorganic sediments from overland flow is low. Conversely, waterbodies here continually receive OM from a combination of autochthonous and allochthonous sources.

Second, as lakes age and accumulate sediments, the proportion of sediment OM derived from emergent vegetation increases (Godshalk and Wetzel 1978; Godshalk and Barko 1985) and is generally recalcitrant to decomposition. The third factor may result from my emphasis on sediments in shallow waters. Here sediments often receive enough light to support benthic primary producers that contribute to sediment OM directly through inorganic C fixation (Wetzel 2001; Ask et al. 2009) and the production of extracellular polymeric substances (EPS) (Gerbersdorf et al. 2009), and indirectly by supporting the growth of microbial communities (Murray et al. 1986; Rier and Stevenson 2001; Carr et al. 2005; Kuehn et al. 2014). Also, sediment OM in shallow waters may have undergone less diagenesis than sediment OM in deeper waters, which may be composed of both freshly deposited OM and older sediment that was transported to deeper waters via sediment focusing.

A fourth factor, the formation of flocs through the aggregation and stabilization of inorganic and organic sediment components (Droppo et al. 1997; Grabowski et al. 2011a), may preserve OC inputs in sediments. Flocs often form as OM adheres to coagulated particles, and eventually they settle to the benthic sediment layer as they grow in size. At the surface of benthic sediments, bacterial and algal communities produce EPS that bridge flocs with polymer fibrils, further stabilizing them (Grabowski et al. 2011b; Gerbersdorf and Wieprecht 2015) and increasing the OC concentration of sediments (Decho 1990; de Winder et al. 1999; Gerbersdorf et al. 2008; Gerbersdorf et al. 2009). High concentrations of dissolved Ca^{2+}, which are typical of groundwater-fed surface waters in the study area (Thobaben and Hamilton 2014; Hamilton 2015) also promote the flocculation process (Grabowski et al. 2011b). When flocs are bound together by iron oxides as they often are (Buffle and Leppard 1995; Liss et al. 1996; Plach et al. 2011; Grabowski et al. 2011a; Plach et al. 2014; Elliott and Warren 2014), the OM can become

resistant to microbial degradation and OC is preserved (Boudot et al. 1989; Keil et al. 1994; Lalonde et al. 2012). This protective mechanism is likely a factor in this study area as dissolved Fe^{2+} is often present at measurable levels in porewaters (Figure 1.6A)(Kinsman-Costello et al. 2015); however, I did not evaluate this directly.

Regardless of the particular mechanisms that enhance OC concentrations in flocculent sediments, the elevated OC concentration impacts the structure of the sediment layer. The most apparent impact is on the density of floc sediments—as the OC concentration of floc sediments increases, the bulk density decreases (Figure 1.11A) and water content increases (Figure 1.11C). Consequently, the range of bulk densities for floc sediments in this study (Figure 1.3B, 0.01-0.55 g cm^{-3}) was on the lower end of the range, 0.09-1.77 g cm^{-3}, reported for 868 measurements made in inundated environments around the globe (Avnimelech et al. 2001), though sediments in that analysis had OC concentrations less than 10%. However, floc densities were also on the low end of the range reported for lake sediments with OC concentrations between 0.5-34% (0.07-1.29 g cm^{-3})(Barko and Smart 1986). Conversely, the organic sediments from the Everglades marsh and arctic lakes in Alaska that I mentioned previously had densities of 0.001-0.4 g cm^{-3} (Corstanje et al. 2006) and 0.06-0.13 g cm^{-3} (Fortino et al. 2016), respectively.

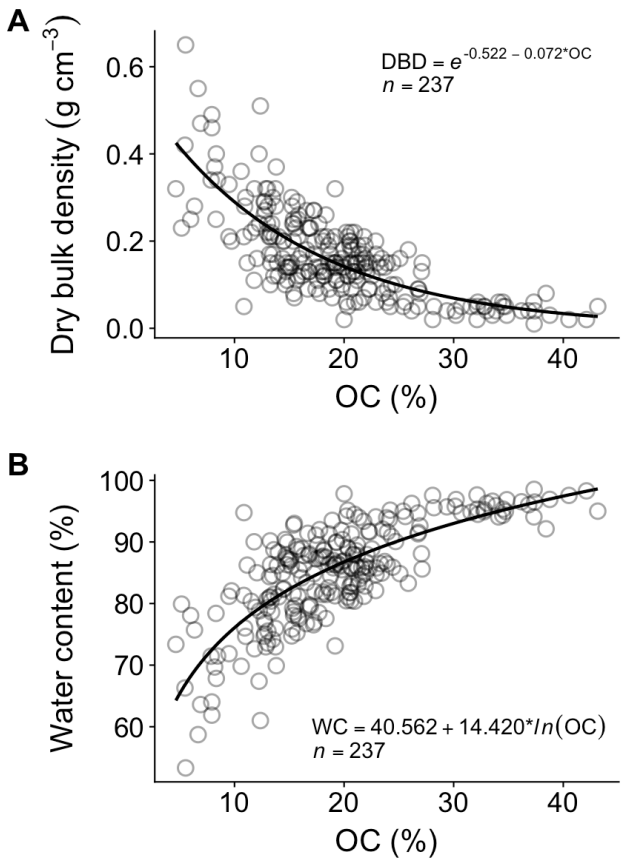

Figure 1.11. (**A**) Relationship between dry bulk density (DBD) and organic carbon (OC) for flocculent sediments from shallow waterbodies in southwestern Michigan, USA. (**B**) Relationship between water content and OC for flocculent sediments. Data in all plots are from the 2014 intact core survey (all core slices in the upper 20 cm) and the 2015 survey of floc abundance (average of upper 20 cm of the floc layer).

Algal biomass

Floc chl *a* contents for all depths sampled (1.2-266.1 μg g^{-1} DW/0.6-26.3 μg cm^{-3}) were typically within ranges observed in sediments of shallow lakes in the Alaskan arctic (2.6-37 μg cm^{-3})(Whalen et al. 2013), shallow waters (< 5 m) of a eutrophic lake in Scotland (24-306 μg g^{-1} DW)(Spears et al. 2006; Spears et al. 2010), and shallow reservoirs and groin fields in Germany (10-248 μg g^{-1} DW/3-83 μg cm^{-3})(Gerbersdorf et al. 2009). Conversely, in all but one of the floc cores, chl *a* contents in the upper 5 cm were greater than the upper range of chl *a* contents

observed for less organic littoral sediments in Canadian Shield lakes (2-22 μg g^{-1} DW)(Cyr and Morton 2006). Similarly, 8 of 10 of the floc cores had mean chl *a* contents in the upper 5 cm greater than the upper range of chl *a* contents observed for floc sediments in Taylor Slough, a marsh in the Florida Everglades (16-56 μg g^{-1} DW).

My observations of chl *a* concentrations in the upper range of those reported for shallow sediments is in accordance with other studies that have found correlations between microphytobenthos biomass and sediment OM content (Håkanson and Jansson 1983; Shimanaga and Shirayama 2000). The presence of algae below the euphotic zone (typically the upper several mm of sediment)(MacIntyre et al. 1996; Underwood and Kromkamp 1999) may result from physical mixing of floc (Wasmund 1984; Cyr 1998) and the vertical migration of microphytobenthos in floc (Round and Eaton 1966; Harper 1969; Underwood and Paterson 2003).

Solute chemistry in floc

The patterns in solute chemistry I observed in floc sediments are congruent with expectations for anoxic accumulations of organic sediments. For DOC, I would expect higher concentrations in porewaters versus overlying waters. As particulate OM undergoes decomposition, a proportion is solubilized to form DOC. Under anoxic conditions, production of DOC outpaces consumption and more recalcitrant compounds accumulate in porewaters (Burdige and Komada 2015). Consistent with my expectation, floc porewater DOC concentrations were consistently greater than SW concentrations (Figure 1.5A). The range of DOC concentrations I observed in floc porewater, 0.9-6.7 mM, was well within the range reported for various freshwater ecosystems (0.3-15.2 mM)(Barko and Smart 1986; Chen and Hur

2015) and similar to the range reported for the floc layer overlying soils in newly constructed wetland in Florida, USA (1.9-3.8 mM)(D'Angelo and Reddy 1994).

Similarly, the production of dissolved P and NH_4^+ typically outpaces losses in organic-rich sediments and these nutrients accumulate in porewaters (Barko and Smart 1986). Dissolved P in porewaters results from OM decomposition and desorption of P from clays, amorphous metal oxides, and similar materials in the absence of oxygen (Wetzel 2001). Mobile P in porewaters diffuses upward, but often accumulates in the upper portion the sediments where it becomes bound again to oxidized metal compounds produced by variable redox conditions in these upper layers (Mortimer 1941; Kamp-Nielsen 1975; Carlton and Wetzel 1988; Löfgren and Boström 1989; Jensen et al. 1992). I observed both the accumulation of SRP in floc porewaters relative to overlying water concentrations (Figure 1.5B) and frequent accumulation of SRP in the upper portions of floc profile (Figure 1.6D), though concentrations (0.4-69.6 μM) were well within the range reported in other North American lake sediments (1.3-302.2 μM)(Barko and Smart 1986).

Ammonium primarily originates from OM decomposition and accumulates in anoxic porewaters where the lack of oxygen inhibits its nitrification to NO_3^-. OM further promotes NH_4^+ accumulation in sediment porewaters as NH_4^+ regularly adsorbs to sediment OM (Raaphorst and Malschaert 1996; Hou et al. 2003; Jellali et al. 2010; Zhang et al. 2015), potentially slowing diffusive loss from sediments. In floc sediments I observed accumulation of NH_4^+ in porewaters relative to concentrations in overlying water (Figure 1.5C) and net production of NH_4^+ in most floc porewater profiles (Figure 1.6E). Similar to SRP, floc NH_4^+ concentrations (1.6-1502.0 μmol N L^{-1}) were well within those reported in other North American lake sediments (114.2-3255.5 μmol N L^{-1})(Barko and Smart 1986).

In the absence of oxygen, heterotrophic microoganisms utilize alternative electron acceptors to oxidize OM. As anaerobic oxidation processes proceed, electron acceptors are usually used in the order of the amount of energy each reduction-oxidation reaction yields. Typically, NO_3^- is utilized first, followed by Fe^{3+}, and then SO_4^{2-}. In anoxic sediment, this usually translates into somewhat predictable solute chemistry as you move from the upper to deeper layers (Burgin et al. 2011). In the upper few mm NO_3^- is consumed by denitrification. In subsequent depths Fe^{2+} is produced via the reduction of Fe^{3+}, followed by the consumption of SO_4^{2-} and the production of H_2S. Finally, CH_4 is produced as a result of methanogenesis—a distinctive form of catabolic metabolism. In floc, the spatial scales and depths at which these zones of consumption and production occurred varied by site (Figure 1.6) and general patterns were lacking; however, with the exception of one unusual site, NO_3^- concentrations were at or near the analytical detection limit below the upper 1 cm.

These observations indicate that floc sediments likely play important roles in determining surface water chemistry by serving as a source or sink for certain important nutrients. Given the nearly undetectable concentrations of NO_3^- in porewaters, floc sediments likely serve to remove NO_3^- from overlying waters and/or from upwelling groundwater. That said, 50% of the samples had NH_4^+ porewater concentrations at least 142 times greater than concentrations in overlying waters at those sites. This extreme gradient means that floc sediments likely serve as a source of inorganic N to overlying waters as NH_4^+ diffuses from concentrated porewaters to more dilute waters (e.g., O'Brien et al. 2012). If production of NO_3^- in the water column from nitrification of NH_4^+ diffusing from floc porewaters exceeds NO_3^- removal by the floc sediment, then floc sediments could become a persistent source of NO_3^- to overlying waters. Similarly, given the extreme difference between SRP concentrations in porewaters and those in the overlying water

(Figure 1.5B), floc likely serves as source of dissolved P to overlying waters. The net effects of floc sediments on sediment-water exchanges of nutrients and other solutes require more investigation.

In addition to the gradient of solute concentrations, diffusive fluxes across the floc-water interface may also be enhanced by the highly porous nature of floc. According to Fick's first law of diffusion, all else being equivalent, sediments with greater porosities will yield greater diffusive fluxes (Berner 1980). While diffusive fluxes for both N and P are determined by more than sediment structure (e.g., interactions with organic and inorganic compounds), given the high porosity of floc sediments (Figure 1.3C, median, 0.94), diffusion coefficients in floc may approach those of free water. However, Flury et al. (2015) demonstrated that the presence of minor amounts of free gas bubbles in sediments can suppress the diffusivities of solutes. Given the volume of occluded gas in floc sediments (Figure 1.7A), this could influence the diffusive fluxes of N and P across the floc-water interface.

Occluded gas

Total volumes of occluded gas in floc sediments (2.2-80.2 L m^{-3}) ranged more widely than those reported in other sediment environments, though I only found a few studies that reported these values. Chanton et al. (1989) observed volumes ranging from 7.6 to 14.8 L m^{-3} in the upper 1 m of tidal freshwater sediments in North Carolina, USA. Martens and Chanton (1989) reported a volume of 15.1 L m^{-3} in the upper 1 m of sediments in a small coastal lagoon in North Carolina, USA. Maximum volumes from both studies were about 50% of the second largest volume I observed in floc sediments (30.1 L m^{-3}).

Floc thickness, floc temperature, and emergent vegetation cover were generally the best predictors of the bulk volume (expressed as L m^{-2}) and CH_4 content of occluded gas (Figure 1.8). The positive correlation between these variables and floc thickness (Figure 1.8A, D, G) likely reflects the contribution of gas produced deeper in the floc layer to the bulk volume and methane content of occluded gas. Intuitively, the bulk volume of gas per sediment surface area increased with floc thickness because there was more sediment volume. The increase in CH_4 content with increasing floc thickness could be explained by a greater stripping of N_2 by bubbles rising through the floc.

Congruent with other studies (e.g., Chanton and Dacey 1991), the CH_4 content of occluded gas in floc was negatively correlated with emergent vegetation cover. Rooted emergent vegetation directly removes methane from the sediment by ventilating excess gas pressure and transporting CH_4 to the atmosphere through the stems, thereby reducing bubble formation and ebullition. These plants also aerate their root systems, a process which releases oxygen that can support CH_4 oxidation.

Floc thickness

Counter to my prediction, vegetation cover was not a good predictor of floc thickness either directly or indirectly. I interpret this result in a couple of ways. First and foremost, I hypothesized that vegetation would directly promote floc accumulation by providing OM and creating a stable (low-energy, low turbulence) environment where intercepted OM would settle to the benthos and accumulate. In this scenario, floc thickness would positively correlate with vegetation cover, at least initially. However, feedbacks between sediments and aquatic vegetation in littoral habitats lead to complex relationships that are challenging to predict (Barko

et al. 1991) and are likely not captured with a single survey of vegetation cover. For example, the accumulation of organic sediment often leads to shifts in both plant abundance and community composition (Barko et al. 1991). Initially, coarse sediments receiving OM inputs are suitable habitat for submersed vegetation to colonize (Sand-Jensen and Sondergaard 1979; Kiorboe 1980). As OM accumulates, changes in sediment conditions such as reductions in sediment densities, persistent anoxia, and changes in nutrient availability, can negatively impact submersed vegetation growth (Barko and Smart 1986; Barko et al. 1991; van Wijck et al. 1992). Subsequently, vegetation types more tolerant of these conditions, mainly floating-leaved and emergent species, may colonize thick organic sediments (Barko et al. 1991; Kłosowski et al. 2011). However, once established, these rooted plants may promote decomposition of OM in the immediate vicinity by aerating sediments with their extensive root structures (Carpenter and Lodge 1986). Thus, plant detritus may be more rapidly mineralized within dense stands of floating-leaved and emergent vegetation than in adjacent habitats with low densities or no vegetation present. Further, colonization of organic sediments can be retarded or prevented if these habitats accumulate natural stressors that are toxic to plants at elevated levels (e.g., NH_4^+, Fe^{2+}, and H_2S)(van Wijck et al. 1992; Lamers et al. 2012; Lamers et al. 2013; Kinsman-Costello et al. 2015; Myrbo et al. 2017). Regardless, it is clear that vegetation cover did not serve as an appropriate proxy for processes that lead to the accumulation of sediment floc layers.

While my analysis did not reveal the input processes that lead to accumulation of floc, it may have done better at indicating processes that preserve OM and promote floc accumulation. Water level drawdowns that expose sediments to the atmosphere promote rapid decomposition of sediment OM and compaction, which both work to reduce floc thickness. Accordingly, while depth from the water surface to the consolidated bottom—the best predictor of floc thickness—

obviously constrains maximum floc thickness, it may also correlate with the amount of time the floc surface is exposed to drying as a result of water level fluctuations. Thus, deeper sites had thicker floc layers. The second most important predictor of floc thickness, floc temperature, also functions to preserve OM in floc accumulations, because decomposition rates often positively correlate with temperature. Consequently, colder sites promote floc accumulation by preserving OM. Because surface temperature influences floc temperature, it also indirectly influenced floc thickness. Cold floc temperatures could also be a proxy for groundwater upwelling, which in addition to keeping temperatures lower, may help maintain floc by inhibiting settling and compaction; settling rates for floc-like material approach groundwater upwelling velocities observed in lake and stream sediments (Maggi 2013; Briggs et al. 2014).

In the SEM, catchment slope had minor predictive value for floc thickness, indirectly and directly. Slope indirectly affected floc thickness by correlation with surface water temperatures, and thus could be a proxy for groundwater inputs and therefore cooler summer temperatures. Most seeps and springs occur where land slopes steeply to the water's edge. Catchment slope also had a positive direct effect, albeit small, on floc thickness. Most studies evaluating catchment predictors of C burial in lakes and reservoirs have observed the opposite relationship, i.e., that catchments with greater slopes had lower sediment C stocks or accumulation rates (Ferland et al. 2012; Mendonça et al. 2017). However, one study focused on C burial found a positive relationship with slope, though this seemed to be a result of increased soil erosion from agricultural land (Kastowski et al. 2011), which is not common in this study area. It is worth noting that average catchment slope did not vary much (~1-6 degrees) for the water bodies in this study, so catchment slope may reflect another important predictor in this study that I did not measure.

CONCLUSIONS

Flocculent sediments were abundant in most of the shallow waterbodies I surveyed in southwestern, Michigan, USA. While I cannot say for sure that this is the case for shallow freshwaters in other regions, I suspect that floc sediments can be found in many similar water bodies in low-relief humid landscapes. But because of their loose structure, floc sediments are often incorrectly sampled using core methods developed for relatively consolidated sediments, or simply avoided in sediment surveys. Thus, surveys that incorrectly sample or avoid floc sediments would be biased towards more consolidated sediments.

The physicochemical properties of floc do not seem to differ much from other organic sediments found in freshwaters, with the exception of their relatively high OC concentrations, low bulk densities, and high volumes of occluded gas bubbles. However, these distinctive features may have consequences for the C burial and the exchange of solutes across the SWI, especially given the prevalence of floc sediments in shallow waters. To understand the ecological importance of the floc layers as an SWI, future research should focus on (1) the physical processes that drive the exchange of oxygen and reactive solutes between overlying waters and loosely structure floc layers (Kincaid, Chapter 4), and (2) the consequences these have for biogeochemical processes and rates.

APPENDIX

Table A1.1. Names, descriptions, and locations of waterbodies sampled.

Site name	Site ID(s)	Location notes	Waterbody type	County	Latitude	Longitude	Surveys
37 Street Marsh	37ST, 37M	Headwaters of Three Lakes; just southwest of 37th St	Through-flow wetland	Kalamazoo	42.366649	-85.399167	1, 4,5
Augusta Creek	AC, AC1, AC2	AC1 = upstream of DNR bridge near East C Ave; AC2 = downstream of DNR bridge	Stream	Kalamazoo	42.392858	-85.35587	1,4,5
Brett Bowers' Pond	BBP	Private property off of East C Ave	Pond	Kalamazoo	42.392265	-85.35562	1
Brook Ledge	BL, RAN	Ransom Creek upstream of looking pond on Brook Lodge property	Through-flow wetland	Kalamazoo	42.356068	-85.362961	1,3,5
Butterfield Lake	BL	--	Lake	Kalamazoo	42.36116	-85.410536	2
Butterfield Lake Outflow	BLO	Portion of Gull Creek downstream of Butterfield Lake & upstream of Greer Rd	Stream	Kalamazoo	42.357909	-85.411955	2
Crane's Pond	CP	Private subdivision	Lake	Kalamazoo	42.359724	-85.394015	1,2
Douglas Lake	DL, DLGN, DLV	DLGN = southwest side, groundwater seep; DLV = southwest side, vegetated	Lake	Kalamazoo	42.35638	85.367397	2,4,5
Douglas Lake Outlet	DLO	Near culvert on south side of East EF Avenue	Lake; littoral wetland	Kalamazoo	42.356638	-85.365535	1
Duck Lake	DUCK	--	Lake	Kalamazoo	42.408537	-85.38212	2
Eagle Creek	EC	Upstream of railroad track crossing	Stream	Kalamazoo	42.336658	-85.337165	1,4,5
Fair Lake	FL	Northeast area of lake; off dock of private property	Lake	Barry	42.492258	85.325184	1
Gilkey Lake Outflow	GLO	Outflow from Gilkey Lake off of Letchs Lane	Through-flow wetland	Barry	42.481548	-85.355481	1
Graham Lake	GL	--	Lake	Kalamazoo	42.363662	-85.40143	2

Table A1.1 (cont'd)

Graham Lake Outflow	GLO	Portion of Gull Creek downstream between Graham & Butterfield Lakes	Stream	Kalamazoo	42.363709	-85.406568	2
Kalamazoo River	KR	Riparian groundwater seepage near River Rd	River	Kalamazoo	42.335607	-85.341133	1
Kellogg Forest Pond	KFP, KFPL2, KFPL3	W.K. Kellogg Experimental Forest	Through-flow wetland	Kalamazoo	42.362832	-85.354426	1,3,4,5
Little Long Lake	LLL, LLLV, LLLNV	Mainly southern half of lake; LLLV = vegetated site; LLLNV = non-vegetated site	Lake	Kalamazoo	42.417624	-85.443422	2,5
Loosestrife Fen	LF	LF = non-vegetated site; LFV = vegetated site	Through-flow wetland	Kalamazoo	42.368423	-85.361267	1,3,5
Lower Crooked Lake	LCL	--	Lake	Barry	42.463628	-85.473193	2
Lux Arbor Pond 10	--	Lux Arbor Reserve; southwest side of pond	Pond	Barry	42.470917	-85.461547	1
Lux Arbor Pond 28	--	Lux Arbor Reserve; north of dirt road crossing	Pond	Barry	42.492874	-85.453312	1
LTER Kettle Pond	KP, KET	Kellogg Biological Station LTER main site	Kettle pond	Kalamazoo	42.412995	-85.374143	1,4
Mill Pond	MP	Part of the Gull Creek system near intersection of N 37th St & E G Ave	Pond	Kalamazoo	42.341407	-85.403298	2
Morrow Lake	ML	Mostly upstream of River Oaks County Park	Reservoir	Kalamazoo	42.276457	-85.444555	2
Sheriff's Marsh - W1	SMW1, SM	West side of N 45th Street; groundwater seep south of culvert	Wetland; groundwater seep	Kalamazoo	42.401364	-85.328643	1,3,4,5
Sheriff's Marsh - W2	SMW2	West side of N 45th Street just west of culvert	Wetland	Kalamazoo	42.401364	-85.328643	1

Table A1.1 (cont'd)

Three Lakes, Lower	LTL, L3L	Most work done in through-flow between Middle & Lower Three Lakes	Lake	Kalamazoo	42.354355	-85.426796	2,3,5
Three Lakes, Upper	UTL, UP3	--	Lake	Kalamazoo	42.348608	-85.438807	2,4
Turkey Marsh	TM	North of E Gull Lake Dr across the road from the Kellogg Biological Station main campus	Wetland	Kalamazoo	42.408563	-85.398913	1,2,5
Windmill Pond	WP	Surrounding Windmill Island on Kellogg Biological Station main campus	Pond	Kalamazoo	42.403328	-85.400226	5
Wintergreen Lake	WL, WLN, WLNV	WLN - vegetated site on north side; WLNV - non-vegetated site on north side	Lake	Kalamazoo	42.398767	-85.383592	2,3,4,5
Wintergreen Lake Outlet	WLO	Outflow of Wintergreen Lake in Kellogg Bird Sanctuary just north of drainage culvert	Through-flow wetland	Kalamazoo	42.395713	-85.39117	1,5

* Indicates in which survey or study the waterbody was sampled: 1 = 2014 intact core survey; 2= 2015 floc abundance survey; 3 = 2015 redox oscillation study; 4 = 2015 chlorophyll a intact core survey; 5 = 2016 cotton strip decomposition study

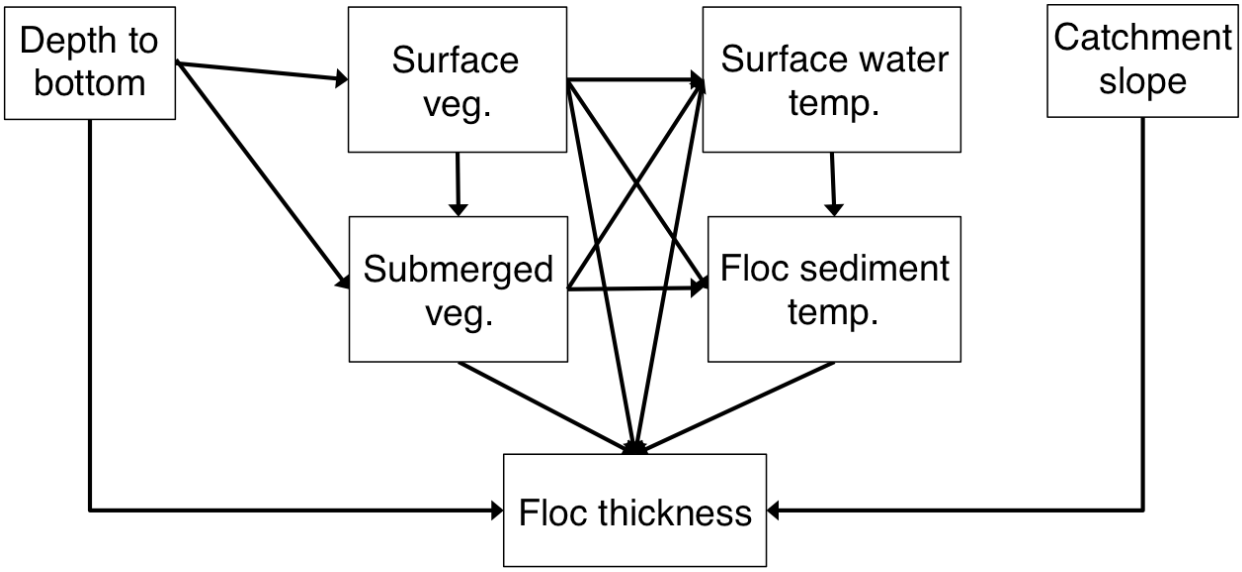

Figure A1.1. Meta-model representing the relationships between waterbody characteristics (depth to bottom, catchment slope), aquatic vegetation cover (surface vegetation and submerged vegetation cover), water and flocculent sediment temperatures, and floc thickness.

LITERATURE CITED

LITERATURE CITED

Abbott BW, Baranov V, Mendoza-Lera C, et al (2016) Using multi-tracer inference to move beyond single-catchment ecohydrology. Earth-Sci Rev 160:19–42. doi: 10.1016/j.earscirev.2016.06.014

Alexander RB, Smith RA, Schwarz GE (2000) Effect of stream channel size on the delivery of nitrogen to the Gulf of Mexico. Nature 403:758–761. doi: 10.1038/35001562

Aminot A, Kirkwood DS, Kérouel R (1997) Determination of ammonia in seawater by the indophenol-blue method: Evaluation of the ICES NUTS I/C 5 questionnaire. Mar Chem 56:59–75. doi: 10.1016/S0304-4203(96)00080-1

Ask J, Karlsson J, Persson L, et al (2009) Terrestrial organic matter and light penetration: Effects on bacterial and primary production in lakes. Limnol Oceangr 54:2034–2040. doi: 10.4319/lo.2009.54.6.2034

Avnimelech Y, Ritvo G, Meijer LE, Kochba M (2001) Water content, organic carbon and dry bulk density in flooded sediments. Aquacult Eng 25:25–33. doi: 10.1016/S0144-8609(01)00068-1

Barko JW, Gunnison D, Carpenter SR (1991) Sediment interactions with submersed macrophyte growth and community dynamics. Aquat Bot 41:41–65. doi: 10.1016/0304-3770(91)90038-7

Barko JW, Smart RM (1986) Sediment-related mechanisms of growth limitation in submersed macrophytes. Ecology 67:1328–1340.

Beaulieu JJ, Tank JL, Hamilton SK, et al (2011) Nitrous oxide emission from denitrification in stream and river networks. PNAS 108:214–219. doi: 10.1073/pnas.1011464108

Berner RA (1980) Early Diagenesis: A Theoretical Approach. Princeton University Press

Bernhardt ES, Blaszczak JR, Ficken CD, et al (2017) Control points in ecosystems: moving beyond the hot spot hot moment concept. Ecosystems 20:665–682. doi: 10.1007/s10021-016-0103-y

Boudot JP, Bel Hadj Brahim A, Steiman R, Seigle-Murandi F (1989) Biodegradation of synthetic organo-metallic complexes of iron and aluminium with selected metal to carbon ratios. Soil Biol Biochem 21:961–966. doi: 10.1016/0038-0717(89)90088-6

Bretz K, Whalen S (2014) Methane cycling dynamics in sediments of Alaskan Arctic Foothill lakes. Inland Waters 4:65–78. doi: 10.5268/IW-4.1.637

Briggs MA, Lautz LK, Buckley SF, Lane JW (2014) Practical limitations on the use of diurnal temperature signals to quantify groundwater upwelling. J Hydrol 519:1739–1751. doi: 10.1016/j.jhydrol.2014.09.030

Buffle J, Leppard GG (1995) Characterization of aquatic colloids and macromolecules. 1. Structure and behavior of colloidal material. Environ Sci Technol 29:2169–2175. doi: 10.1021/es00009a004

Burdige DJ, Komada T (2015) Sediment pore waters. In: Hansell DA, Carlson CA (eds) Biogeochemistry of Marine Dissolved Organic Matter. Elsevier, pp 535–577

Burgin AJ, Yang WH, Hamilton SK, Silver WL (2011) Beyond carbon and nitrogen: how the microbial energy economy couples elemental cycles in diverse ecosystems. Front Ecol Environ 9:44–52. doi: 10.1890/090227

Carlton RG, Wetzel RG (1988) Phosphorus flux from lake sediments: Effect of epipelic algal oxygen production. Limnol Oceangr 33:562–570. doi: 10.4319/lo.1988.33.4.0562

Carpenter SR, Lodge DM (1986) Effects of submersed macrophytes on ecosystem processes. Aquat Bot 26:341–370. doi: 10.1016/0304-3770(86)90031-8

Carr GM, Morin A, Chambers PA (2005) Bacteria and algae in stream periphyton along a nutrient gradient. Freshwater Biol 50:1337–1350. doi: 10.1111/j.1365-2427.2005.01401.x

Chanton JP, Dacey JWH (1991) Effects of vegetation on methane flux, reservoirs, and carbon isotopic composition. In: Sharkey T, Holland E, Mooney H (eds) Trace gas emissions by plants. Academic, New York, pp 65–92

Chanton JP, Martens CS, Kelley CA (1989) Gas transport from methane-saturated, tidal freshwater and wetland sediments. Limnol Oceangr 34:807–819.

Chen M, Hur J (2015) Pre-treatments, characteristics, and biogeochemical dynamics of dissolved organic matter in sediments: A review. Water Res 79:10–25. doi: 10.1016/j.watres.2015.04.018

Cheng FY, Basu NB (2017) Biogeochemical hotspots: role of small water bodies in landscape nutrient processing. Water Resour Res 53:5038–5056. doi: 10.1002/2016WR020102

Corstanje R, Grunwald S, Reddy KR, et al (2006) Assessment of the spatial distribution of soil properties in a northern Everglades marsh. J Environ Qual 35:938. doi: 10.2134/jeq2005.0255

Crawford JT, Stanley EH, Spawn SA, et al (2014) Ebullitive methane emissions from oxygenated wetland streams. Global Change Biol 20:3408–3422. doi: 10.1111/gcb.12614

Cyr H (1998) How does the vertical distribution of chlorophyll vary in littoral sediments of small lakes? Freshwater Biol 40:25–40. doi: 10.1046/j.1365-2427.1998.00319.x

Cyr H, Morton KE (2006) Distribution of biofilm exopolymeric substances in littoral sediments of Canadian Shield lakes: the effects of light and substrate. Can J Fish Aquat Sci 63:1763–1776. doi: 10.1139/f06-079

D'Angelo EM, Reddy KR (1994) Diagenesis of organic matter in a wetland receiving hypereutrophic lake water: I. Distribution of dissolved nutrients in the soil and water column. J Environ Qual 23:928–936.

de Winder B, Staats N, Stal LJ, Paterson DM (1999) Carbohydrate secretion by phototrophic communities in tidal sediments. Journal of Sea Research 42:131–146. doi: 10.1016/S1385-1101(99)00021-0

Dean WE (1974) Determination of carbonate and organic matter in calcareous sediments and sedimentary rocks by loss on ignition: comparison with other methods. J Sediment Res 44:242–248. doi: 10.1306/74D729D2-2B21-11D7-8648000102C1865D

Dean WE, Gorham E (1998) Magnitude and significance of carbon burial in lakes, reservoirs, and peatlands. Geol 26:535–538. doi: 10.1130/0091-7613(1998)026<0535:MASOCB>2.3.CO;2

Decho AW (1990) Microbial exopolymer secretions in ocean environments: their role(s) in food webs and marine processes. Oceanogr Mar Biol Annu Rev 28:75–153.

Downing J (2010) Emerging global role of small lakes and ponds: little things mean a lot. Limnetica 29:9–24.

Downing JA, Cole JJ, Middelburg JJ, et al (2008) Sediment organic carbon burial in agriculturally eutrophic impoundments over the last century. Global Biogeochem Cycles. doi: 10.1029/2006GB002854

Droppo IG, Leppard GG, Flannigan DT, Liss SN (1997) The freshwater floc: a functional relationship of water and inorganic floc constituents affecting suspended sediment properties. Water Air Soil Pollut 99:43–54. doi: 10.1023/A:1018359726978

Elliott AVC, Warren LA (2014) Microbial engineering of floc Fe and trace element geochemistry in a circumneutral, remote lake. Environ Sci Technol 48:6578–6587. doi: 10.1021/es403754t

Ferland M-E, del Giorgio PA, Teodoru CR, Prairie YT (2012) Long-term C accumulation and total C stocks in boreal lakes in northern Québec. Global Biogeochem Cycles. doi: 10.1029/2011GB004241

Flury S, Glud RN, Premke K, McGinnis DF (2015) Effect of sediment gas voids and ebullition on benthic solute exchange. Environ Sci Technol 49:10413–10420. doi: 10.1021/acs.est.5b01967

Fortino K, Whalen SC, Smoak JM (2016) Patterns in the percent sediment organic matter of arctic lakes. Hydrobiologia 777:149–160. doi: 10.1007/s10750-016-2771-1

Gardner WS, McCarthy MJ, Carini SA, et al (2009) Collection of intact sediment cores with overlying water to study nitrogen- and oxygen-dynamics in regions with seasonal hypoxia. Cont Shelf Res 29:2207–2213. doi: 10.1016/j.csr.2009.08.012

Gerbersdorf SU, Jancke T, Westrich B, Paterson DM (2008) Microbial stabilization of riverine sediments by extracellular polymeric substances. Geobiology 6:57–69. doi: 10.1111/j.1472-4669.2007.00120.x

Gerbersdorf SU, Westrich B, Paterson DM (2009) Microbial extracellular polymeric substances (EPS) in fresh water sediments. Microb Ecol 58:334–349. doi: 10.1007/s00248-009-9498-8

Gerbersdorf SU, Wieprecht S (2015) Biostabilization of cohesive sediments: revisiting the role of abiotic conditions, physiology and diversity of microbes, polymeric secretion, and biofilm architecture. Geobiology 13:68–97. doi: 10.1111/gbi.12115

Godshalk GL, Barko JW (1985) Vegetative succession and decomposition in reservoirs. In: Gunnison D (ed) Microbial Processes in Reservoirs. Springer Netherlands, Dordrecht, pp 59–77

Godshalk GL, Wetzel RG (1978) Decomposition of aquatic angiosperms. II. Particulate components. Aquat Bot 5:301–327. doi: 10.1016/0304-3770(78)90074-8

Golterman HL (2004) The chemistry of phosphate and nitrogen compounds in sediments. Kluwer Academic Publishers, Dordrecht

Golterman HL, Clymo RS (1969) Methods for Chemical Analysis of Fresh Waters. Blackwell, Oxford

Gosselink JG, Hatton R, Hopkinson CS (1984) Relationship of organic carbon and mineral content to bulk density in Louisiana marsh soils. Soil Science 137:177–180.

Grabowski RC, Droppo IG, Wharton G (2011a) Erodibility of cohesive sediment: The importance of sediment properties. Earth-Sci Rev 105:101–120. doi: 10.1016/j.earscirev.2011.01.008

Grabowski RC, Droppo IG, Wharton G (2011b) Erodibility of cohesive sediment: The importance of sediment properties. Earth-Sci Rev 105:101–120. doi: 10.1016/j.earscirev.2011.01.008

Grannemann NG, Hunt RJ, Nicholas JR, et al (2000) The importance of ground water in the Great Lakes Region. USGS Water-Resources Investigations Report 00–4008. U.S. Geological Survey, Lansing, MI, USA

Grimm NB, Fisher SG (1984) Exchange between interstitial and surface water: Implications for stream metabolism and nutrient cycling. Hydrobiologia 111:219–228. doi: 10.1007/BF00007202

Hamilton SK (2015) Water quality and movement in agricultural landscapes. In: Hamilton SK, Doll JE, Robertson GP (eds) The Ecology of Agricultural Lanscapes: Long-Term Research on the Path to Sustainability. Oxford University Press, New York, New York, USA, pp 275–309

Hansen K (1959) Sediments from Danish lakes. J Sediment Res 29:38–46. doi: 10.1306/74D70876-2B21-11D7-8648000102C1865D

Harper MA (1969) Movement and migration of diatoms on sand grains. Br Phycol J 4:97–103. doi: 10.1080/00071616900650081

Harris D, Horwáth WR, van Kessel C (2001) Acid fumigation of soils to remove carbonates prior to total organic carbon or CARBON-13 isotopic analysis. Soil Sci Soc Am J 65:1853–4. doi: 10.2136/sssaj2001.1853

Harrison JA, Maranger RJ, Alexander RB, et al (2009) The regional and global significance of nitrogen removal in lakes and reservoirs. Biogeochemistry 93:143–157. doi: 10.1007/s10533-008-9272-x

Harrison XA (2014) Using observation-level random effects to model overdispersion in count data in ecology and evolution. PeerJ 2:e616. doi: 10.7717/peerj.616

Harrison XA (2015) A comparison of observation-level random effect and Beta-Binomial models for modelling overdispersion in Binomial data in ecology & evolution. PeerJ 3:e1114. doi: 10.7717/peerj.1114

Håkanson L, Jansson M (1983) Principles of Lake Sedimentology. Springer Berlin Heidelberg, Berlin, Heidelberg

Helton AM, Poole GC, Meyer JL, et al (2011) Thinking outside the channel: modeling nitrogen cycling in networked river ecosystems. Front Ecol Environ 9:229–238. doi: 10.1890/080211

Hou LJ, Liu M, Jiang HY, et al (2003) Ammonium adsorption by tidal flat surface sediments from the Yangtze Estuary. Environ Geol 45:72–78. doi: 10.1007/s00254-003-0858-2

Ioffe BV, Vitenberg AG (1984) Head-Space Analysis and Related Methods in Gas Chromatography. Wiley, New York

Jaeger B (2017) r2glmm: Computes R squared for mixed (multilevel) models. R package version 0.1.2. Retrieved from: https://CRAN.R-project.org/package=r2glmm

Jellali S, Diamantopoulos E, Kallali H, et al (2010) Dynamic sorption of ammonium by sandy soil in fixed bed columns: Evaluation of equilibrium and non-equilibrium transport processes. J Environ Manage 91:897–905. doi: 10.1016/j.jenvman.2009.11.006

Jensen HS, Kristensen P, Jeppesen E, Skytthe A (1992) Iron:phosphorus ratio in surface sediment as an indicator of phosphate release from aerobic sediments in shallow lakes. Hydrobiologia 235-236:731–743. doi: 10.1007/BF00026261

Kamp-Nielsen L (1975) A kinetic approach to the aerobic sediment-water exchange of phosphorus in Lake Esrom. Ecological Modelling 1:153–160. doi: 10.1016/0304-3800(75)90030-7

Kastowski M, Hinderer M, Vecsei A (2011) Long-term carbon burial in European lakes: Analysis and estimate. Global Biogeochem Cycles. doi: 10.1029/2010GB003874

Keil RG, Montluçon DB, Prahl FG, Hedges JI (1994) Sorptive preservation of labile organic matter in marine sediments. Nature 370:549–552. doi: 10.1038/370549a0

Kinsman-Costello LE, O'Brien JM, Hamilton SK (2015) Natural stressors in uncontaminated sediments of shallow freshwaters: The prevalence of sulfide, ammonia, and reduced iron. Environ Toxicol Chem 34:467–479. doi: 10.1002/etc.2801

Kiorboe T (1980) Distribution and production of submerged macrophytes in Tipper Grund (Ringkobing Fjord, Denmark), and the impact of waterfowl grazing. J Appl Ecol 17:675–687.

Kuehn KA, Francoeur SN, Findlay RH, Neely RK (2014) Priming in the microbial landscape: periphytic algal stimulation of litter-associated microbial decomposers. Ecology 95:749–762. doi: 10.1890/13-0430.1

Kłosowski S, Jabłońska E, Szańkowski M (2011) Aquatic vegetation as an indicator of littoral habitats and various stages of lake aging in north-eastern Poland. Ann Limnol - Int J Lim 47:281–295. doi: 10.1051/limn/2011008

Lalonde K, Mucci A, Ouellet A, Gélinas Y (2012) Preservation of organic matter in sediments promoted by iron. Nature 483:198–200. doi: 10.1038/nature10855

Lamers LPM, Govers LL, Janssen ICJM, et al (2013) Sulfide as a soil phytotoxin—a review. Front Plant Sci 4:1–14. doi: 10.3389/fpls.2013.00268

Lamers LPM, van Diggelen JMH, Op den Camp HJM, et al (2012) Microbial transformations of nitrogen, sulfur, and iron dictate vegetation composition in wetlands: a review. Front Microbio 3:1–12. doi: 10.3389/fmicb.2012.00156

Lefcheck JS (2016) piecewiseSEM: Piecewise structural equation modelling in R for ecology, evolution, and systematics. Methods Ecol Evol 7:573–579. doi: 10.1111/2041-210X.12512

Lerman A (1979) Geochemical Processes: Water and Sediment Environments. Wiley, New York

Liss SN, Droppo IG, Flannigan DT, Leppard GG (1996) Floc Architecture in Wastewater and Natural Riverine Systems. Environ Sci Technol 30:680–686. doi: 10.1021/es950426r

Lovley DR, Phillips EJP (1987) Rapid assay for microbially reducible ferric iron in aquatic sediments. Appl Environ Microbiol 53:1536–1540.

Löfgren S, Boström B (1989) Interstitial water concentrations of phosphorus, iron and manganese in a shallow, eutrophic swedish lake—Implications for phosphorus cycling. Water Res 23:1115–1125. doi: 10.1016/0043-1354(89)90155-3

MacIntyre HL, Geider RJ, Miller DC (1996) Microphytobenthos: The ecological role of the

"secret garden" of unvegetated, shallow-water marine habitats. I. distribution, abundance and primary production. Estuaries 19:186–16. doi: 10.2307/1352224

Maggi F (2013) The settling velocity of mineral, biomineral, and biological particles and aggregates in water. J Geophys Res Oceans 118:2118–2132. doi: 10.1002/jgrc.20086

Martens CS, Chanton JP (1989) Radon as a tracer of biogenic gas equilibration and transport from methane-saturated sediments. J Geophys Res 94:3451–9. doi: 10.1029/JD094iD03p03451

McClain ME, Boyer EW, Dent CL, et al (2003) Biogeochemical hot spots and hot moments at the interface of terrestrial and aquatic ecosystems. Ecosystems 6:301–312. doi: 10.1007/s10021-003-0161-9

Megonigal JP, Hines ME, Visscher PT (2004) Anaerobic metabolism: Linkages to trace gases and aerobic processes. In: Schlesinger WH (ed) Biogeochemistry. Oxford, U.K, pp 317–424

Mendonça R, Müller RA, Clow D, et al (2017) Organic carbon burial in global lakes and reservoirs. Nature Communications 1–6. doi: 10.1038/s41467-017-01789-6

Mortimer CH (1941) The exchange of dissolved substances between mud and water in lakes. J Ecol 29:280–329.

Murphy J, Riley JP (1962) A modified single solution method for the determination of phosphate in natural waters. Analytica Chimica Acta 27:31–36. doi: 10.1016/S0003-2670(00)88444-5

Murray RE, Cooksey KE, Priscu JC (1986) Stimulation of bacterial DNA synthesis by algal exudates in attached algal-bacterial consortia. Appl Environ Microbiol 52:1177–1182.

Myrbo A, Swain EB, Engstrom DR, et al (2017) Sulfide generated by sulfate reduction is a primary controller of the occurrence of wild rice (*Zizania palustris*) in shallow aquatic ecosystems. J Geophys Res Biogeosci 122:2736–2753. doi: 10.1002/2017JG003787

Nakagawa S, Schielzeth H (2012) A general and simple method for obtaining R^2 from generalized linear mixed-effects models. Methods Ecol Evol 4:133–142. doi: 10.1111/j.2041-210x.2012.00261.x

O'Brien JM, Hamilton SK, Kinsman-Costello LE, et al (2012) Nitrogen transformations in a through-flow wetland revealed using whole-ecosystem pulsed. Limnol Oceangr 57:221–234. doi: 10.4319/lo.2012.57.1.0221

Plach JM, Elliott AVC, Droppo IG, Warren LA (2011) Physical and ecological controls on freshwater floc trace metal dynamics. Environ Sci Technol 45:2157–2164. doi: 10.1021/es1031745

Plach JM, Lin S, Droppo IG, Warren LA (2014) Iron cycling in a littoral freshwater beach: Implications for floc trace metal dynamics. J Great Lakes Res 40:47–57. doi: 10.1016/j.jglr.2014.01.002

R Core Team (2017) R: A language and environment for statistical computing. Vienna: R Foundation for Statistical Computing. Available online at: https://www.R-project.org/

Raaphorst WV, Malschaert JFP (1996) Ammonium adsorption in superficial North Sea sediments. Cont Shelf Res 16:1415–1435. doi: 10.1016/0278-4343(95)00081-X

Raymond PA, Hartmann J, Lauerwald R, et al (2013) Global carbon dioxide emissions from inland waters. Nature 503:355–359. doi: 10.1038/nature12760

Rier ST, Stevenson RJ (2001) Relation of environmental factors to density of epilithic lotic bacteria in 2 ecoregions. J N Am Benthol Soc 20:520–532. doi: 10.2307/1468085

Round FE, Eaton JW (1966) Persistent, vertical-migration rhythms in benthic microflora: III. The rhythm of epipelic algae in a freshwater pond. J Ecol 54:609–615. doi: 10.2307/2257806

RStudio Team (2017) RStudio: Integrated development for R. Boston, MA: RStudio Inc.

Sand-Jensen K, Sondergaard M (1979) Distribution and quantitative development of aquatic macrophytes in relation to sediment characteristics in oligotrophic Lake Kalgaard, Denmark. Freshwater Biol 9:1–11. doi: 10.1111/j.1365-2427.1979.tb01481.x

Shimanaga M, Shirayama Y (2000) Response of benthic organisms to seasonal change of organic matter deposition in the bathyal Sagami Bay, central Japan. Oceanologica Acta 23:91–107. doi: 10.1016/S0399-1784(00)00103-1

Shipley B (2009) Confirmatory path analysis in a generalized multilevel context. Ecology 90:363–368. doi: 10.1890/08-1034.1

Shipley B (2013) The AIC model selection method applied to path analytic models compared using a d-separation test. Ecology 94:560–564. doi: 10.1890/12-0976.1

Smith SV, Renwick WH, Bartley JD, Buddemeier RW (2002) Distribution and significance of small, artificial water bodies across the United States landscape. Sci Total Environ 299:21–36. doi: 10.1016/S0048-9697(02)00222-X

Spears BM, Carvalho L, Perkins R, et al (2010) The contribution of epipelon to total sediment microalgae in a shallow temperate eutrophic loch (Loch Leven, Scotland). Hydrobiologia 646:281–293. doi: 10.1007/s10750-010-0187-x

Spears BM, Carvalho L, Perkins R, et al (2006) Spatial and historical variation in sediment phosphorus fractions and mobility in a large shallow lake. Water Res 40:383–391. doi: 10.1016/j.watres.2005.11.013

Stookey LL (1970) Ferrozine: a new spectrophotometric reagent for iron. Anal Chem 42:779–781. doi: 10.1021/ac60289a016

Thobaben ET, Hamilton SK (2014) The relative importance of groundwater and its ecological implications in diverse glacial wetlands. Am Midl Nat 172:205–218. doi: 10.1674/0003-

0031-172.2.205

Tranvik LJ, Downing JA, Cotner JB, et al (2009) Lakes and reservoirs as regulators of carbon cycling and climate. Limnol Oceangr 54:2298–2314. doi: 10.4319/lo.2009.54.6_part_2.2298

Underwood G, Kromkamp J (1999) Primary production by phytoplankton and microphytobenthos in estuaries. Adv Ecol Res 29:93–153.

Underwood GJC, Paterson DM (2003) The importance of extracellular carbohydrate production by marine epipelic diatoms. Adv Bot Res 40:183–240. doi: 10.1016/S0065-2296(05)40005-1

van Wijck C, de Groot C-J, Grillas P (1992) The effect of anaerobic sediment on the growth of *Potamogeton pectinatus* L.: the role of organic matter, sulphide and ferrous iron. Aquat Bot 44:31–49. doi: 10.1016/0304-3770(92)90079-X

Wasmund N (1984) Production and distribution of the microphytobenthos in the sediment of Lake Mikolajskie. Internat Rev Hydrobiol 69:215–229. doi: 10.1002/iroh.19840690210

Wetzel RG (2001) Limnology: Lake and River Ecosystems, 3rd edn. Academic Press, San Diego

Wetzel RG (1992) Gradient-dominated ecosystems: sources and regulatory functions of dissolved organic matter in freshwater ecosystems. Hydrobiologia 229:181–198. doi: 10.1007/BF00007000

Whalen SC, Lofton DD, McGowan GE, Strohm A (2013) Microphytobenthos in shallow arctic lakes: fine-scale depth distribution of chlorophyll a, radiocarbon assimilation, irradiance, and dissolved O_2. Arct Antarct Alp Res 45:285–295. doi: 10.1657/1938-4246-45.2.285

Zhang L, Wang S, Jiao L, et al (2015) Effects of organic matter content and composition on ammonium adsorption in lake sediments. Environ Sci Pollut Res 23:6179–6187. doi: 10.1007/s11356-015-5820-9

CHAPTER 2

DECOMPOSITION IN FLOCCULENT SEDIMENTS OF SHALLOW FRESHWATERS

ABSTRACT

Shallow waterbodies are abundant in many landscapes across the globe and are increasingly acknowledged for their role in freshwater carbon (C) cycling. In these ecosystems, the fate of C is largely determined by sediment processes, which have received much less attention in shallow freshwaters than deeper freshwater and marine settings. In this study I investigated rates of organic matter decomposition in a rarely investigated, but common sediment type—flocculent organic sediment—and how temperature and other environmental factors affect decomposition rates. I then compared the results to those reported for other freshwater settings. In spite of the high accumulation of organic matter, decomposition rates in floc sediments were on average 1.7 times greater than rates measured in oxic overlying waters, and were generally only eclipsed by temperature-adjusted rates reported in streams, which are well oxygenated, flowing environments. Rates were positively correlated with sediment porewater concentrations of soluble reactive phosphorus and dissolved iron, and negatively correlated with ammonium. Warmer temperatures also resulted in increased decomposition rates, and the temperature sensitivity results suggest that rates of decomposition in flocculent sediments could increase 12-56% with a 1-4°C increase in water temperatures, a range of increase likely for this region in the next 100 years if climate change continues at the current pace.

INTRODUCTION

Analyses of global carbon (C) budgets suggest that freshwaters store significant amounts of organic carbon (OC) in their sediments (Cole et al. 2007; Tranvik et al. 2009; Battin et al. 2009). Interestingly, subsequent studies have demonstrated that the greatest areal rates of OC burial tend to occur in small lakes, reservoirs, and ponds (Kortelainen et al. 2004; Downing et al. 2008; Brainard and Fairchild 2012; Ferland et al. 2012). In these systems inputs of allochthonous and autochthonous OC are high, settling times in oxygenated water columns are short, and sediment resuspension is limited or only occurs episodically, especially in small, wind-protected waterbodies (Ferland et al. 2012; Ferland et al. 2014). Consequently, sediment processes play a large role in determining the fate of OC (i.e., burial vs. mineralization) in freshwaters; however, these process have received much less attention in freshwater sediments than in marine sediments (Burdige 2007; Sobek et al. 2011), especially in shallow waterbodies (Downing 2010).

Decomposition in sediments is regulated by a few main interacting factors including the physicochemical environment (particularly temperature and the availability of terminal electron acceptors such as oxygen, nitrate, manganese, iron, and sulfate), the quantity and quality of OC, and the activity of microbes and detritivorous invertebrates (Fenchel et al. 2012). In fine sediments, including organic sediments, oxygen is often depleted within the first few millimeters of the sediment layer versus several cm in sandy sediments (Glud 2008; Sobek et al. 2009). Thus, decomposition beneath the surface of organic sediments likely occurs with limited oxygen, potentially reducing rates relative to more oxygenated environments. Also, anoxic sediment porewaters tend to accumulate inorganic nutrients (e.g., ammonium and phosphorus) (Wetzel 2001) and potentially toxic substances (e.g., ammonia and dissolved sulfide and iron) (Kinsman-Costello et al. 2015), though their effect on decomposition depends on conditions that vary

among sediments. For example, in the absence of C limitation, decomposition is often constrained by the relative availability of N and P (i.e., N:P ratio) in organic matter and in the environment (Güsewell and Gessner 2009), which depend on differing production, removal, and adsorption processes for N and P in sediments. Further, while very high concentrations of sulfide or ammonium can inhibit the activity of decomposers, levels of inhibition depend on factors including environmental conditions (temperature and pH) and the community composition of decomposers (e.g., some organisms are more tolerant of these substances than others) (Chen et al. 2008).

Environmental conditions characteristic of sediments underlying shallow water columns may modulate these key factors and thereby influence decomposition rates. For example, shallow-water sediments tend to receive more light and experience greater temperatures than sediments in deeper waters, at least seasonally. Light availability promotes the growth of algae and cyanobacteria in the upper layers of the sediment. These organisms influence decomposition by generating diel oscillations of oxygen and dissolved inorganic carbon concentrations via photosynthesis and respiration, affecting redox potential and pH in the sediment (Revsbech et al. 1988; Fenchel et al. 2012), and by releasing organic substrates, thereby stimulating microbial catabolism and nutrient mineralization (Wetzel 2001; Fenchel et al. 2012; Rier et al. 2014; Kuehn et al. 2014). Warmer temperatures also promote metabolic activity, which often results in greater rates of sediment decomposition in shallow waters relative to sediments in colder waters (Gudasz et al. 2010; Gudasz et al. 2015).

In this study, I examine decomposition rates and their controls in an understudied organic sediment commonly found in shallow freshwaters—flocculent (hereafter called floc) sediment. In shallow waterbodies that are continuously inundated, floc sediments—loosely consolidated

organic deposits with dry bulk densities frequently <0.1 g cm^{-3} and water contents frequently >90% (Kincaid, Chapter 1)—often occur as thick layers. In a recent survey of shallow lakes, wetlands, and the margins of streams in southwestern Michigan, floc accumulations ranged from 0.01 to >2 meters in thickness and were found in a wide variety of semi- to permanently inundated habitats with productive aquatic and/or riparian vegetation and a lack of strong current or wave action (Kincaid, Chapter 1). These habitats include, but are not limited to, the littoral zones of lakes, small reservoirs, persistently inundated wetlands, stream outlets in lakes, depositional zones in flowing systems, and groundwater seeps. Despite the common occurrence of floc in a diversity of shallow waterbodies, little is known about how these sediments influence ecosystem processes, including decomposition and nutrient cycling. I begin addressing this knowledge gap by quantifying rates of decomposition in floc for three seasons and examining how physicochemical conditions in floc accumulations affect these rates.

The primary objective of this study was to understand how decomposition rates in floc accumulations compare to those reported for other freshwater settings. To accomplish this, I quantified decomposition rates by deploying a standardized substrate—cotton strips—within and above the floc layer during three seasons. The cotton strip assay has been used in a variety of freshwater ecosystems and habitats, and thus I was able to compare the rates I measured to those reported in the literature for a variety of other freshwater settings (e.g., stream and riparian habitats). I predicted that because floc layers are evidently persistently anoxic—as evidenced by the consistent presence of reduced iron or hydrogen sulfide in floc porewaters and nearly undetectable levels of nitrate (Kincaid, Chapter 1)—decomposition rates in floc would be reduced relative to rates measured in more oxic environments (including the water overlying the

floc sediment surface). This would imply that C turnover times are long in these abundant accumulations, which might explain, in part, why these thick layers accumulate over time.

My second objective was to determine which environmental variables are the best predictors of decomposition rates in floc. To do this, I measured decomposition rates within floc layers across naturally occurring gradients in porewater chemistry. Again I used the cotton strip assay, which allowed us to control for OC quality and assess the effect of site differences on decomposition rates (Harrison et al. 1988). Lastly, to understand how decomposition rates in floc will respond to rising water temperatures, I quantified the apparent temperature sensitivity of this process and compared these values to those predicted by metabolic theory and reported in the literature in other freshwater settings. In spite of the high accumulation of organic matter, I show that decomposition rates in floc sediments are as high or higher than many other freshwater sediments that have been studied, and not much different than the decomposition rates measured on the sediment surfaces of flowing, well-oxygenated streams.

METHODS

Site selection

I measured decomposition rates in thick accumulations (>10 cm) of floc and in the water just above the sediment surface in a variety of shallow (<1 m) freshwater ecosystems. All sites were located in Kalamazoo County, MI, USA and included the littoral zones of lakes, shallow through-flow wetlands, and depositional zones on the margins of stream channels. The sites remain inundated in most or all years, often because they receive groundwater discharge. Most sites were devoid of vegetation, but a few sites had stands of emergent vegetation (*Nuphar advena, Nymphaea odorata, Brasenia schreberi*) or were among low densities of mixed

communities of submerged aquatic vegetation (e.g., *Ceratophyllum demersum*, *Chara* spp., *Myriophyllum* spp., *Potamogeton* spp.).

Cotton strip decomposition assays

I measured decomposition rates by deploying vertical arrays of cotton strips (95% cellulose; Figure 2.1) during three seasons in 2016: late spring (June: 2–22 June), mid-summer (August: 26 July – 5 Aug), and autumn (October: 6–20 Oct). The cotton strip approach is appealing for several reasons. These strips have low nutrient contents and are ~95% cellulose, which is the main detrital polymer in terrestrial ecosystems and is part of the complex material, lignocellulose, that makes up the majority of OC deposited in freshwater habitats (Megonigal et al. 2004). The floc accumulations I chose are located in diverse habitats and the sources and forms of organic material in these accumulations are likely variable among these settings. Thus, the use of standardized cotton strips allows us to control for OC quality and assess the effect of site differences on decomposition rates (Harrison et al. 1988). Further, the cotton strip assay has been employed in a variety of freshwater ecosystems and habitats, which allows me to compare these rates to those measured in other settings.

Figure 2.1. (**A**) Illustration of a cotton strip array in the lab (numbers are depths relative to the floc-water interface when deployed in the field) and (**B**) two replicate arrays deployed in the field.

I standardized the individual cotton strips following the protocol described by (Tiegs et al. 2013a). Briefly, I cut cotton strips (8 x 2 cm) from bolts of Fredrix-brand unprimed 12-oz. heavy-weight cotton fabric, Style #548 (Fredrix, Lawrenceville, GA, USA). I then created vertical arrays by attaching seven strips to frames made of galvanized steel using thin cable binders (2.3 mm in width; Figure 2.1A). At each site I slowly inserted two vertical arrays into the floc layer, leaving the top cotton strip above the floc layer, but still underwater (Figure 2.1B). The distances from the floc-water interface to the middle of each cotton strip were 1.4 cm above and -1.4, -4.3, -7.1, -9.9, -12.8, and -15.6 cm below the interface. During the August deployment, the upper cotton strips at a few sites were buried in floc during an intense storm event. At those sites, all strips were located in the floc layer and depths were adjusted so the bottom strip was

located at -18.4 cm below the floc-water interface. At the end of the deployment, I carefully removed the arrays from the floc, rinsed them gently with deionized water, and soaked the arrays in 80% ethanol for approximately 30 seconds to arrest microbial activity. After disassembling the arrays, I dried the cotton strips at 40°C for 24 hours.

Tensile strength loss determination

I estimated decomposition rates using tensile strength losses (TSL) (Tiegs et al. 2013a). I measured tensile strengths on each cotton strip after deployment in the field using a tensiometer (Mark-10 brand, Model #MG100, Copiague, NY, USA) at a fixed rate of 2 cm min^{-1}. I determined initial tensile strengths on a set of control strips that were not deployed in the field, but were rinsed and dried like the deployed strips. I then expressed TSL on the deployed strips as percent of the initial tensile strength of control strips lost per day of deployment (TSL day^{-1}, hereafter referred to as non-adjusted TSL rates). This linear model describes TSL through time more accurately than the exponential model typically used in leaf decomposition studies (Tiegs et al. 2013a). To evaluate differences in TSL not due to temperature, I also calculated temperate-adjusted loss rates (per degree day; TSL $degday^{-1}$, hereafter referred to as temperate-adjusted TSL rates) by replacing time (days) with cumulative daily mean temperature (i.e., degree days) (Woodward et al. 2012; Tiegs et al. 2013a; Griffiths and Tiegs 2016).

Temperature measurements and water chemistry

During each deployment, I measured water temperature within and above the floc layer over time using Thermocron iButton® temperature loggers (models 1912H and 1922L, Maxim Integrated, San Jose, CA), recording water temperatures hourly at 2 cm above and -2 and -15 cm

below the floc-water interface. I calculated daily means at each of these depths. I estimated daily mean temperatures for strips located at depths without thermal loggers (i.e., -4.3, -7.1, -9.9, and -12.8 cm) by linearly interpolating daily means between -2 and -15 cm.

I also sampled overlying water and floc porewater at each site once during each deployment, though in August I only sampled the floc porewater. To sample the overlying water, I collected approximately 250 mL of water in a clean bottle and stored it on ice until returning to the laboratory. Once in the laboratory, I filtered the samples through 0.45 μm pore-size Supor polyethersulfone membrane filters (Pall Corp., Port Washington, New York). To sample porewater in the upper 10 cm of the floc layer I carefully inserted a 10 cm long Rhizon sampler (0.15 μm mean pore size; cat. no. 19.21.21, Rhizosphere Research Products, Wageningen, The Netherlands) vertically into the floc layer and slowly extracted 20 mL of porewater using a spring-loaded 30-mL syringe connected to the Rhizon via Tygon PVC tubing. I added subsamples of the filtered porewater into reagents in the field to produce stable colorimetric complexes with dissolved Fe^{2+} and ΣH_2S. The remaining filtered portion stayed cold on ice until return to the laboratory. I stored all filtered samples at 4°C until analysis within 5 days of sample collection.

I measured concentrations of major ions using Dionex membrane-suppression ion chromatography. I measured soluble reactive phosphorus (SRP) concentration colorimetrically using the molybdate blue method and long-path-length spectrophotometry (Murphy and Riley 1962) and dissolved organic carbon (DOC) using the non-purgeable organic carbon (NPOC) method on a Shimadzu carbon analyzer equipped for high-temperature, Pt-catalyzed combustion and gas chromatographic measurement of the resultant CO_2. I measured dissolved Fe^{2+} in porewaters colorimetrically using a ferrozine reaction method modified from (Lovley and

Phillips 1987) and (Stookey 1970), in which I added filtered porewater to a solution of 50 mM 4-(2-hydroxethyl)-1-piperazineethanesulfonic acid buffer containing ferrozine (1 g l^{-1}). I measured ΣH_2S in porewaters using the methylene blue spectrophotometric method (Golterman and Clymo 1969).

Fungal biomass

I estimated fungal biomass as ergosterol content (Newell 1992; Gessner and Newell 2002) on field-deployed cotton strips from a subset of depths from all sites in October. After gently rinsing the cotton strips with deionized water, I collected two disc subsamples (1.1 cm diameter) from strips deployed at 1.4 cm above and -1.4, -7.1, and -15.6 cm below the floc-water interface. I placed both subsamples in 10 mL HPLC-grade methanol and refrigerated them in the dark at 4°C until analyzed. To extract ergosterol, I placed both subsamples in 5 mL methanol and incubated them in a 65°C water bath for 2 hours. I then saponified the samples by adding a solution of 4% KOH in 95% ethanol and heating them for an additional 30 minutes. Pentane was added to partition the ergosterol extracted from the cotton discs, after which I evaporated the sample to dryness with nitrogen gas, and then dissolved the sample again in 0.5 mL HPLC-grade methanol. I quantified ergosterol using Dionex high performance liquid chromatography (Gulis and Suberkropp 2006).

Data analysis

Seasonal differences in decomposition rates—To test for seasonal differences in TSL rates, I first conducted non-parametric Kruskal-Wallis rank sum tests for TSL rates, analyzing the data for overlying water and floc layers independently. Following the rejection of the null hypothesis (α =

0.05), I conducted pairwise comparisons of TSL rates among seasons using two-sided Conover-Iman tests ($\alpha = 0.05/2$). Again, these were done independently for TSL rates measured in the overlying water versus those measured in floc layers. To control the false discovery rate I adjusted *p*-values using the Benjamini-Hochberg procedure (Benjamini and Hochberg 1995).

Differences in and predictors of decomposition rates between overlying water and floc—To test for differences in TSL rates between those measured in the overlying water and those measured within floc layers across all sites for each season, I first conducted a non-parametric Friedman rank sum test to evaluate differences in rates measured at any depth. This test treats each cotton strip on a single vertical array as a repeated measure and thus is a more conservative approach than the traditional non-parametric Kruskal-Wallis test. Following the rejection of a Friedman test ($\alpha = 0.05$) for a season, I compared TSL rates measured in the overlying water to each depth in the floc using Wilcoxon signed rank tests ($\alpha = 0.05$). To control the false discovery rate I adjusted *p*-values using the Benjamini-Hochberg procedure (Benjamini and Hochberg 1995).

I then assessed which environmental variables best explained relative differences in TSL rates measured in the water versus the average of those measured within the floc layer at each site. To do this I first calculated a TSL ratio for each site:

$$TSL\ ratio = \frac{Mean\ TSL_{water}}{Mean\ TSL_{floc}} \quad (1)$$

Non-adjusted and temperature-adjusted TSL ratios correlated positively with the mean of TSL rates measured in the water at each site (TSL day^{-1}: $r = 0.83$, $p < 0.001$; TSL $degday^{-1}$: $r = 0.87$, $p < 0.001$), but not with the mean of rates measured in floc at each site (TSL day^{-1}: $r = -0.06$, $p = 0.75$; TSL $degday^{-1}$: $r = 0.01$, $p = 0.94$) indicating that differences in TSL ratios were largely driven by changes in the magnitude of TSL rates in the overlying water at each site. Given this, I

assessed which water chemistry variables were the best predictors of temperature-adjusted TSL ratios in June and October (I did not collect overlying water samples in August). To do this I fit a generalized least squares (GLS) model starting with temperature-adjusted TSL ratios as a response variable and season and concentrations of SRP, DOC, NH_4-N, NO_3-N, SO_4^{2-}, Mg^{2+}, Ca^{2+}, and Cl^- as covariates. All continuous covariates had Pearson correlation coefficients < 0.7 and I centered each of them at their means and scaled them by their standard deviations.

Differences in fungal biomass on cotton strips in October—To test for differences in ergosterol concentrations on cotton strips in the overlying water versus those on cotton strips deployed in floc layers, I used the same procedure as described previously (i.e., Friedman rank sum tests followed by Wilcoxon signed rank test followed by the Benjamini-Hochberg procedure).

Predictors of decomposition rates in floc—I assessed which floc porewater chemistry variables were the best predictors of temperature-adjusted TSL rates in floc by fitting a linear mixed effects (LME) model. The full model began with temperature-adjusted TSL rates as the response variable, season, depth, and concentrations of floc porewater solutes (SRP, Fe^{2+}, ΣH_2S, DOC, SO_4^{2-}, NH_4^+, and Ca^{2+}) as covariates, and site as a random effect. The inclusion of site as a random effect allowed us to account for between site variation and correlations between rates measured in the same site while assessing the independent variables. Because the cotton strip assay is thought to best approximate average in situ decomposition rates at tensile strength losses of 50% (Harrison et al. 1988), I limited the data to cotton strips with 25-75% TSL. I also excluded rates measured at -18.4 cm in the floc as there were very few of these and they only occurred in August. I did not include floc porewater NO_3^- as a covariate as most of my

measurements were at or below the detection limit. All continuous covariates had correlations < 0.7 and I centered each of them at their means and scaled them by their standard deviations.

Apparent temperature sensitivity of decomposition in the floc—I assessed the apparent temperature sensitivity of TSL rates in floc sediments using the Boltzmann-Arrhenius function derived from metabolic theory (Brown et al. 2004). This function quantifies temperature sensitivity as activation energy (E_a); the greater the value of the E_a, the more sensitive biological activity is to temperature. Because the decomposition of cellulose involves multiple organisms and many biochemical reactions, the E_a of this process actually represents an apparent (i.e., empirical) temperature sensitivity. To quantify E_a, I used the same Boltzmann-Arrhenius function recently used to estimate the temperature sensitivity of leaf litter breakdown in streams (Follstad Shah et al. 2017):

$$\ln r = \ln r_0 - E_a \times (1/k_B T - 1/k_B T_0) \quad (2)$$

where r_0 is a normalization constant, E_a is the apparent activation energy (eV), k_B is the Boltzmann constant (8.62×10^{-5} eV K^{-1}), T is temperature in Kelvin (K), and T_0 is a standard temperature. The final term ($1/k_B T - 1/k_B T_0$) in this equation is the inverse absolute temperature and is used to center the temperature data on a standard temperature (Allen et al. 2005; Yvon-Durocher et al. 2012). I used a standard temperature of 18°C (291.15 K) as this was close to the median daily mean temperature in the floc during the cotton strip array deployments. For these purposes, r represents the non-adjusted TSL rates. I then obtained the value of E_a from the slope of the relationship between the inverse absolute temperature and ln r.

To estimate E_a I used a LME model with non-adjusted TSL rates as the response variable, inverse normalized temperature (eV) as a covariate, and site as a random effect. Once again, I

limited the data to cotton strips with 25-75% TSL. The inclusion of site as a random effect allowed us to account for between site variation and correlations between rates measured in the same site while assessing the independent variables. This particular random intercept model assumes that variability in site characteristics influences non-adjusted TSL rates but not its temperature sensitivity. To test this assumption, I also fit a model with a random intercept (site) and slope (inverse normalized temperature).

Model building and statistical inference—I conducted all statistical analyses in R v.3.4.3 (R Core Team 2017) using RStudio v.1.1.383 (RStudio Team 2017). I fit GLS and LME models using the 'nlme' package (Pinheiro et al. 2017). Model selection for both model types began with the inclusion of all fixed effects (Zuur et al. 2009). I then assessed whether the inclusion of the random site effect improved model fit using likelihood ratio tests. These comparisons included one model with and one model without the random term. I selected the most parsimonious model consisting of significant factors ($\alpha = 0.05$) by sequentially removing one fixed effect and comparing the new reduced model forms to more complex models using Akaike's information criterion (AIC) scores and likelihood ratio (L) tests. When testing for the significance of random effects I fit models using restricted estimated maximum likelihood (REML); when comparing models with different fixed effects I fit models with maximum likelihood (ML). I refit the final, most simple model, with REML to provide the best estimates of standard errors and random effects.

I assessed models for linearity, normality, and homoscedasticity by plotting normalized residuals based on the REML fit against fitted values and predictor variables. I also assessed

goodness of fit using quantile-quantile plots. I report model parameters along with their standard errors (SE).

RESULTS

Seasonal variation in cellulosic decomposition

There were seasonal differences in median TSL rates ($p < 0.05$, Appendix Table A2.1) that generally reflected patterns in seasonal temperatures (Figure 2.2). In August, median non-adjusted rates were more than 4-fold and 2-fold greater than median rates in the coldest season (October) in the overlying water and floc layers, respectively (Figure 2.2B). This pattern held true even when rates were adjusted for temperature (TSL degday^{-1}, Figure 2.2C), though the magnitude of change between the seasons was not as large.

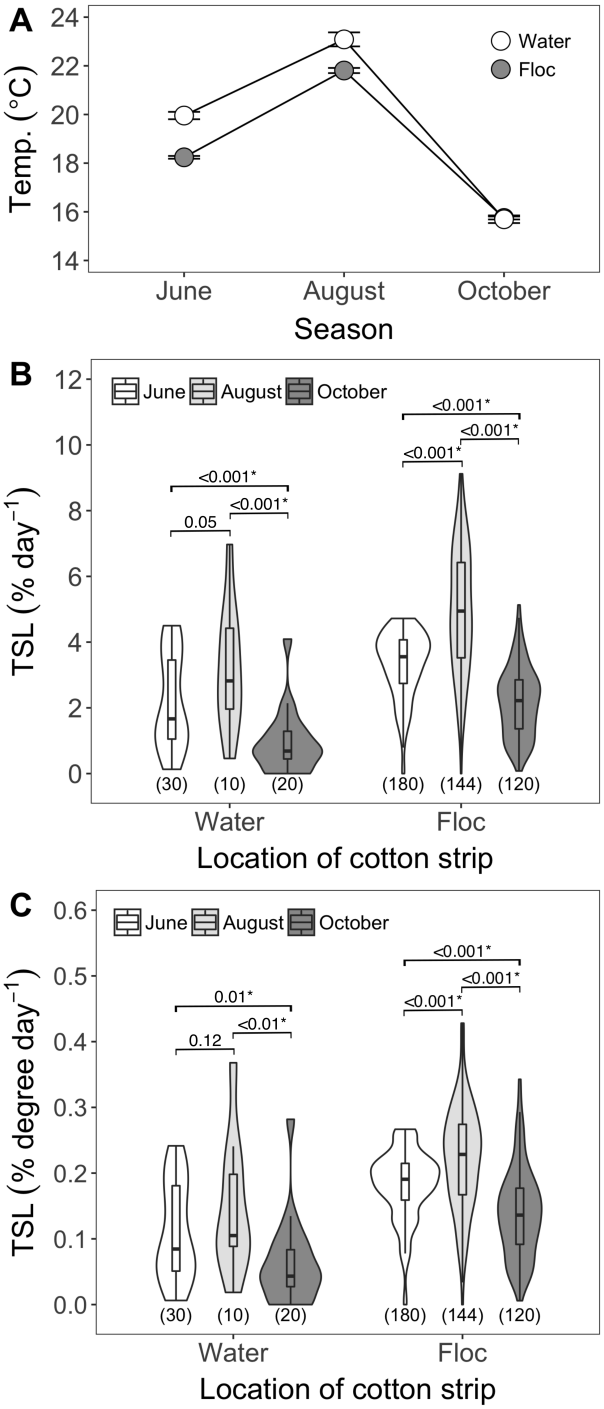

Figure 2.2. (**A**) Mean temperatures, (**B**) non-adjusted tensile strength loss (TSL), and (**C**) temperature-adjusted TSL across all sites for cotton strips in the overlying water and in floc layer. Data used in each plot are site means. Error bars in (**A**) represent ± standard error of the mean. Violin plots in (**B** & **C**) show the density distribution of TSL rates. Boxplots within the violin plots represent the median and interquartile range. Values above brackets in plots (**B** & **C**) are *p*-values for pairwise comparisons; (*) indicates significant *p*-values (Appendix Table A2.1). Values in parentheses in plots (**B** & **C**) are the number of measurements.

Differences in cellulosic decomposition rates between overlying water and the floc layer

Median non-adjusted TSL rates were generally greater in the floc layer than in the overlying water for all seasons (Figure 2.3A), and the difference was significant for floc depths in June ($\chi^2_{(6)} = 27.61$, $p < 0.001$) and October ($\chi^2_{(6)} = 20.20$, $p = 0.002$), but not August ($\chi^2_{(6)} = 6.56$, $p = 0.36$). This pattern remained after adjusting rates for temperature (June: $\chi^2_{(6)} = 41.57$, $p < 0.001$; August: $\chi^2_{(6)} = 9.64$, $p = 0.14$; October: $\chi^2_{(6)} = 20.16$, $p = 0.003$; Figure 2.3B).

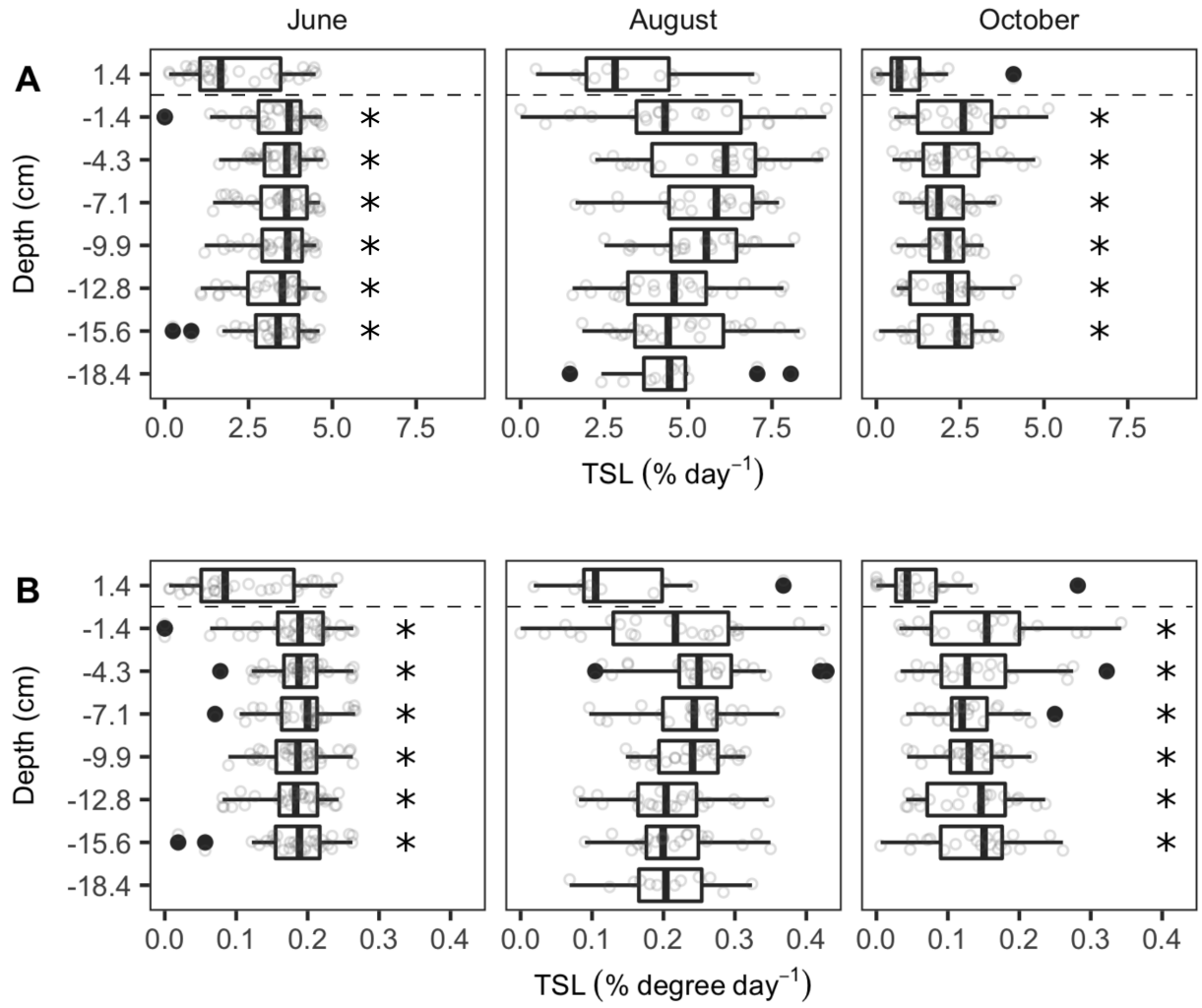

Figure 2.3. (**A**) Non-adjusted tensile strength loss (TSL) and (**B**) temperature-adjusted TSL at each depth above (1.4 cm) and below (-1.4 to -18.4 cm) the floc-water interface (depicted as dashed horizontal line) for all sites. (*) indicates that rates at these depths are significantly different than those above the floc-water interface for that season according to post hoc comparisons (Appendix Table A2.2).

I also assessed the relative differences in TSL rates measured in the overlying water versus those measured in the floc layers at each site (TSL ratio; Figure 2.4). On average, tensile strength losses in the overlying water were 60% (TSL d^{-1}) and 57% (TSL $degday^{-1}$) of those in the floc. The most important water chemistry predictor of temperature-adjusted TSL ratios was the concentration of Ca^{2+} followed by the concentration of Mg^{2+} ($\beta_{Ca} = 0.22 \pm 0.08$, $p = 0.008$; $\beta_{Mg} = -0.14 \pm 0.08$, $p = 0.08$; Model M10 in Appendix Table A2.3), though their effects were in opposite directions. Relative differences between mean temperature-adjusted TSL rates in the overlying water and the floc layer decreased, or rather the temperature-adjusted TSL ratio moved closer to one, as the concentration of Ca^{2+} in the surface water increased.

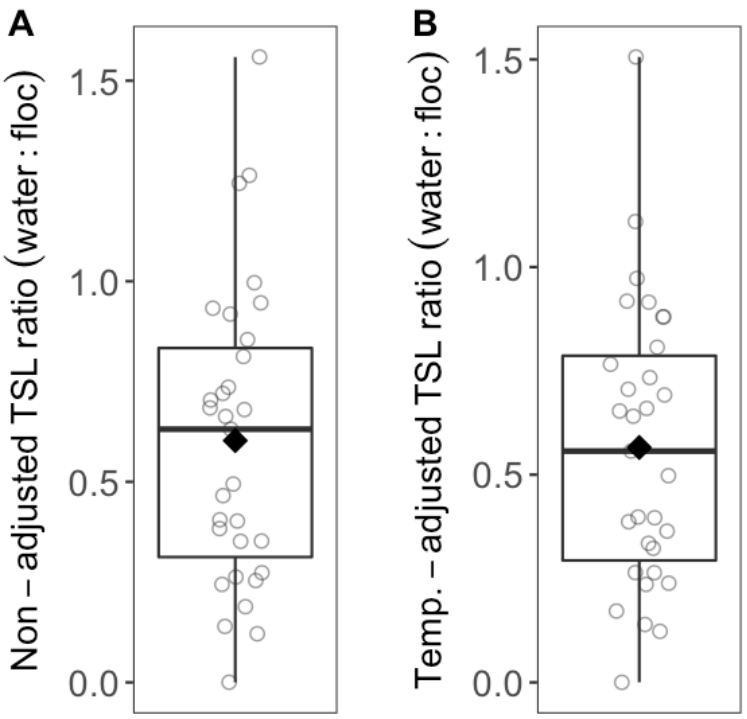

Figure 2.4. The relative difference in tensile strength loss (TSL) rates measured in the water versus those measured in the floc layer at each site. Each ratio is the mean TSL rate measured in the water at that site divided by the mean TSL rate measured in the floc layer. (**A**) includes ratios for non-adjusted TSL rates (% per day) and (**B**) includes ratios for temperature-adjusted TSL rates (% per degree day). Open circles are the ratios at each site and the ◆ is the mean of for all sites and seasons.

Differences in fungal biomass on cotton strips in October

I estimated fungal biomass on cotton strips because the initial decomposition of plant detritus in lakes and wetlands is largely accomplished by fungal assemblages (Komínková et al. 2000; Kuehn et al. 2000; Kuehn 2016). Ergosterol concentrations on all cotton strips were close to the analytical detection limit. Median concentrations across all sites in October were greatest on cotton strips in the overlying water (Figure 2.5), though they were only significantly greater than on cotton strips deployed at -7.1 cm ($\chi^2_{(3)} = 14.64$, $p = 0.002$; Appendix Table A2.4).

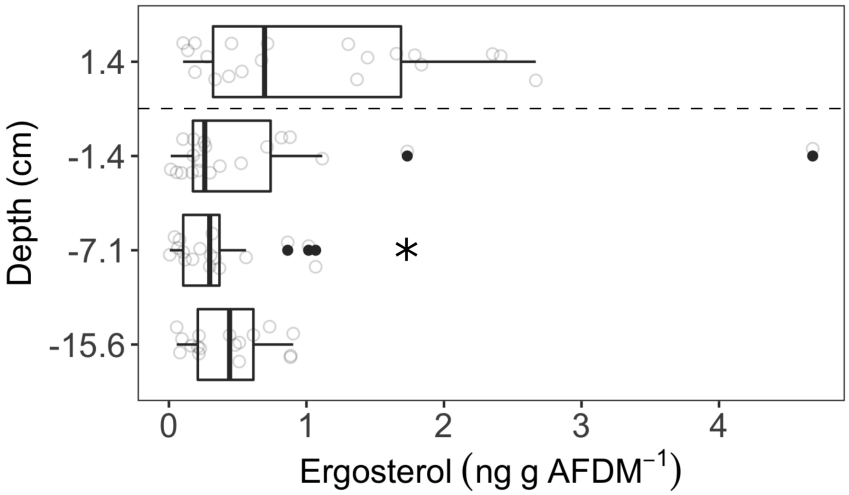

Figure 2.5. Fungal biomass estimated as ergosterol concentrations on cotton strips deployed above (1.4 cm) and below (-1.4, -7.1, and -15.6 cm) the floc-water interface (depicted by dashed horizontal line) for all sites in October. (*) indicates that concentrations at that depth are significantly different than those in the overlying water (1.4 cm) according to post hoc comparisons (Appendix Table A2.4).

Predictors of cellulosic decomposition rates in the floc layer

Floc temperature had a strong positive effect on non-adjusted TSL rates, and when evaluated in isolation, temperature explained nearly half of the variation in these rates (Figure 2.6).

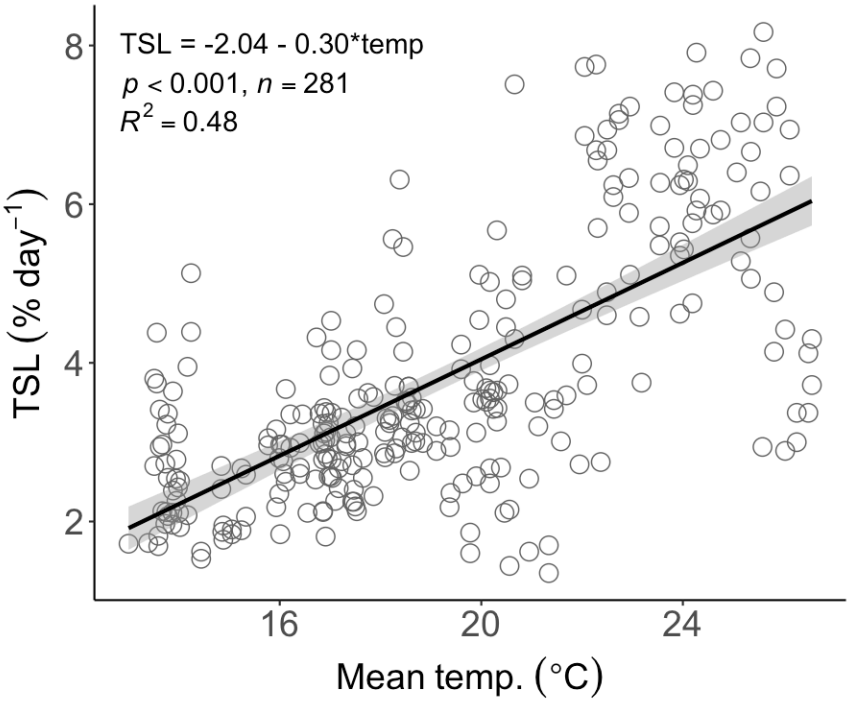

Figure 2.6. Linear relationship between non-adjusted tensile strength loss rates (TSL, % per day) and mean temperature in the floc layers for all seasons and depths. A line of best fit (solid black line) and 95% confidence intervals (gray area) are overlain.

After adjusting TSL rates for temperature, there was still considerable variation in TSL across sites (Figure 2.3B), and thus I assessed which floc porewater chemistry variables were the best predictors of temperature-adjusted TSL rates. The best predictor of temperature-adjusted TSL rates was the concentration of SRP, followed by the concentrations of Fe^{2+} and NH_4^+, though the first two were positively related to TSL degday^{-1} rates and the latter, negatively (β_{SRP} = 0.02 ± 0.005, $p < 0.001$; β_{Fe} = 0.01 ± 0.004, $p = 0.02$; $\beta_{NH4\text{-}N}$ = -0.01 ± 0.005, $p = 0.01$; Model M9 in Appendix Table A2.5).

Apparent temperature sensitivity of cellulosic decomposition in floc

The apparent activation energy (E_a) of decomposition in the upper ~16 cm of floc was 0.82 ± 0.04 eV (95% CI: 0.74-0.89 eV; Figure 2.7A; Model M2 in Appendix Table A2.6). The depth-specific E_a estimates were lowest at -1.4 cm below the floc-water interface and increased with depth in the sediment (Figure 2.7B).

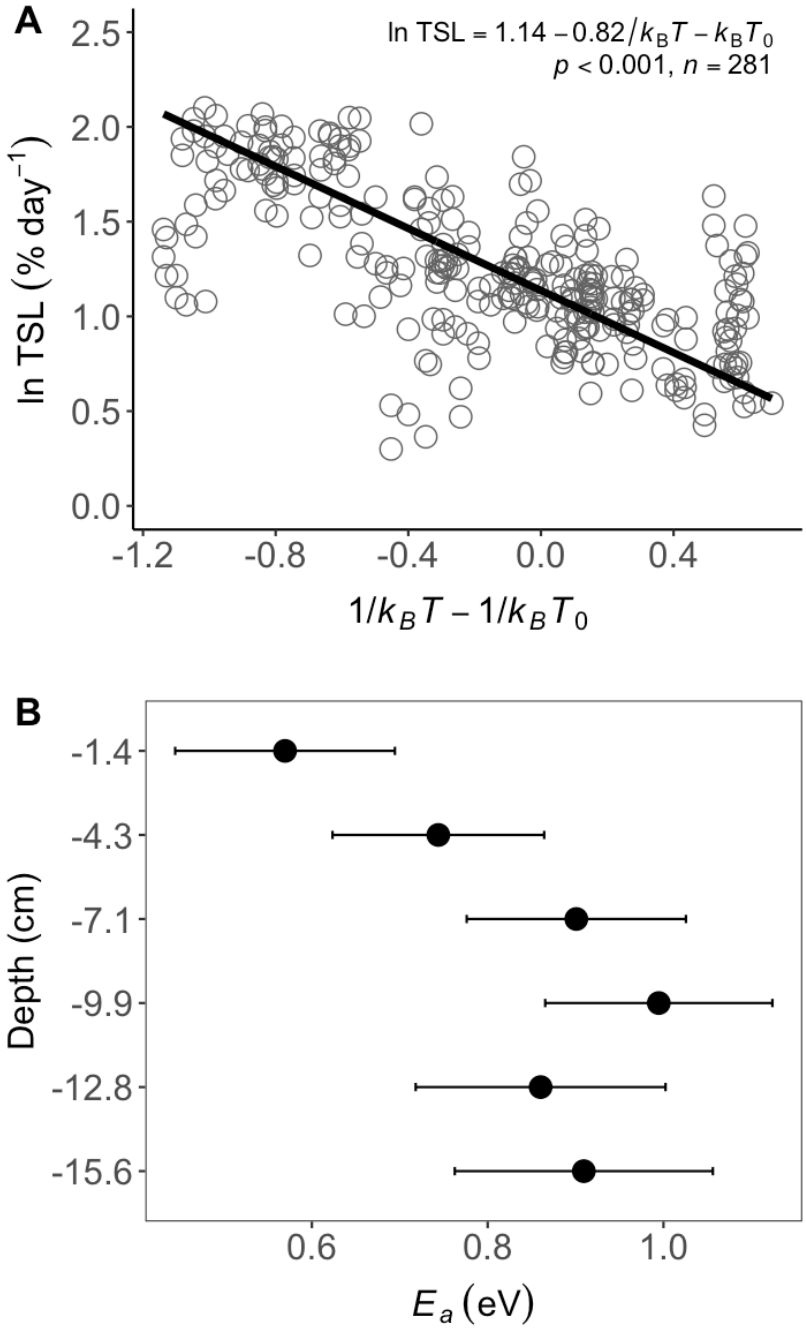

Figure 2.7. (**A**) The apparent activation energy (E_a, eV) of non-adjusted tensile strength loss rates (TSL, % per day) of cotton strips deployed in flocculent sediment. The x-axis is the inverse absolute temperature (T) in Kelvin (K) multiplied by the Boltzmann constant (k_B, 8.62×10^{-5} eV K^{-1}) and normalized by a standard water temperature (T_0), 291.15 K or 18°C. The slope approximates the inverse of E_a. (**B**) The apparent activation energy of TSL at each depth in the floc layer. Bars represent the 95% confidence intervals.

DISCUSSION

Decomposition rates in flocculent sediments

The decomposition rates in floc layers I report here are on the upper end of the range of values reported for streams and riparian zones, which is where most studies using the cotton strip assay have been conducted. In a single coordinated field experiment in >500 streams that measured TSL rates on cotton strips deployed in surface water environments of streams and riparian zones, Tiegs et al. (unpublished data) found mean non-adjusted TSL rates of 3.27 ± 0.15 and 1.48 ± 0.10% in streams and riparian zones, respectively; the mean across all floc depths and seasons in this study was 3.56 ± 0.08%. When adjusted for exposure to different temperatures, the mean TSL rate in floc layers across all seasons (0.18 ± 0.003%) was less than that of stream environments (0.31 ± 0.016%), but nearly equivalent to mean temperature-adjusted TSL rates measured in riparian zones (0.17 ± 0.015%). In summary, decomposition within floc, as measured by temperature-adjusted TSL rates, occurred as quickly as decomposition in surface water riparian environments, but more slowly than decomposition in streams.

Why are decomposition rates greater in floc layers than in overlying water?

Contrary to my prediction, decomposition rates were consistently greater in floc layers than in the overlying water, even when rates were adjusted for exposure to different temperatures. Median TSL rates in the overlying water were significantly lower than median TSL rates measured in most depths in the floc layers in June and October (Figure 2.3). Further, the majority of sites (>90%) had TSL ratios <1 (Figure 2.4), demonstrating that the disparity between rates in the overlying water and the floc layer is common and is not the result of a few anomalous sites or differences in field deployment times. The absence of significant differences

between TSL rates measured in the overlying water and those measured in the floc layer in August (Figure 2.3) could be due to a seasonal homogenization of TSL rates in the overlying water and floc layers, but is more likely an artifact of low replication due to burial of cotton strips in the overlying water by sediment disturbance after a large storm event. Regardless, relative to rates measured in overlying water, decomposition occurred rapidly within the floc layer.

My prediction that decomposition rates would be greatly reduced in floc layers was based on the assumption that decomposition is restricted under anoxic conditions as others have observed (Reddy and Patrick 1975; Godshalk and Wetzel 1978). However, several studies in marine sediments, where the effect of oxygen on organic-matter decomposition has received considerable attention (Burdige 2007), have revealed that the effect of oxygen on the degradation of particulate organic matter in marine sediment depends on the nature of the substrate. In short, fresh, less refractory organic matter is degraded at similar rates regardless of whether oxygen is present, while aged, more refractory organic matter is degraded at greatly reduced rates under anoxic conditions (Kristensen et al. 1995; Hulthe et al. 1998; Kristensen and Holmer 2001). Rates in this study could perhaps be explained because cellulose—the main constituent of cotton strips—is one of the more easily degraded biopolymers (Pérez et al. 2002). Alternatively, studies have demonstrated that exposure to oscillating redox conditions can stimulate overall mineralization of organic matter (Reddy and Patrick 1975; Aller 1994; Aller et al. 1996; Hulthe et al. 1998). Though I did not measure redox potential while the cotton strips were deployed, I have observed redox oscillations in the floc layer potentially associated with diurnal photosynthetic activity, bioturbation, and/or the introduction of oxidants (e.g., oxygen and NO_3^-) into the floc layer following convective mixing events with overlying water (Kincaid, Chapter 4)

that could have stimulated decomposition of cotton strips within the floc. However, the enhanced decomposition rates in the floc compared to overlying water suggest there are other factors besides the availability of oxygen that result in greater rates of decomposition in floc sediments than those rates measured in the overlying water.

Degradation of cellulose requires the production of extracellular enzymes by bacterial and fungal communities (Leschine 1995; Lynd et al. 2002); thus, greater TSL rates in floc relative to overlying water might, in part, be due to a greater abundance of microorganisms in floc, which would aid in rapid colonization and decomposition of cotton strips. Given that fungi are thought to be critically important decomposers of biopolymers like cellulose in soils (Boer et al. 2005) and stream ecosystems (Kuehn 2016), I estimated fungal biomass on cotton strips after retrieving them from the field, but I found that it was low overall on the cotton strips and tended to be greater on cotton strips deployed in the water overlying floc layers than on those deployed within floc layers (Figure 2.5). This may be explained by oxygen limitation, as many fungi are considered obligate aerobes although some can survive and remain active under anoxic conditions, including in lake sediments (Wurzbacher et al. 2010). Further, because fungal biomass is often positively correlated with the size of particulate organic matter in which the fungi dwell (Sinsabaugh et al. 2002), the low biomass of fungi on cotton strips might be due to the small size of average floc aggregates. Regardless, fungal biomass did not explain the greater decomposition rates in floc compared to overlying water.

I did not measure the biomass of bacteria on the cotton strips, and bacteria can play significant roles in degrading OC where they are abundant (Benner et al. 1986; Tanaka 1991). Bacteria are typically more abundant by several orders of magnitude in sediments compared to an equivalent volume of overlying water (Wetzel 2001; Fenchel et al. 2012). Lastly, measuring

extracellular enzyme activities instead of, or in combination with, microbial biomass might be a better indicator of the contribution of microbial activity to the breakdown and mineralization of sediment as extracellular enzymes associated with microbial communities are the proximate drivers of the degradation of biopolymers like cellulose (Chróst 1991; Burns and Dick 2002). However, this would be difficult once cotton strips are removed from the sediments and porewater in which they are deployed, and would only provide potential rates.

As mentioned in the introduction, algal communities may also enhance decomposition rates in floc sediments underlying shallow water columns by altering the pH and redox potential and by releasing organic substrates that stimulate microbial mineralization processes. While I did not measure algal biomass in floc during this study, I have consistently observed algal pigments (i.e., chlorophyll *a*) at varying concentrations >30 cm below the floc-water interface in similar waterbodies (Kincaid, Chapter 1). Thus, future investigations discerning the role of algae in stimulating decomposition processes in floc and sediments in general would improve our understanding of C cycling in shallow waterbodies (Rier et al. 2014; Kuehn et al. 2014).

The relatively low TSL rates measured in the overlying water may have resulted from the suppression of extracellular enzyme activities by organic acids such as polyphenols. Dissolved polyphenols derived from plant litter can complex with extracellular enzymes and inactivate them, thereby decreasing C and nutrient mineralization; however, divalent cations (e.g., Ca^{2+}) can decrease this inhibition by bonding to organic acids, and in turn decrease their capacity to complex with extracellular enzymes (Wetzel 1990; Wetzel 1992). In this study, the mean Ca^{2+} concentration in overlying waters (52.3 mg L^{-1}; range, 20.1-95.5 mg L^{-1}) was approximately half the mean concentration of Ca^{2+} in floc porewaters (106.9 mg L^{-1}; range, 37.3-193.7 mg L^{-1}) and temperature-adjusted TSL ratios moved closer to one as the concentration of Ca^{2+} in the

overlying water increased. This suggests that polyphenols in the dissolved OC pool may have suppressed enzyme activities, and consequently TSL rates, in overlying waters where Ca^{2+} concentrations were too low to inhibit the complexation of organic acids with ecoenzymes. While I did not test this mechanism directly, it warrants further exploration.

Predictors of decomposition in floc layers

Temperature is a fundamental driver of many biological processes, including the metabolism of microorganisms (Yvon-Durocher et al. 2010), and unsurprisingly, it was a good predictor of TSL rates in floc layers. Non-adjusted TSL rates were positively correlated with mean floc temperature (Figure 2.6) and mean rates in both floc layers and overlying water followed patterns in seasonal water temperatures, with the greatest rates occurring in August, the warmest month in this study (Figs. 3A & 4A). The positive relationship between temperature and microbially driven OC decomposition in aquatic ecosystems is well established (Gudasz et al. 2010; Boyero et al. 2011; Follstad Shah et al. 2017), though seasonal variation in sediment degradation rates can also be influenced by other factors like seasonal changes in the sources and quality of OC inputs (Schulz 1995).

The most important predictor of temperature-adjusted TSL rates within floc layers was the concentration of SRP in porewaters; TSL rates increased with increasing SRP concentrations (Appendix Table A2.5). This suggests one of several things: (1) decomposition is limited by phosphorus (P), (2) sites with greater decomposition potential increase SRP availability through mineralization of OC, or (3) SRP co-varies with another predictor of decomposition that I did not measure. Studies manipulating the concentration of P provide evidence in support of P limitation of decomposition in sediments. For example, decomposition or community respiration rates

increased with P enrichment for cotton strips deployed in sediments of an oligotrophic marsh (Newman et al. 2001), white pine (*Pinus strobus*) cellulose incubated in anoxic laboratory incubations of lake sediments (Federle and Vestal 1980), and cellulose sponges deployed in streams in Alaska (Rüegg et al. 2011). Similarly, cotton strips deployed in the sediment of wetland ponds in Alaska decomposed more quickly in ponds with greater surface water SRP concentrations (Vizza et al. 2017). And in similar ponds in Alaska with thick and ubiquitous floc layers, Tiegs et al. (2013b) found that microbial decomposition rates of plant litter increased with increasing P content of the litter. Further, Godshalk and Wetzel (1978) found that litter of two aquatic vascular plant species decomposed faster in the littoral zone of a hypereutrophic lake that was particularly enriched in SRP (Wintergreen Lake, which is one of my study sites) than in a similar habitat in a nearby mesotrophic lake with much lower SRP concentrations, despite stronger reducing conditions in the hypereutrophic lake. These studies together provide evidence for P limitation of OC decomposition in these freshwater sediments.

Though Fe^{2+} concentrations only had about half the predictive power of SRP, temperature-adjusted TSL rates tended to increase with increasing concentrations of Fe^{2+} in floc porewaters. The presence of Fe^{2+} in the floc porewaters may be an indicator of one or two processes that may contribute to enhanced decomposition rates. First, microbial reduction of ferric iron (Fe^{3+}) to Fe^{2+} is an important pathway in the anaerobic degradation of sediment OM, for example in freshwater lakes (Thamdrup 2000; Lovley et al. 2004; Lau et al. 2015) and Arctic peat soils (Lipson et al. 2010). Second, in sediments P is often sorbed as the inorganic phosphate (PO_4^{3-}) ion to inorganic metal oxides, particularly poorly crystalline iron oxides. In the absence of oxygen Fe^{3+} is reduced to Fe^{2+} and Fe-bound P is released to sediment porewaters (Boström et al. 1988). Increased available P, as explained earlier, then enhances decomposition rates.

The negative relationship between temperature-adjusted TSL rates in floc and NH_4^+ concentrations in the floc porewaters may be another indicator that decomposition rates were P limited. The majority of sites had dissolved N:P ratios in the floc porewaters above the Redfield ratio and as this ratio increased temperature-adjusted TSL rates tended to decrease, though the trend was only significant ($p < 0.05$) for June and October when considering all depths together (Figure 2.8). Similarly, Vizza et al. (2017) found that decomposition rates of cotton strips in wetland ponds were negatively related to surface water TN:TP ratios.

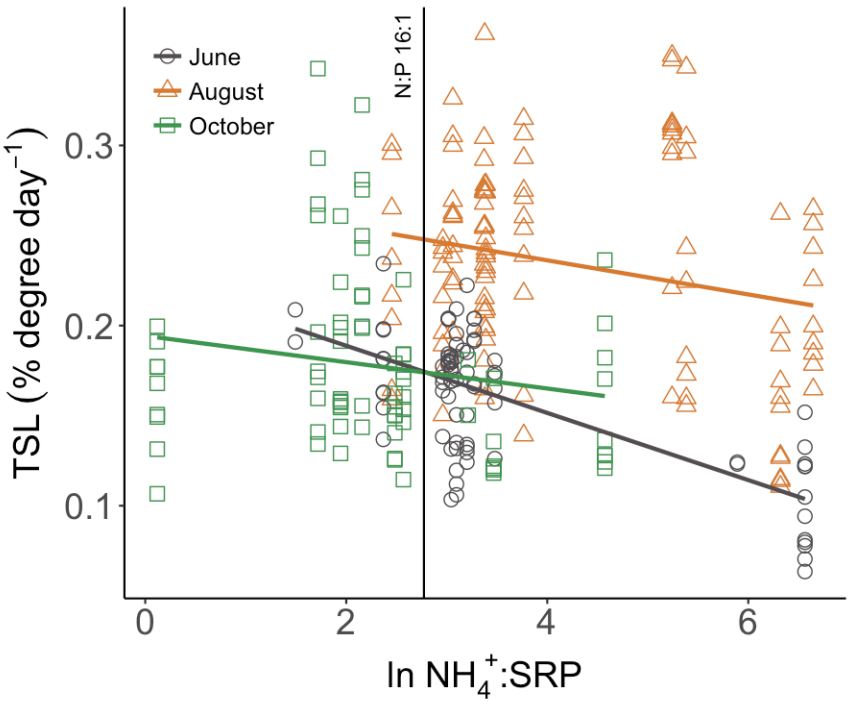

Figure 2.8. Linear relationships for each season between temperature-adjusted tensile strength loss rates (TSL, % per degree day) in floc and the natural log of the molar ratio of NH_4-N to SRP concentrations in the floc porewaters. The data are limited to cotton strips with TSL between 25-75%. Linear regressions were significant ($p < 0.05$) for June and October, but not for August. The vertical line shows the 16:1 molar N:P ratio.

Ammonia inhibition could also have contributed to the negative relationship between temperature-adjusted TSL rates in floc and NH_4^+ concentrations in the floc porewaters. While we

cannot rule this mechanism out conclusively, it is unlikely ammonia toxicity resulted in reduced TSL rates because the maximum concentration of NH_4^+ that I measured in floc porewaters (~21 mg N L^{-1}) was 2-3 orders of magnitude less than inhibitory concentrations reported in the literature (Chen et al. 2008). On a similar note, when I assessed which floc porewater chemistry variables were the best predictors of temperature-adjusted TSL rates, ΣH_2S concentration was a marginally significant negative predictor ($p = 0.08$, Model M7 in Appendix Table A2.5), but again, the maximum concentration of ΣH_2S that I measured in floc porewaters (~160 μM) was 1-2 orders of magnitude less than inhibitory concentrations reported in the literature (Chen et al. 2008). Therefore, ammonia and sulfide likely did not inhibit decomposition rates in floc.

Apparent temperature sensitivity of decomposition in floc

The overall apparent activation energy (E_a) of decomposition rates in floc across all depths, sites, and seasons (0.82 ± 0.04 eV) is considerably greater than predicted for respiration in general and for short-term ecosystem respiration in aquatic systems, both ~0.6 eV (Brown et al. 2004; Allen et al. 2005; Yvon-Durocher et al. 2012). Differences in the temperature dependence of decomposition can be driven by differences in organic matter quality (Bosatta and Ågren 1999; Cornwell et al. 2008; Makkonen et al. 2012; Follstad Shah et al. 2017); however, Tiegs et al. (unpublished data) found that the E_a of TSL for cotton strips deployed in stream and riparian area surface water habitats (~0.6 eV; $n > 500$) was similar to the E_a predicted for respiration of OC in soil and aquatic ecosystems. This similarity suggests that the greater E_a for decomposition of cotton strips in floc is not driven by differences in organic matter quality, but rather, by environmental differences.

While I did not directly examine the environmental factors that contribute to a greater E_a in this study, I suggest they may result from the contribution of anaerobic processes to decomposition. The E_a estimate in the upper cms of the floc layer where oxygen may be present transiently is ~0.6 eV (Figure 2.7B). In deeper layers of the floc layer, where oxygen is unavailable the majority of the time and anaerobic processes dominate, E_a increases and reflects the E_a for methane production in freshwater sediment incubations (0.93 eV) (Yvon-Durocher et al. 2014).

CONCLUSIONS

Shallow waterbodies are abundant in many landscapes across the globe and are increasingly acknowledged for their role in freshwater C cycling. In these ecosystems, the fate of C is largely determined by sediment processes, which have received much less attention than in deeper freshwater and marine settings. My primary goal in this study was to investigate decomposition rates in shallow-water sediments, in this case, flocculent organic sediment, and compare these to rates in other freshwater settings where the cotton strip assay has been deployed.

Contrary to my expectation, decomposition rates in floc sediments measured in this study were on average 1.7 times greater than rates measured in overlying waters, and were generally only eclipsed by temperature-adjusted rates reported in streams, which are generally flowing and well oxygenated. This result does agree with some studies, particularly in marine sediments, that demonstrate that decomposition under anoxic conditions is not always retarded relative to oxic environments. Further, it does not seem that slow decomposition explains the apparently high OC accumulation rates that produce thick layers of floc in certain environments.

Accumulation of floc can only occur when OC inputs exceed decomposition, and thus floc sediments may be sustained by particularly high rates of OC input. The environments in which I observed thick accumulations of floc often had obviously high autochthonous inputs from aquatic vascular plants and/or allochthonous inputs of terrigenous OC deposited by advective flows from upstream. The latter would be more recalcitrant to decomposition and result in accumulation, but floc can often be found in shallow productive waters far from shorelines or advective inputs of terrigenous OC. Another possibility is that the flocculent nature of the particulate matter inhibits decomposition in some way that is not exhibited with fixed cotton strips inserted into the floc. The factors promoting the accumulation of floc thus remain a mystery; more information on inputs, transformations, and losses of OC is needed.

Short-term assays using either natural leaf litter or cellulose strips provide useful comparative assays of decomposition rates, although mass loss from litter may be faster if it includes the initial leaching of soluble organic and inorganic matter, which is more important with fresh litter. Given that decomposition usually slows in the latter stages when more recalcitrant organic matter remains, short-term assays using either litter bags or cotton strips may overestimate loss rates over longer time scales, but cotton strips may well represent the decomposition of structural biopolymers, the main component of aged litter.

Decomposition of OC in floc layers may be limited by the availability of P or the ratio of N to P available in the porewaters. Predictably, warmer temperatures led to increased decomposition rates and the temperature sensitivity results suggest that rates of decomposition in flocculent sediments could increase 12-56% with a 1-4°C increase in water temperatures, a range that is likely for this region in the next 100 years if climate change continues at the current pace

(Winslow et al. 2015). If decomposition outpaces OC inputs in a warmer world, stocks of sediment OC in freshwaters may decline.

In conclusion, floc sediments in shallow waters support relatively rapid rates of decomposition, and further studies are necessary to understand how general these patterns are in other shallow-water organic sediments. However, given that floc sediments are abundant, our understanding of OC cycling and burial in shallow freshwaters would particularly benefit from research that investigates the controls on the decomposition of OC aggregated in floc particles and how quickly this OC pool turns over, or alternatively, is recalcitrant to degradation in this form.

APPENDIX

Table A2.1. Results of Kruskal-Wallis rank sum tests and Conover-Iman test of multiple comparisons using rank sums to test for differences in tensile strength loss rates between seasons.

			Kruskal-Wallis			Conover-Iman	
Rate[†]	Location	Season Comparison	χ^2	d.f.[‡]	p	t[§]	Adjusted p[‖]
TSL day^{-1}	Water		16.96	2	<0.001		
		August vs. June				1.75	0.05
		August vs. October				4.4	<0.001*
		June vs. October				3.68	<0.001*
	Floc		167.35	2	<0.001		
		August vs. June				8.69	<0.001*
		August vs. October				16.35	<0.001*
		June vs. October				8.9	<0.001*
TSL degday^{-1}	Water		9.4	2	0.009		
		August vs. June				1.2	0.12
		August vs. October				3.01	0.003
		June vs. October				2.52	0.01
	Floc		88.39	2	<0.001		
		August vs. June				4.94	<0.001*
		August vs. October				10.48	<0.001*
		June vs. October				6.31	<0.001*

[†] Tensile strength loss rate (TSL day^{-1}, % per day; TSL degday^{-1}, % per degree day)
[‡] degrees of freedom
[§] t-test statistic for Conover-Iman test
[‖] p-values adjusted using the Benjamini-Hochberg procedure; * indicates significant p-values ($\alpha = 0.05/2$ in combination with p adjustment procedure)

Table A2.2. Results of Wilcox signed rank tests to compare differences in tensile strength loss rates (TSL day^{-1}, % per day; TSL degree day^{-1}, % per degree day) between those measured in the overlying water and those measured in each subsequent depth in the floc, by season. These comparisons were only made following the rejection of a Friedman test ($\alpha = 0.05$). The Benjamini-Hochberg procedure was used to adjust *p*-values to control the false discovery rate.

		TSL day^{-1}		TSL degday^{-1}	
Season	Depth Comparison	$V^{\dagger}$	Adjusted $p^{\ddagger}$	V	Adjusted p
June	+1.4 vs. -1.4	31.0	<0.001*	22.0	<0.001*
June	+1.4 vs. -4.3	40.0	<0.001*	11.0	<0.001*
June	+1.4 vs. -7.1	45.0	0.001*	15.0	<0.001*
June	+1.4 vs. -9.9	70.5	0.002*	35.0	<0.001*
June	+1.4 vs. -12.8	98.0	0.006*	60.0	0.001*
June	+1.4 vs. -15.6	98.0	0.006*	50.0	0.001*
October	+1.4 vs. -1.4	14.0	0.002*	15.0	0.002*
October	+1.4 vs. -4.3	28.0	0.005*	29.0	0.006*
October	+1.4 vs. -7.1	32.0	0.007*	35.0	0.009*
October	+1.4 vs. -9.9	21.0	0.003*	22.0	0.003*
October	+1.4 vs. -12.8	24.5	0.004*	27.0	0.005*
October	+1.4 vs. -15.6	18.5	0.002*	18.0	0.002*

† Wilcoxon signed rank test statistic

‡ *p*-values adjusted using the Benjamini-Hochberg procedure; * indicates significant *p*-values ($p < 0.05$)

Table A2.3. Results of generalized least squares modeling to select the best predictors of temperature-adjusted tensile strength loss (TSL degree day^{-1}, % degree day^{-1}) ratios using surface water chemistry variables.

Model Code[1]	Model Type[2]	Method[3]	Model[4]	AIC	*L* ratio	*p*	d.f.[5]	Comparison
Testing whether the inclusion of site as a random effect improves the model								
M1	gls	REML	season + all chem	52			11	
M2	lme	REML	season + all chem, random = ~1|site	54	<0.001	1.00	12	M1 vs. M2
Selecting the most parsimonious model								
M1	gls	ML	season + all chem	16				
M3	gls	ML	season + all chem (less Cl^-)	14	0.00	0.97	10	M1 vs. M3
M4	gls	ML	season + all chem (less Cl^- & Ca^{2+})	21	8.77	0.003	9	M1 vs. M4
M5	gls	ML	season + all chem (less Cl^- & Mg^{2+})	18	6.16	0.01	9	M3 vs. M5
M6	gls	ML	season + all chem (less Cl^- & SO_4^{2-})	12	<0.001	0.98	9	M3 vs. M6
M7	gls	ML	season + all chem (less Cl^-, SO_4^{2-}, & NO_3-N)	11	0.48	0.49	8	M6 vs. M7
M8	gls	ML	season + all chem (less Cl^-, SO_4^{2-}, NO_3-N, & DOC)	11	2.07	0.15	7	M7 vs. M8
M9	gls	ML	season + all chem (less Cl^-, SO_4^{2-}, NO_3-N, DOC, & NH_4-N)	10	0.75	0.39	6	M8 vs. M9
M10*	gls	ML	season + all chem (less Cl^-, SO_4^{2-}, NO_3-N, DOC, NH_4-N, & SRP)	11	3.44	0.06	5	M9 vs. M10

[1] * Denotes the most parsimonious model, TSL = 0.71 – 0.34 season(October) – 0.14 Mg^{2+} + 0.22 Ca^{2+}; season estimate is relative to June; estimates for continuous covariates are standardized coefficients; n = 23

[2] Model types: gls = generalized least squares, lme = linear mixed effect

[3] Method used to fit model: REML = restricted estimation maximum likelihood, ML = full maximum likelihood

[4] The covariate 'all chem' includes SRP + NH_4^+ + DOC + NO_3^- + SO_4^{2-} + Mg^{2+} + Ca^{2+} + Cl^-; these continuous covariates were centered to the mean and scaled by standard deviation

[5] degrees of freedom for likelihood ratio tests

Table A2.4. Results of Wilcox signed rank tests to compare differences in ergosterol concentrations (ng g $AFDM^{-1}$) between those measured in the overlying water (depth +1.4) and those measured in each subsequent depth in the floc (depths -1.4, -7.1, and -15.6). These comparisons were only made following the rejection of a Friedman test ($\alpha = 0.05$). The Benjamini-Hochberg procedure was used to adjust *p*-values to control the false discovery rate.

Season	Depth Comparison	V[1]	Adjusted p[2]
October	+1.4 vs. -1.4	46.0	0.07
October	+1.4 vs. -7.1	55.0	0.02*
October	+1.4 vs. -15.6	48.0	0.06

[1] Wilcoxon signed rank test statistic
[2] *p*-values adjusted using the Benjamini-Hochberg procedure; * indicates significant *p*-values ($p < 0.05$)

Table A2.5. Results of linear mixed effects modeling to select the best predictors of temperature-adjusted tensile strength loss (TSL degday^{-1}, % degree day^{-1}) rates using floc porewater chemistry variables.

Model Code[1]	Model Type[2]	Method[3]	Model[4]	AIC	*L* ratio	*p*	d.f.[5]	Comparison
Testing whether the inclusion of site as a random effect improves the model								
M1	gls	REML	season + depth + all chem	-748			16	
M2	lme	REML	season + depth + all chem, random = ~1|site	-763	17.65	<0.001	17	M1 vs. M2
Selecting the most parsimonious model								
M1	lme	ML	season + depth + all chem, random = ~1|site	-891			17	
M3	lme	ML	season + depth + all chem (less Ca^{2+}), random = ~1|site	-889	3.60	0.06	16	M1 vs. M3
M4	lme	ML	season + depth + all chem (less Ca^{2+} & DOC), random = ~1|site	-890	1.32	0.25	15	M3 vs. M4
M5	lme	ML	season + depth + all chem (less Ca^{2+}, DOC, & SO_4^{2-}), random = ~1|site	-891	0.51	0.48	14	M4 vs. M5
M6	lme	ML	season + depth + all chem (less Ca^{2+}, DOC, SO_4^{2-}, & NH_4-N), random = ~1|site	-883	10.03	0.002	13	M5 vs. M6
M7	lme	ML	season + depth + all chem (less Ca^{2+}, DOC, SO_4^{2-}, & H_2S), random = ~1|site	-890	3.13	0.08	13	M5 vs. M7
M8	lme	ML	season + depth + all chem (less Ca^{2+}, DOC, SO_4^{2-}, H_2S, & Fe^{2+}), random = ~1|site	-887	4.80	0.03	12	M7 vs. M8
M9*	lme	ML	season + depth + all chem (less Ca^{2+}, DOC, SO_4^{2-}, H_2S, & SRP), random = ~1|site	-879	13.68	<0.001	12	M7 vs. M9

[1] * Denotes the most parsimonious model, TSL = 0.16 + 0.07 season(August) – 0.03 season(October) – 0.010 depth(-12.8) – 0.003 depth(-9.9) + 0.001 depth(-7.1) + 0.008 depth(-4.3) + 0.007 depth(-1.4) + 0.02 SRP + 0.01 Fe^{2+} – 0.01 NH_4^+; season estimates are relative to June; depth estimates are relative to -15.6; estimates for continuous covariates are standardized coefficients; n = 270

[2] Model types: gls = generalized least squares, lme = linear mixed effect

[3] Method used to fit model: REML = restricted estimation maximum likelihood, ML = full maximum likelihood

[4] The covariate 'all chem' includes SRP + Fe^{2+} + H_2S + NH_4^+ + SO_4^{2-} + DOC + Ca^{2+}; these continuous covariates were centered to the mean and scaled by standard deviation

[5] degrees of freedom for likelihood ratio tests

Table A2.6. Results of linear mixed effects modeling to predict tensile strength loss rates (ln TSL day^{-1}, % per day) and estimate the apparent activation energy.

Model Code[1]	Model Type[2]	Method[3]	Model[4]	AIC	*L* ratio	*p*	d.f.[5]	Comparison
M1	gls	REML	inverse temperature	137			3	
M2*	lme	REML	inverse temperature, rand. = ~1|site	21	118.76	<0.001	4	M1 vs. M2
M3	lme	REML	inverse temperature, rand. = inverse temperature|site	19	5.27	0.07	6	M2 vs. M3
M3	lme	REML	inverse temperature, rand. = inverse temperature|site	19	124.03	<0.001	6	M1 vs. M3

[1] * Denotes the most parsimonious model, ln TSL = $1.14 - 0.82/k_BT - k_BT_0$, $p < 0.001$, n = 281
[2] Model types: gls = generalized least squares, lme = linear mixed effect
[3] Method used to fit model: REML = restricted estimation maximum likelihood, ML = full maximum likelihood
[4] Inverse temperature = $1/k_BT\text{-}1/k_BT_0$, where k is Boltzmann's constant, T is ambient temperature in K, and T_0 is a standard temperature (291.15K); rand. = random effect
[5] degrees of freedom for likelihood ratio tests

LITERATURE CITED

LITERATURE CITED

Allen AP, Gillooly JF, Brown JH (2005) Linking the global carbon cycle to individual metabolism. Funct Ecology 19:202–213. doi: 10.1111/j.1365-2435.2005.00952.x

Aller RC (1994) Bioturbation and remineralization of sedimentary organic matter: effects of redox oscillation. Chem Geol 114:331–345. doi: 10.1016/0009-2541(94)90062-0

Aller RC, Blair NE, Xia Q, Rude PD (1996) Remineralization rates, recycling, and storage of carbon in Amazon shelf sediments. Cont Shelf Res 16:753–786. doi: 10.1016/0278-4343(95)00046-1

Battin TJ, Luyssaert S, Kaplan LA, et al (2009) The boundless carbon cycle. Nature Geosci 2:598–600. doi: 10.1038/ngeo618

Benjamini Y, Hochberg Y (1995) Controlling the false discovery rate: A practical and powerful approach to multiple testing. J R Statist Soc B 57:289–300.

Benner R, Moran MA, Hodson RE (1986) Biogeochemical cycling of lignocellulosic carbon in marine and freshwater ecosystems: Relative contributions of procaryotes and eucaryotes. Limnol Oceangr 31:89–100. doi: 10.4319/lo.1986.31.1.0089

Boer W de, Folman LB, Summerbell RC, Boddy L (2005) Living in a fungal world: impact of fungi on soil bacterial niche development. FEMS Microbiol Rev 29:795–811. doi: 10.1016/j.femsre.2004.11.005

Bosatta E, Ågren GI (1999) Soil organic matter quality interpreted thermodynamically. Soil Biol Biochem 31:1889–1891. doi: 10.1016/S0038-0717(99)00105-4

Boström B, Andersen JM, Fleischer S, Jansson M (1988) Exchange of phosphorus across the sediment-water interface. Hydrobiologia 170:229–244. doi: 10.1007/BF00024907

Boyero L, Pearson RG, Gessner MO, et al (2011) A global experiment suggests climate warming will not accelerate litter decomposition in streams but might reduce carbon sequestration. Ecol Lett 14:289–294. doi: 10.1111/j.1461-0248.2010.01578.x

Brainard AS, Fairchild GW (2012) Sediment characteristics and accumulation rates in constructed ponds. J Soil Water Conserv 67:425–432. doi: 10.2489/jswc.67.5.425

Brown JH, Gillooly JF, Allen AP, et al (2004) Toward a metabolic theory of ecology. Ecology 85:1771–1789. doi: 10.1890/03-9000

Burdige DJ (2007) Preservation of organic matter in marine sediments: Controls, mechanisms, and an imbalance in sediment organic carbon budgets? Chem Rev 107:467–485. doi: 10.1021/cr050347q

Burns RG, Dick RP (2002) Enzymes in the Environment: Activity, Ecology, and Applications. Marcel Dekker, New York

Chen Y, Cheng JJ, Creamer KS (2008) Inhibition of anaerobic digestion process: A review. Bioresour Technol 99:4044–4064. doi: 10.1016/j.biortech.2007.01.057

Chróst RJ (1991) Microbial Enzymes in Aquatic Environments, 1st edn. Springer-Verlag, New York

Cole JJ, Prairie YT, Caraco NF, et al (2007) Plumbing the global carbon cycle: Integrating inland waters into the terrestrial carbon budget. Ecosystems 10:172–185. doi: 10.1007/s10021-006-9013-8

Cornwell WK, Cornelissen JHC, Amatangelo K, et al (2008) Plant species traits are the predominant control on litter decomposition rates within biomes worldwide. Ecol Lett 11:1065–1071. doi: 10.1111/j.1461-0248.2008.01219.x

Downing J (2010) Emerging global role of small lakes and ponds: little things mean a lot. Limnetica 29:9–24.

Downing JA, Cole JJ, Middelburg JJ, et al (2008) Sediment organic carbon burial in agriculturally eutrophic impoundments over the last century. Global Biogeochem Cycles. doi: 10.1029/2006GB002854

Federle TW, Vestal JR (1980) Lignocellulose mineralization by Arctic lake sediments in response to nutrient manipulation. Appl Environ Microbiol 40:32–39.

Fenchel T, King G, Blackburn TH (2012) Bacterial biogeochemistry: the ecophysiology of mineral cycling, Third. Academic Press, London

Ferland M-E, del Giorgio PA, Teodoru CR, Prairie YT (2012) Long-term C accumulation and total C stocks in boreal lakes in northern Québec. Global Biogeochem Cycles. doi: 10.1029/2011GB004241

Ferland M-E, Prairie YT, Teodoru C, del Giorgio PA (2014) Linking organic carbon sedimentation, burial efficiency, and long-term accumulation in boreal lakes. J Geophys Res Biogeosci 119:836–847. doi: 10.1002/2013JG002345

Follstad Shah JJ, Kominoski JS, Ardón M, et al (2017) Global synthesis of the temperature sensitivity of leaf litter breakdown in streams and rivers. Global Change Biol 19:202–12. doi: 10.1111/gcb.13609

Gessner MO, Newell SY (2002) Biomass, growth rate, and production of filamentous fungi in plant litter. In: Hurst CJ, Crawford RL, Knudsen GR, et al. (eds) Manual of Environmental Microbiology. American Society for Microbiology Press, Washington, D.C., USA, pp 390–408

Glud RN (2008) Oxygen dynamics of marine sediments. Mar Biol Res 4:243–289. doi:

10.1080/17451000801888726

Godshalk GL, Wetzel RG (1978) Decomposition of aquatic angiosperms. II. Particulate components. Aquat Bot 5:301–327. doi: 10.1016/0304-3770(78)90074-8

Golterman HL, Clymo RS (1969) Methods for Chemical Analysis of Fresh Waters. Blackwell, Oxford

Griffiths NA, Tiegs SD (2016) Organic-matter decomposition along a temperature gradient in a forested headwater stream. Freshw Sci 35:518–533. doi: 10.1086/685657

Gudasz C, Bastviken D, Steger K, et al (2010) Temperature-controlled organic carbon mineralization in lake sediments. Nature 466:478–481. doi: 10.1038/nature09186

Gudasz C, Sobek S, Bastviken D, et al (2015) Temperature sensitivity of organic carbon mineralization in contrasting lake sediments. J Geophys Res Biogeosci 120:1215–1225. doi: 10.1002/2015JG002928

Gulis V, Suberkropp KF (2006) Fungi: Biomass, production, and sporulation of aquatic hyphomycetes. In: Hauer FR, Lamberti GA (eds) Methods in Stream Ecology. Elsevier, pp 311–325

Güsewell S, Gessner MO (2009) N : P ratios influence litter decomposition and colonization by fungi and bacteria in microcosms. Funct Ecology 23:211–219. doi: 10.1111/j.1365-2435.2008.01478.x

Harrison AF, Latter PM, Whalton DWH (1988) Cotton strip assay: an index of decomposition in soil. NERC/ITE, Grange-over-Sands

Hulthe G, Hulth S, Hall POJ (1998) Effect of oxygen on degradation rate of refractory and labile organic matter in continental margin sediments. Geochim Cosmochim Ac 62:1319–1328. doi: 10.1016/S0016-7037(98)00044-1

Kinsman-Costello LE, O'Brien JM, Hamilton SK (2015) Natural stressors in uncontaminated sediments of shallow freshwaters: The prevalence of sulfide, ammonia, and reduced iron. Environ Toxicol Chem 34:467–479. doi: 10.1002/etc.2801

Komínková D, Kuehn KA, Büsing N, et al (2000) Microbial biomass, growth, and respiration associated with submerged litter of *Phragmites australis* decomposing in a littoral reed stand of a large lake. Aquat Microb Ecol 22:271–282. doi: 10.3354/ame022271

Kortelainen P, Pajunen H, Rantakari M, Saarnisto M (2004) A large carbon pool and small sink in boreal Holocene lake sediments. Global Change Biol 10:1648–1653. doi: 10.1111/j.1365-2486.2004.00848.x

Kristensen E, Ahmed SI, Devol AH (1995) Aerobic and anaerobic decomposition of organic matter in marine sediment: Which is fastest? Limnol Oceangr 40:1430–1437. doi: 10.4319/lo.1995.40.8.1430

Kristensen E, Holmer M (2001) Decomposition of plant materials in marine sediment exposed to different electron acceptors (O2, NO_3^-, and SO_4^{2-}), with emphasis on substrate origin, degradation kinetics, and the role of bioturbation. Geochim Cosmochim Ac 65:419–433. doi: 10.1016/S0016-7037(00)00532-9

Kuehn KA (2016) Lentic and lotic habitats as templets for fungal communities: traits, adaptations, and their significance to litter decomposition within freshwater ecosystems. Fungal Ecol 19:135–154. doi: 10.1016/j.funeco.2015.09.009

Kuehn KA, Francoeur SN, Findlay RH, Neely RK (2014) Priming in the microbial landscape: periphytic algal stimulation of litter-associated microbial decomposers. Ecology 95:749–762. doi: 10.1890/13-0430.1

Kuehn KA, Lemke MJ, Suberkropp K, Wetzel RG (2000) Microbial biomass and production associated with decaying leaf litter of the emergent macrophyte *Juncus effusus*. Limnol Oceangr 45:862–870. doi: 10.4319/lo.2000.45.4.0862

Lau MP, Sander M, Gelbrecht J, Hupfer M (2015) Solid phases as important electron acceptors in freshwater organic sediments. Biogeochemistry 123:49–61. doi: 10.1007/s10533-014-0052-5

Leschine SB (1995) Cellulose degradation in anaerobic environments. Annu Rev Microbiol 49:399–426. doi: 10.1146/annurev.mi.49.100195.002151

Lipson DA, Jha M, Raab TK, Oechel WC (2010) Reduction of iron (III) and humic substances plays a major role in anaerobic respiration in an Arctic peat soil. J Geophys Res. doi: 10.1029/2009JG001147

Lovley DR, Holmes DE, Nevin KP (2004) Dissimilatory Fe(III) and Mn(IV) reduction. Adv Microb Physiol 49:219–286. doi: 10.1016/S0065-2911(04)49005-5

Lovley DR, Phillips EJP (1987) Rapid assay for microbially reducible ferric iron in aquatic sediments. Appl Environ Microbiol 53:1536–1540.

Lynd LR, Weimer PJ, van Zyl WH, Pretorius IS (2002) Microbial cellulose utilization: Fundamentals and biotechnology. Microbiol Mol Biol Rev 66:506–577. doi: 10.1128/MMBR.66.3.506-577.2002

Makkonen M, Berg MP, Handa IT, et al (2012) Highly consistent effects of plant litter identity and functional traits on decomposition across a latitudinal gradient. Ecol Lett 15:1033–1041. doi: 10.1111/j.1461-0248.2012.01826.x

Megonigal JP, Hines ME, Visscher PT (2004) Anaerobic metabolism: Linkages to trace gases and aerobic processes. In: Schlesinger WH (ed) Biogeochemistry. Oxford, U.K, pp 317–424

Murphy J, Riley JP (1962) A modified single solution method for the determination of phosphate in natural waters. Analytica Chimica Acta 27:31–36. doi: 10.1016/S0003-2670(00)88444-5

Newell SY (1992) Estimating fungal biomass and productivity in decomposing litter. In: Carroll GC, Wicklow DT (eds) The Fungal Community: Its Organization and Role in the Ecosystem. Marcel Dekker, New York, New York, USA, pp 521–561

Newman S, Kumpf H, Laing JA, Kennedy WC (2001) Decomposition responses to phosphorus enrichment in an Everglades (USA) slough. Biogeochemistry 54:229–250. doi: 10.1023/A:1010659016876

Pérez J, Muñoz-Dorado J, la Rubia de T, Martínez J (2002) Biodegradation and biological treatments of cellulose, hemicellulose and lignin: an overview. Int Microbiol 5:53–63. doi: 10.1007/s10123-002-0062-3

Pinheiro J, Bates D, DebRoy S, et al (2017) nlme: Linear and nonlinear mixed effects models. R package version 3.1-131.1. Retrieved from: https://CRAN.R-project.org/package=nlme

R Core Team (2017) R: A language and environment for statistical computing. Vienna: R Foundation for Statistical Computing. Available online at: https://www.R-project.org/

Reddy KR, Patrick WH Jr. (1975) Effect of alternate aerobic and anaerobic conditions on redox potential, organic matter decomposition and nitrogen loss in a flooded soil. Soil Biol Biochem 7:87–94. doi: 10.1016/0038-0717(75)90004-8

Revsbech NP, Nielsen J, Hansen PK (1988) Benthic primary production and oxygen profiles. In: Blackburn TH, Sørensen J (eds) Nitrogen Cycling in Marine Environments. SCOPE, Wiley, pp 69–83

Rier ST, Shirvinski JM, Kinek KC (2014) *In situ* light and phosphorus manipulations reveal potential role of biofilm algae in enhancing enzyme-mediated decomposition of organic matter in streams. Freshwater Biol 59:1039–1051. doi: 10.1111/fwb.12327

RStudio Team (2017) RStudio: Integrated development for R. Boston, MA: RStudio Inc.

Rüegg J, Tiegs SD, Chaloner DT, et al (2011) Salmon subsidies alleviate nutrient limitation of benthic biofilms in southeast Alaska streams. Can J Fish Aquat Sci 68:277–287. doi: 10.1139/F10-145

Schulz S (1995) Effect of algal deposition on acetate and methane concentrations in the profundal sediment of a deep lake (Lake Constance). FEMS Microbiol Ecol 16:251–259. doi: 10.1016/0168-6496(94)00088-E

Sinsabaugh RL, Carreiro MM, Alvarez S (2002) Enzyme and microbial dynamics of litter decomposition. In: Burns RG, Dick RP (eds) Enzymes in the Environment: Activity, Ecology, and Applications. Marcel Dekker, New York, pp 249–265

Sobek S, Durisch-Kaiser E, Zurbrügg R, et al (2009) Organic carbon burial efficiency in lake sediments controlled by oxygen exposure time and sediment source. Limnol Oceangr 54:2243–2254. doi: 10.4319/lo.2009.54.6.2243

Sobek S, Zurbrügg R, Ostrovsky I (2011) The burial efficiency of organic carbon in the sediments of Lake Kinneret. Aquat Sci 73:355–364. doi: 10.1007/s00027-011-0183-x

Stookey LL (1970) Ferrozine: a new spectrophotometric reagent for iron. Anal Chem 42:779–781. doi: 10.1021/ac60289a016

Tanaka Y (1991) Microbial decomposition of reed (*Phragmites communis*) leaves in a saline lake. Hydrobiologia 220:119–129. doi: 10.1007/BF00006544

Thamdrup B (2000) Bacterial manganese and iron reduction in aquatic sediments. In: Schink B (ed) Advances in Microbial Ecology. Springer, pp 41–84

Tiegs SD, Clapcott JE, Griffiths NA, Boulton AJ (2013a) A standardized cotton-strip assay for measuring organic-matter decomposition in streams. Ecol Indic 32:131–139. doi: 10.1016/j.ecolind.2013.03.013

Tiegs SD, Entrekin SA, Reeves GH, et al (2013b) Litter decomposition, and associated invertebrate communities, in wetland ponds of the Copper River Delta, Alaska (USA). Wetlands 33:1151–1163. doi: 10.1007/s13157-013-0470-5

Tranvik LJ, Downing JA, Cotner JB, et al (2009) Lakes and reservoirs as regulators of carbon cycling and climate. Limnol Oceangr 54:2298–2314. doi: 10.4319/lo.2009.54.6_part_2.2298

Vizza C, Zwart JA, Jones SE, et al (2017) Landscape patterns shape wetland pond ecosystem function from glacial headwaters to ocean. Limnol Oceangr 10:7–15. doi: 10.1002/lno.10575

Wetzel RG (2001) Limnology: Lake and River Ecosystems, 3rd edn. Academic Press, San Diego

Wetzel RG (1990) Land-water interfaces: metabolic and limnological regulators. Verh Int Verein Limnol 24:6–24.

Wetzel RG (1992) Gradient-dominated ecosystems: sources and regulatory functions of dissolved organic matter in freshwater ecosystems. Hydrobiologia 229:181–198. doi: 10.1007/BF00007000

Winslow LA, Read JS, Hansen GJA, Hanson PC (2015) Small lakes show muted climate change signal in deepwater temperatures. Geophys Res Lett 42:355–361. doi: 10.1002/2014GL062325

Woodward G, Gessner MO, Giller PS, et al (2012) Continental-scale effects of nutrient pollution on stream ecosystem functioning. Science 336:1438–1440. doi: 10.1126/science.1219534

Wurzbacher CM, Bärlocher F, Grossart HP (2010) Fungi in lake ecosystems. Aquat Microb Ecol 59:125–149. doi: 10.3354/ame01385

Yvon-Durocher G, Allen AP, Bastviken D, et al (2014) Methane fluxes show consistent temperature dependence across microbial to ecosystem scales. Nature 507:488–491. doi: 10.1038/nature13164

Yvon-Durocher G, Caffrey JM, Cescatti A, et al (2012) Reconciling the temperature dependence of respiration across timescales and ecosystem types. Nature 487:472–476. doi: 10.1038/nature11205

Yvon-Durocher G, Jones JI, Trimmer M, et al (2010) Warming alters the metabolic balance of ecosystems. Philos Trans Royal Soc B 365:2117–2126. doi: 10.1098/rstb.2010.0038

Zuur AF, Ieno EN, Walker N, et al (2009) Mixed effects modelling for nested data. In: Mixed Effects Models and Extensions in Ecology with R. Springer New York, New York, NY, pp 101–142

CHAPTER 3

NITRATE REMOVAL BY FLOCCULENT SEDIMENTS IN SHALLOW FRESHWATERS

ABSTRACT

Increased loading of nitrogen (N) as a result of anthropogenic activities has degraded freshwater and coastal marine waters. Watershed networks of lakes, wetlands, and fluvial systems retain or remove a large portion of the N that would otherwise be transported to coastal ecosystems. Small, shallow waterbodies often disproportionately contribute to N removal relative to larger, deeper waterbodies, but have not received as much study. Sediment-water interactions strongly affect N transformations and removal from overlying water in shallow waterbodies. In this study I considered the potential for a rarely investigated, but common sediment type in shallow waterbodies—flocculent organic sediment (floc)—to remove nitrate (NO_3^-) from overlying waters. Given the high organic matter content of floc, I hypothesized that NO_3^- removal rates would be greater than in more consolidated, less organic sediments in similar settings. To test this I conducted *in situ* NO_3^- removal assays in a variety of shallow freshwaters with variable accumulations of floc in southwestern Michigan, examined their controls, and compared measured rates with those reported in the literature across a range of aquatic ecosystems and sediment types. Nitrate removal rates for floc were related to dissolved oxygen concentrations, temperature, and depth of overlying water, but not to the organic matter content of floc. The median removal rate for floc was greater than the median rate for other sediment types, but this difference may only exist under conditions where overlying waters are enriched with NO_3^-. I discuss possible explanations for the lower than predicted rates and suggest further

study is necessary to evaluate the role of flocculent sediments as ecosystem control points for NO_3^- removal.

INTRODUCTION

Anthropogenic activities associated with food and energy production have drastically increased the availability of nitrogen (N) in the biosphere (Vitousek et al. 1997; Galloway et al. 2004; Galloway et al. 2008). A significant amount of this N enters freshwater ecosystems as reactive forms (e.g., dissolved inorganic N) via overland and subsurface flow pathways (Galloway et al. 2003; Gruber and Galloway 2008; Baron et al. 2012). In many agricultural or densely populated watersheds, N loading increases to the point where elevated concentrations of N, and particularly nitrate (NO_3^-), persist in surface waters, often entering via contaminated groundwater (Rupert 2008; Puckett et al. 2011) or via leaching and runoff during increasingly common weather whiplashes (dry-wet transitions) in agricultural regions (Loecke et al. 2017). At elevated concentrations, NO_3^- can interfere with the use of freshwater for drinking, recreation, and industry (Townsend et al. 2003; Camargo and Alonso 2006) and has been implicated in coastal eutrophication and the occurrence of hypoxic zones (Smith et al. 1999; Boesch et al. 2001; Rabalais et al. 2001; Camargo and Alonso 2006).

Although N loading to coastal marine waters is increasing in many parts of the world (Yan et al. 2010; Yasin et al. 2010; Seitzinger et al. 2010; Strokal et al. 2014), a robust body of research has demonstrated that watershed networks of lakes, wetlands, and fluvial systems retain a large portion of the N that would otherwise be transported to coastal ecosystems (Howarth et al. 1996; Alexander et al. 2000; Peterson et al. 2001; Seitzinger et al. 2002; Mulholland et al. 2008; Harrison et al. 2009; Jordan et al. 2011; Finlay et al. 2013). Nitrogen entering these

systems has multiple potential fates including temporary assimilation by aquatic biota, burial in sediment, or permanent gaseous removal via denitrification (Wetzel 2001; Saunders and Kalff 2001). And it seems that waterbodies on the lower end of the size distributions (i.e., headwater streams, wetlands <0.1 km^2, and lakes ≤ 50 km^2) are hot spots for these N retentive and sink processes (Alexander et al. 2000; Seitzinger et al. 2006; Alexander et al. 2008; Wollheim et al. 2008; Harrison et al. 2009; Cheng and Basu 2017).

It is well established that small streams are particularly important in mediating N export through fluvial networks (Smith et al. 1997; Alexander et al. 2000; Peterson et al. 2001; Seitzinger et al. 2002; Mulholland et al. 2008), but only more recently have small lentic waterbodies been recognized as important N sinks (Harrison et al. 2009; Jordan et al. 2011; Cheng and Basu 2017). Using a spatially explicit, global model of lentic N removal, Harrison et al. (2009) estimated that lakes and reservoirs greater than 0.001 km^2 remove 19.7 Tg N $year^{-1}$. This is roughly one-third of the N entering surface freshwaters globally and is comparable to estimates of N removal by streams and rivers. Further, of those waterbodies, small lakes (0.001-50 km^2) remove nearly half of this N (9.3 Tg N $year^{-1}$) at a rate equivalent to 16% more uptake per unit area than larger lakes (Harrison et al. 2009). While these modeling estimates remain to be tested, they provide enticing evidence that small lakes and reservoirs, which are usually shallow and often productive, may function as control points for mediating N export to downstream waterbodies; thus, investigating the controls on N retention in these small waterbodies is important to understand their aggregate role at watershed scales.

Mass-balance studies in lakes have found that N removal rates correlate positively with N loading rates and water residence times, and negatively with mean lake depths (Kelly et al. 1987; Dillon and Molot 1990; Molot and Dillon 1993; Windolf et al. 1996; Saunders and Kalff 2001).

The negative relationship with depth is likely the result of the decreased influence of sediment-water interactions in deeper water columns. Furthermore, deeper lakes are more prone to seasonal thermal stratification, reducing the volume of through-flowing water in contact with the sediment. Thus, N transformations and removal by sediment-water interactions are expected to more strongly affect N concentrations in the overlying water in small lentic waterbodies.

In southwestern Michigan many shallow aquatic ecosystems accumulate flocculent organic sediments, hereafter called floc. These deposits consist of loosely consolidated layers (typical dry bulk densities ≤ 0.1 g cm^{-3} and water contents frequently >90%) of fine and coarse particulate organic matter as well as variable amounts of mineral matter, and often exceed 10 cm in thickness (Kincaid, Chapter 1). Thick accumulations of floc are most common in semi- to permanently-flooded shallow waterbodies that have productive aquatic and/or riparian vegetation and lack strong current or wave action. Floc also accumulates where inflowing water slows down and deposits its organic matter load, as for example where streams and rivers enter natural lakes and artificial reservoirs. Thus, floc is common in the littoral zones of lakes, small reservoirs, persistently flooded wetland habitat, depositional zones in lotic systems, and groundwater seeps. Despite the very common occurrence of these sediments in a diversity of shallow waterbodies, their biogeochemical importance has been little studied, and they are often incorrectly sampled using core methods developed for relatively consolidated sediments, or simply avoided (e.g., not sampled, or poured off the top of sediment cores).

Floc may promote rapid removal of NO_3^- from overlying water columns in shallow aquatic ecosystems where it is abundant. Most importantly, floc accumulations have high levels of organic matter, frequently exceeding 40% of sediment dry weight as measured by loss-on-ignition (Kincaid, Chapter 1). Organic carbon availability in sediments supports heterotrophic

microbial activity, thereby stimulating both assimilatory uptake of NO_3^- and respiratory denitrification. And when N demand cannot be met by mineralization of organic N, heterotrophs may assimilate NO_3^- from water (Caraco et al. 1998). Additionally, the organic carbon supply indirectly enhances denitrification potential by increasing sediment oxygen demand, producing more anaerobic habitat and decreasing the thickness of the oxic surface layer in the sediment through which NO_3^- has to diffuse before becoming available to denitrifiers. Often NO_3^--rich water traveling along surface and subsurface flowpaths must pass over or through accumulations of floc located at the shallow margins of waterbodies or at the confluence of lotic and lentic systems. In this case, floc layers may act as hot spots or even ecosystem control points (McClain et al. 2003; Bernhardt et al. 2017) for NO_3^- removal from surface waters.

Given the high organic matter content of floc, I hypothesized that NO_3^- removal rates would be greater than in more consolidated, less organic sediments in similar settings. To test this I measured potential NO_3^- removal rates in a variety of shallow freshwaters with variable accumulations of floc in southwestern Michigan. In this paper, I report those rates, examine their potential controls, and compare them with NO_3^- removal rates reported in the literature across a range of aquatic ecosystems with variable sediment compositions as a first assessment of the importance of this understudied sediment in watershed N removal.

METHODS

Site selection

In September 2015 and 2016, I conducted NO_3^- removal assays in shallow freshwater ecosystems in Kalamazoo County, Michigan, USA with thick accumulations (>10 cm) of flocculent sediments. I targeted locations with water columns <1 m deep that were also largely

devoid of vascular plant growth, although there were often plants growing nearby. If vegetation was present but it was weakly rooted or not rooted, I carefully removed the plants before the beginning of the experiments; places where vegetation removal would have been disruptive to the sediments were avoided. I conducted the experiments in 12 shallow aquatic ecosystems, including the littoral zones of lakes (LTER kettle pond, site name hereafter [LTER], Wintergreen Lake [Wintergreen]), an isolated depressional wetland (Turkey Marsh [Turkey]), shallow through-flow wetlands (Kellogg Research Forest Pond [KRFP], Three Lakes [Three], Loosestrife Fen [Loosestrife], Ransom Creek [Ransom], Sheriffs Marsh [Sheriffs], Wintergreen Lake Outlet [Wintergreen Out], Windmill Pond [Windmill]), and in depositional zones on the margins of stream channels (Eagle Creek [Eagle], Gull Run [Gull]) (Table 3.1).

Nitrate removal assays

I conducted NO_3^- removal assays *in situ* using open-ended mesocosms inserted into the sediments and extending above the water level. I constructed the mesocosms by removing the bottom of storage containers made of rigid, opaque polypropylene. To accommodate different water levels and open sediment areas, I used different sizes of containers; thus, internal surface areas ranged from 0.16 – 0.28 m^2 (Table 3.1). To isolate a volume of floc and overlying water, I carefully inserted the mesocosms into the flocculent sediment layer to a depth of at least 10 cm. The tops of the mesocosms were never more than 10 cm above the surface of the overlying water.

Table 3.1. Physical and chemical characteristics of sediments and overlying waters in the mesocosms used for *in situ* NO_3^- removal experiments. Surface water temperatures and dissolved oxygen (DO) concentrations represent averages from both pre-and post-enrichment periods. Nutrient concentrations are averages from samples collected during the pre-enrichment period only.

		Sediment			Surface water							
Site	Year	Area (m^2)	OM (%)	chl *a* (ug g^{-1})	Depth (m)	Temp. (°C)	Min. DO (mg l^{-1})	Mean DO (mg l^{-1})	NO_3-N (μM)	NH_4-N (μM)	SRP (μM)	DIN:SRP
Eagle	2016	0.16	42	14.2	0.11	19.7	7.0	8.6	7.2	4.2	0.08	142.5
Gull	2016	0.18	45	20.5	0.22	21.6	6.3	6.9	4.1	7.1	0.06	186.7
KRFP	2015	0.16	40	57.1	0.25	21.0	NA	NA	63.2	3.3	0.68	97.8
KRFP	2016	0.25	42	11.5	0.29	17.4	5.1	6.8	42.9	43.6	1.25	69.2
Loosestrife	2015	0.16	24	48.0	0.07	15.6	NA	NA	5.5	3.2	1.50	5.8
Loosestrife	2016	0.16	28	12.6	0.06	21.7	7.0	11.6	2.7	2.4	0.06	85.0
LTER	2016	0.18	21	32.2	0.28	21.7	7.3	9.9	0.1	1.4	0.09	16.7
Ransom	2016	0.25	18	4.7	0.35	20.9	4.6	5.3	1.9	10.5	0.18	68.9
Sheriffs	2015	0.16	50	24.0	0.10	10.6	NA	NA	1.5	41.7	0.28	154.3
Sheriffs	2016	0.16	55	8.1	0.19	16.8	3.8	4.9	2.8	34.6	0.11	340.0
Three	2015	0.16	22	42.1	0.40	15.0	NA	NA	11.8	9.0	0.19	109.5
Three	2016	0.25	23	8.5	0.40	23.0	3.8	6.0	2.1	24.9	0.22	122.7
Turkey	2016	0.18	26	20.2	0.16	17.6	0.4	0.6	1.3	16.2	0.23	76.1
Windmill	2016	0.18	57	97.0	0.27	17.8	3.4	6.3	1.5	52.5	0.62	87.1
Wintergreen	2015	0.16	23	113.0	0.30	15.3	NA	NA	17.1	5.0	0.48	46.0
Wintergreen	2016	0.28	30	33.7	0.35	26.1	8.8	12.7	1.3	5.8	0.07	101.4
Wintergreen Out	2016	0.28	35	26.4	0.60	22.6	0.8	1.6	0.9	0.3	0.08	15.0

The mesocosms and experimental design changed slightly between experiments in 2015 and 2016. In 2015, I installed mesocosms without any openings on the sides and allowed them to settle for 2 diel cycles before commencing the experiments. In 2016, I added two holes on opposite sides of the container to permit overlying water inside and outside of the mesocosm to exchange for 2 diel cycles prior to beginning the experiment and avoid possible water level disequilibrium between outside and inside the chambers. Immediately before starting the NO_3^- tracer studies, I sealed these holes by inserting tightly fitting rubber stoppers.

I measured NO_3^- removal rates in the mesocosms by enriching the overlying water with NO_3^- and a conservative solute tracer (Br^-) and monitoring changes in concentrations over 3 diel cycles. I increased the concentrations of NO_3^--N and Br^- in the mesocosms to approximately 2 mg l^{-1} by adding a concentrated solution of $NaNO_3$ and NaBr. Following the addition of the enrichment solution, I gently stirred the mesocosm to mix the water column while not mobilizing the floc. Immediately following enrichment and mixing, I sampled the overlying water in the mesocosm. In 2015, I sampled each mesocosm 22 hrs (time of day: PM), 46-48 hrs (PM), and 67-73 hrs (PM) after the initial sampling time. In 2016, I sampled each mesocosm 16-17 hrs (AM), 24-26 hrs (PM), 44-49 hrs (PM), and 64-65 hrs (AM) after the initial sampling time.

I calculated areal NO_3^- removal rates as first-order rate constants (k), estimating k as the slope of the linear relationship between the natural log of NO_3-N:Br^- ratios and time elapsed (days). I fit first-order models even though NO_3^- removal displayed zero order kinetics (i.e., NO_3^- decreased linearly with time), because first-order removal behavior is most commonly observed in the literature. In a few cases, the relationship became non-linear when nearly all of the NO_3^- was removed from the water column before the last temporal sampling event (e.g., Loosestrife in Figure 3.1). In these cases, I estimated k using only data points where NO_3-N:Br^- ratios were

>0.001 and the relationship with time remained linear. Linear regressions were always significant ($p < 0.05$). I then multiplied the total mass of NO_3-N at the beginning of the enrichment period by k and standardized this rate using the surface area of the sediment in the mesocosms. Negative values denote removal (presumably mainly due to fluxes from the water column to the sediment; the water above the sediments was not visibly rich in particulate matter and algae). Because I made the measurements by elevating the NO_3^- concentration in the overlying water column above ambient concentrations, the rates should be considered potential, rather than actual, NO_3^- removal rates (O'Brien and Dodds 2010).

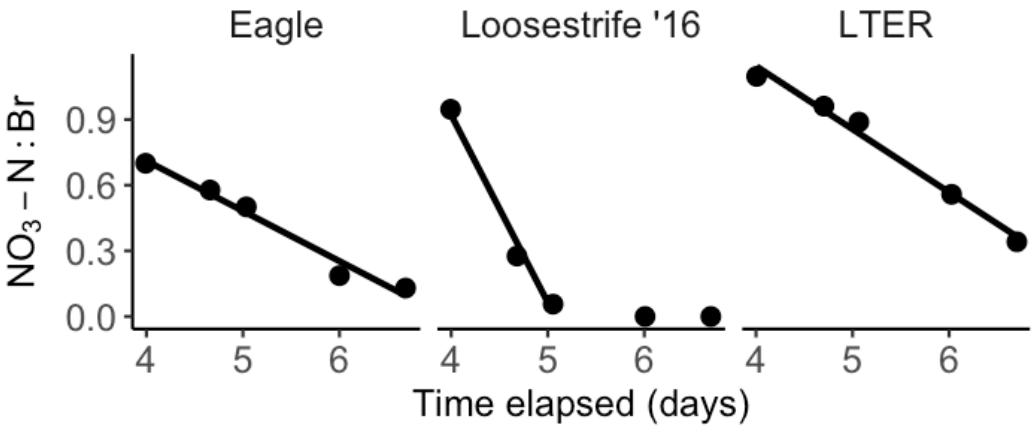

Figure 3.1. Examples of NO_3^- removal in the mesocosms at three sites including Loosestrife, a case where NO_3^- concentrations became depleted and hence only early measurements were used to generate comparable estimates.

Surface water sampling and analyses

I sampled the overlying water in the mesocosms using a 140-mL syringe fitted with a length of Tygon PVC clear tubing, obtaining a depth integrated sample by withdrawing water from throughout the vertical extent of the water column. I stored the sample in a clean bottle on ice until returning to the laboratory. In the laboratory I filtered the samples through 0.45 μm pore-size Supor polyethersulfone membrane filters (Pall Corp., Port Washington, New York) and

stored the samples at 4°C until analysis within 5 days. In 2016, I also measured dissolved oxygen profiles in the mesocosm during each sampling event using a Hydrolab minisonde.

I measured NO_3^-, Br^-, and porewater NH_4^+ using Dionex membrane-suppression ion chromatography and, for samples of overlying water, I measured NH_4^+ and soluble reactive phosphorus (SRP) concentrations colorimetrically using the phenylhypochlorite technique (Aminot et al. 1997) and molybdate blue method (Murphy and Riley 1962), respectively.

Sediment sampling and analyses

Following the termination of the NO_3^- removal assays, I measured particulate organic matter content and chlorophyll *a* (chl *a*) concentrations in the floc layer. Using a plastic coring tube (internal diameter 5.4 cm), I sampled the upper 10 cm of sediment in two random locations in each mesocosm. I determined organic matter content (% w/w) by loss on ignition upon combusting subsamples of dried sediment at 550°C for two hours. To determine chl *a* concentrations, I extracted pigments from the sediment in 90% acetone for 24 hours at 4°C, followed by measurement of chl *a* concentrations on filtered subsamples using a calibrated Turner Designs fluorometer (TD-700, Turner Designs, Sunnyvale, CA, USA).

Compilation of NO_3^- removal rates from the literature

To compare NO_3^- removal rates for floc to those made for other sediment types, I compiled studies that measured NO_3^- fluxes across the sediment-water interface in both freshwater and marine settings. Methods for flux measurements varied and included *ex situ* incubations in sediment cores and *in situ* methods including assays conducted in closed systems (e.g., benthic chambers and mesocosms) and whole ecosystems (e.g., tracer studies in through-

flow wetlands). I included measurements made at ambient NO_3^- concentrations, or close to ambient in the case of many ^{15}N isotope addition experiments, as well as those that elevated the concentrations of NO_3^-. When values were not available in text or tables, I extracted values from plots using the online tool, WebPlotDigitizer (http://arohatgi.info/WebPlotDigitizer/). I maintained measurements made in different locations within a water body as discrete observations, but averaged repeated measurements made over time for each water body. Nitrate fluxes and supporting information are compiled in Appendix Table A3.1. In total, 141 measurements were compiled from sediments in lakes, streams, wetlands, estuaries, and coastal and deeper water marine ecosystems.

Data analysis

I conducted all data analyses in R v.3.4.3 (R Core Team 2017) using RStudio v.1.1.383 (RStudio Team 2017). To test for overall differences in NO_3^- removal rates among sediment types independent of NO_3^- enrichment, I first conducted a non-parametric Kruskal-Wallis rank sum test. Following the rejection of a Kruskal-Wallis test ($\alpha = 0.05$), I did pairwise comparisons for each sediment type using Dunn's test (Dunn et al. 2014; Dinno 2017). To control the family-wise error rates, I applied a Bonferroni *p*-value correction. To test for differences between sediment types with consideration of NO_3^- enrichment, I followed the same procedure.

RESULTS

Sediment characteristics

Sediment characteristics varied widely among mesocosm sites (Table 3.1). Organic matter content of the upper 10 cm of flocculent sediment ranged from 18 to 57% (mean of 34%)

by weight. Chlorophyll-*a* concentrations ranged from 4.7 to 113.0 ug g^{-1} dry sediment (mean of 33.7 ug g^{-1}).

Water column characteristics

Physicochemical characteristics of the shallow overlying water columns (0.06-0.6 m) also varied among mesocosm sites (Table 3.1). Mean water temperatures ranged from 10.6 to 26.1°C. Mean dissolved oxygen concentrations ranged from 0.6 to 12.7 mg l^{-1}, but with the exception of two sites, remained above 3 mg l^{-1}. Background inorganic N concentrations varied by several orders of magnitude among sites, with NO_3^- concentrations ranging from 0.1 to 63.2 μmol N l^{-1} and ammonium ranging from 0.3 to 52.5 μmol N l^{-1}. Background SRP concentrations ranged from 0.06 to 1.5 μmol P l^{-1}. Background molar ratios of dissolved inorganic N (DIN; NO_3^- + NH_4^+) to SRP ratios ranged from 5.8 to 340.0.

Nitrate removal rates

Nitrate removal from the water column proceeded linearly in all experiments (e.g., Figure 3.1). In 3 of the 17 experiments, NO_3^- concentrations decreased below detection limits before the end of the experiment, but I was able to estimate first order removal rate constants (*k*; day^{-1}) and areal removal rates for all experiments (Table 3.2). Negative values for the rate constants imply net removal from the water column. Nitrate removal rates ranged from -0.25 to -7.28 mmol N m^{-2} h^{-1} with a median and mean of -0.39 and -0.98 mmol N m^{-2} h^{-1}, respectively.

Table 3.2. Nitrate removal rates for each site. Negative values denote removal (presumably mainly due to fluxes from the water column to the sediment).

Site	Year	First order removal constant, *k* (day^{-1})	Areal removal rate (mmol N m^{-2} h^{-1})
Eagle	2016	-0.68	-0.321
Gull	2016	-0.22	-0.316
KRFP	2015	-0.10	-0.260
	2016	-0.13	-0.251
Loosestrife	2015	-0.41	-0.314
	2016	-2.55	-0.807
LTER	2016	-0.44	-0.797
Ransom	2016	-0.18	-0.394
Sheriffs	2015	-0.47	-0.394
	2016	-0.40	-0.359
Three	2015	-0.08	-0.259
	2016	-0.35	-0.850
Turkey	2016	-7.82	-7.283
Windmill	2016	-0.24	-0.398
Wintergreen	2015	-0.25	-0.573
	2016	-0.46	-1.150
Wintergreen Out	2016	-0.41	-1.997

Where it was observed, dissolved oxygen depletion in the overlying water was associated with increased rates of NO_3^- removal. The two greatest (most negative) rates occurred in mesocosms that reached minimum dissolved concentrations <3 mg l^{-1} (Figure 3.2A; sites Turkey and Wintergreen Out). The site with the greatest removal rate, Turkey, went anoxic at the beginning of the NO_3^- enrichment period as recently senesced leaves from a riparian tree fell into the mesocosm; NO_3^- at this site fell below detection limits before the second sampling period, approximately 17 hours after enrichment. Because site Turkey had such anomalously high NO_3^-

uptake rates, I did not include it when assessing the influence of other variables on NO_3^- removal.

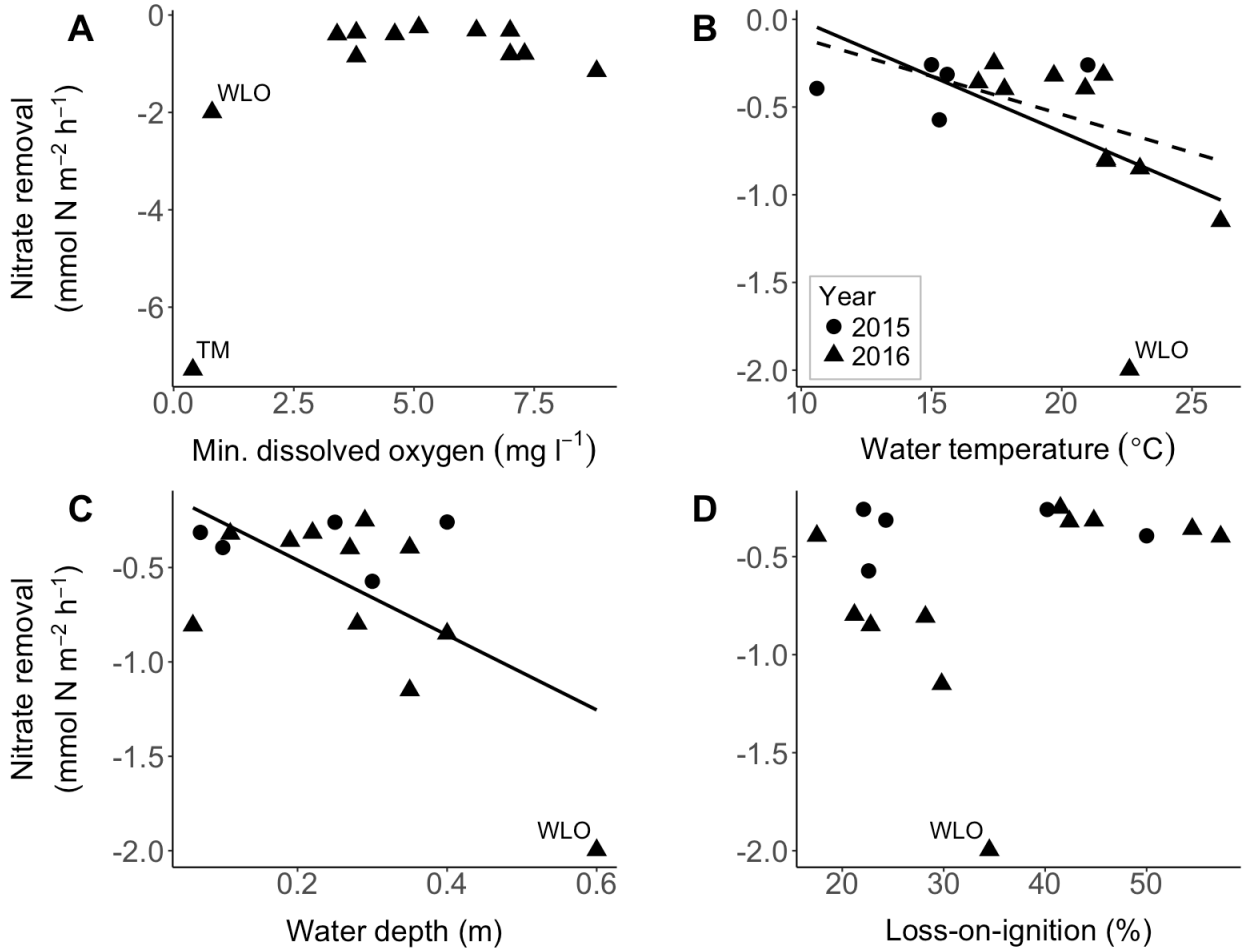

Figure 3.2. Relationships between NO_3^- removal rates and (**A**) minimum surface water dissolved oxygen concentration, (**B**) mean surface water temperature, (**C**) surface water depth, and (**D**) floc organic matter content measured as loss-on-ignition. The rate from Turkey Marsh (TM) was an outlier and was excluded from regression fits in **B**-**D**. Lines in **B** and **C** indicate relationships between NO_3^- removal rates and the covariate including (bold) the rate from Wintergreen Lake Outlet (WLO) and excluding WLO (dashed).

Water temperature and water depth also were related to NO_3^- removal rates. Nitrate removal rates increased with increasing mean water temperature regardless of the inclusion of site WLO in the regression (Figure 3.2B; with site WLO: NRR = 0.63 – 0.06x, R^2 = 0.29, p = 0.03; without site WLO: NRR = 0.33 – 0.04x, R^2 = 0.38, p = 0.01). Increasing water depth also

increased NO_3^- removal rates, though this relationship was heavily influenced by the inclusion of site WLO (Figure 3.2C; with site WLO: NRR = -0.06 – 0.02x, R^2 = 0.38, p = 0.01; without site WLO: NRR = -0.36 – 0.01x, R^2 = 0.05, p = 0.41). Organic matter percentage in the floc did not influence NO_3^- removal rates (Figure 3.2D; with site WLO: NRR = -0.88 + 0.01x, R^2 = 0.05, p = 0.39; without site WLO: NRR = -0.78 – 0.01x, R^2 = 0.16, p = 0.14).

Response of NH_4^+, SO_4^{2-}, and SRP to enrichment

I evaluated fluxes of other solutes in addition to NO_3^- and Br^- during the enrichment period for experiments conducted in 2016 (Appendix Table A3.2); the 2016 modified experimental setup allowed mesocosms to equilibrate with the surrounding water after installation. This was done in case concentrated porewater was released during mesocosm installation, or there was a change in water levels. Four of the 12 experiments resulted in significant increases of NH_4^+ in overlying water ranging from 0.01 to 0.10 mmol N m^{-2} h^{-1}. Conversely, NH_4^+ was removed from the water column at a rate of -0.07 mmol N m^{-2} h^{-1} at one site. Two of the sites that released NH_4^+ also released SO_4^{2-} to the overlying water column resulting in fluxes of 0.61 and 0.85 mmol m^{-2} h^{-1}. Sulfate was removed at one site at -0.03 mmol m^{-2} h^{-1}. There was no detectable release or removal of SRP during the NO_3^- removal experiments. None of these responses were correlated with first-order removal constants (k) or areal removal rates for NO_3^- ($p > 0.05$)

DISCUSSION

Rates of NO_3^- removal by sediments are controlled by multiple factors, including temperature, NO_3^- concentration, labile organic carbon availability, and dissolved oxygen

availability. For the NO_3^- removal assays, I enriched the overlying water with NO_3^- thereby alleviating any NO_3^- limitation and allowing us to evaluate other controls on potential NO_3^- removal rates. I observed greater rates of NO_3^- removal at sites with warmer water (Figure 3.2B), likely because increases in temperature generally lead to increased rates of biochemical reactions and microbial respiration. More specifically, temperature influences rates of NO_3^- directly by increasing the affinity for NO_3^- as a substrate in both algae and bacteria (Reay et al. 1999) and increasing the diffusion rate for NO_3^- (Golterman 2000), and indirectly by increasing both chemical and biological sediment oxygen demand (Walker and Snodgrass 1986; Klein et al. 2017). Correspondingly, researchers studying N removal in wastewater treatment wetlands found similar relationships between temperature and NO_3^- removal rates (Beutel et al. 2009; Chang et al. 2013). Similar temperature effects were found for NO_3^- removal rates in shallow wetland sediments in France, though the effect was greater in sediments with more organic matter (El-Habr and Golterman 1990).

Nitrate fluxes between overlying water and sediment in lakes are also temperature dependent, though the direction of the response may depend on trophic status of the lake. In an oligotrophic lake higher temperatures led to an increase in NO_3^- fluxes from the sediment to overlying water (Anthony and Lewis 2012), whereas higher temperatures in a eutrophic lake led to reduced NO_3^- fluxes from the sediment (Liikanen et al. 2002). This suggests that dissolved oxygen may interact with temperature to regulate the balance between N processes in the sediment that control the fate of N in overlying water, specifically assimilatory uptake vs. dissimilatory pathways (e.g., nitrification and denitrification). Greater sediment oxygen demand in eutrophic systems promotes hypoxic or anoxic conditions that limit nitrate production from nitrification and favor nitrate removal via denitrification. Most of the waterbodies in this study

are eutrophic and sites with minimum dissolved oxygen concentrations <3 mg l^{-1} had the highest fluxes of NO_3^- into the sediment.

I did not observe a relationship between NO_3^- removal rates and the organic matter content of floc (Figure 3.2D), despite the 3-fold difference in organic matter contents of floc in my study sites (Table 3.1). The absence of this relationship may result from several factors. First, NO_3^- removal via dissimilatory pathways may not be carbon limited in these highly organic sediments. Second, the organic matter in floc might be lower quality (e.g., high C:N ratio) and more recalcitrant to degradation; thus, an increase in organic matter content would not necessarily represent a large increase in labile forms of organic carbon. This latter situation would impact NO_3^- removal rates directly by limiting organic carbon available as a substrate for NO_3^- reducers, and indirectly by lowering sediment oxygen demand and decreasing rates of denitrification. While either scenario is plausible, I suggest the quality of organic matter in the floc may have limited NO_3^- removal rates in this study. Based on floc cores collected from the 5 sites assayed in 2015, the mean C:N molar ratio for the upper 12 cm of floc was 11.6 (range: 9.2-15.3), which was similar to the median C:N molar ratio of the upper 20 cm of floc measured in nearby waterbodies (11.7, Kincaid, Chapter 1). Ingersoll and Baker (1998) demonstrated that the ideal C:N ratio for nitrate removal efficiency in treatment wetlands was 5—a value much lower than I measured in floc. Further, Bastviken et al. (2005) demonstrated that denitrification potential in wetland sediments was inversely related to the C:N ratio of the dominant plant species.

Nitrate removal rates for floc relative to other sediment types

The median NO_3^- removal rate for flocculent sediments (Figure 3.3A, -0.39 mmol N m^{-2} h^{-1}), which includes rates measured in this study and three other studies (Svensson et al. 2001; O'Brien et al. 2012a; McCarthy et al. 2016), was greater (more negative) than the median rate for other sediment types (Figure 3.3A; Appendix Table A3.3). The particularly large (most negative) NO_3^- removal rate for floc sediments (-9.6 mmol N m^{-2} h^{-1}; this outlier is not shown in Figure 3.3) was measured prior to this study in one of the through-flow wetland sites (KRFP) (O'Brien et al. 2012a). That large removal rate was less than the maximum rate reported in the literature (-175 mmol N m^{-2} h^{-1}; this outlier is not shown in Figure 3.3) for a silty sand mixture in Lake Erie, USA (Small et al. 2014), but was an order of magnitude greater than the maximum rates reported for sand and mud, both approximately -0.9 mmol N m^{-2} h^{-1}.

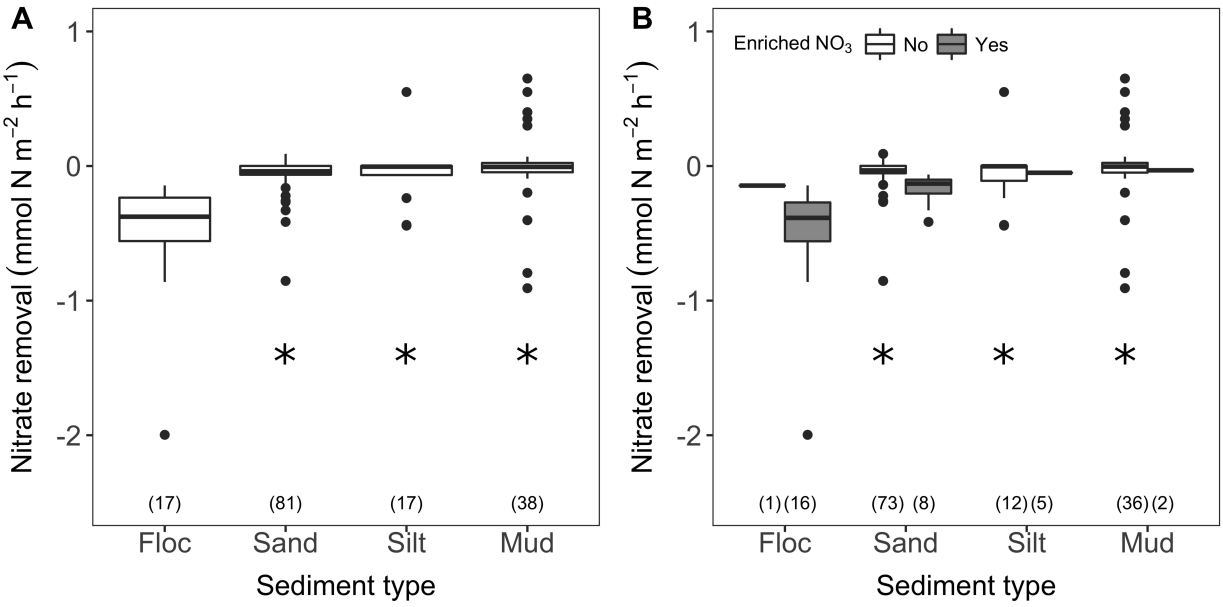

Figure 3.3. (**A**) Nitrate removal rates reported in the literature for major sediment types in freshwater and marine environments. Negative values imply net removal from the water column. For clarity purposes, rates more negative than -2 mmol N m^{-2} h^{-1} are not shown. (**B**) I further distinguish between measurements made by adding additional NO_3^- of any amount to the water column (enriched) versus those made at ambient nutrient conditions (no enrichment). Three of the floc measurements are from the literature (Svensson et al. 2001; O'Brien et al. 2012a; McCarthy et al. 2016); the remaining 14 values are from this study. Measurements were made using different methods (i.e., *in situ* mesocosms and benthic chambers and in the lab using sediment cores; Table S1. Asterisks (*) indicate that rates for these sediment types are significantly different ($P < 0.05$; Table S3) than those for floc (**A**) and significantly different than those for floc measured by enriching the overlying water with NO_3^- (enriched, **B**).

The difference between NO_3^- removal rates for floc versus those measured for other sediment types may only exist under conditions where overlying waters are enriched with NO_3^- and therefore could be an effect of NO_3^- availability rather than the presence of flocculent sediments. As noted in previous studies, enrichment of overlying water with even small amounts of NO_3^- tends to increase NO_3^- fluxes to sediment relative to incubations with ambient NO_3^- concentrations (Gardner and McCarthy 2009; Han et al. 2014). And when I separate the NO_3^- removal rates by enrichment condition (i.e., those measured using enrichment versus those measured under ambient nutrient conditions), I find that median NO_3^- removal rates for floc

measured using enrichment are only statistically greater than removal rates for other sediment types measured under ambient conditions (Figure 3.3B; Appendix Table A3.3).

Why were rates of NO_3^- removal not greater for organic-rich, flocculent sediments, as I had hypothesized? Here I propose possible explanations for the lower than predicted rates. First, because the measurements were not made using isotopically-labeled NO_3^-, the rates represent the net result of both NO_3^- additions plus potentially stimulated removal and release processes in the mesocosms. Isotopically-labeled (i.e., $^{15}NO_3^-$) additions would have allowed us to evaluate gross NO_3^- removal rates as well as the fate of the removed N (e.g., permanent removal via denitrification versus temporary uptake and subsequent release by microbes and algae), although these can be technically challenging in short-term chamber incubations (O'Brien et al. 2012b). Second, as demonstrated by researchers modeling sediment oxygen demand in freshwater lakes, processes like biological oxygen demand control the development of conditions favorable to anaerobiosis and thereby influence NO_3^- uptake. However, they may depend less on the quantity of organic matter present in the sediment and more on the biodegradability or the flux of organic carbon to the sediments (Walker and Snodgrass 1986). Thus, it may be that organic matter in floc is neither high quality nor readily biodegradable. In this study, the maximum NO_3^- removal rate I measured was at a site that rapidly became anoxic as it received an input of labile carbon in the form of recently senesced leaves from a deciduous tree in the riparian zone. And several studies have demonstrated that the availability of easily biodegradable carbon improves N removal efficiency in wetlands used for treatment of N enriched wastewater (Gersberg et al. 1983; Kozub and Liehr 1999; Misiti et al. 2011). Third, these organic-rich floc layers tend to accumulate high levels of ammonium N in porewaters (Table 3.1, site means ranged from 28 to 1347 uM). And though I did not observe a clear relationship between concentrations of ammonium in the

overlying water and NO_3^- removal rates, it is possible that production of NO_3^- from nitrification of ammonium N diffusing from the organic-rich floc layers could decrease net NO_3^- removal rates. Lastly, under oxic conditions in the water column, denitrification in floc may be supported by NO_3^- supplied via nitrification in the porewaters rather than NO_3^- from the overlying water column as has been demonstrated in other studies (Lohse et al. 1993; Rysgaard et al. 2003; Farías et al. 2004). The presence of microalgae in sediment, which I observed in the floc sediments (Table 4.1), can also reduce the use of NO_3^- from the water column during the day by promoting coupled nitrification-denitrification in the upper layers of sediment (Risgaard-Petersen et al. 2003), though they can also inhibit nitrifying bacteria if their photosynthetic activity exceeds community respiration (Risgaard-Petersen 2003).

CONCLUSIONS

Organic-rich, flocculent sediment layers remove NO_3^- from overlying water columns at rates comparable to those of other sediment types. However, I cannot conclude that removal rates are much greater than those measured for other sediment types, despite being organic-rich. That said, given the abundance of this sediment type in shallow waterbodies and the tendency for them to accumulate along the margins of these ecosystems, where they intercept overland and subsurface flows from their catchments, they may still serve as important ecosystem control points. In other words, if floc continuously removes NO_3^- from intercepted flows throughout the year, even at modest rates, then they might serve as a permanent control point for NO_3^- in the watershed (Bernhardt et al. 2017). Progress towards the understanding of their function as a control point requires future studies that evaluate the fate of the removed NO_3^- (i.e., temporary assimilation or permanent removal via denitrification), assess temporal patterns and drivers of

NO_3^- removal by floc in shallow and deeper waters, quantify other N processes associated with floc (e.g., ammonification of organic N and subsequent exchange of ammonium with overlying waters), evaluate the influence of microalgae and vascular vegetation on N cycling, and identify physical exchange mechanisms and rates (e.g., bioturbation, advective flows due to wave action, buoyancy-driven flows resulting from rapid cooling or heating of overlying waters, etc.) that may enhance transport of oxygen and NO_3^- into loosely consolidated floc layers.

APPENDIX

Table A3.1. Nitrate flux values (mmol N m^{-2} hr^{-1}) reported in the literature for major sediment types in freshwater and marine systems. Measurements made in different locations within a water body are maintained as discrete observations, but repeated measurements made over time in each water body were averaged. Negative fluxes indicate movement of nitrate from the water column to the sediment. Citations listed below table.

Source	Eco.*	Exp. Unit†	Site Name	Country/US State	Subsite/Treatment	Sed.‡	Enr.§	NO_3-N Flux
Anthony_Lewis_2012	L	SC	Grand Lake	CO	N/A	Sand	No	0.007
Asmus_etal_2000	M_C	BC	Ria Formosa	PORTUGAL	Mud	Mud	No	0.002
Asmus_etal_2000	M_C	BC	Ria Formosa	PORTUGAL	Sand	Sand	No	0.005
Asmus_etal_2000	M_C	BC	Sylt-Romo Bay	PORTUGAL	Arenicola flat	Sand	No	-0.112
Asmus_etal_2000	M_C	BC	Sylt-Romo Bay	PORTUGAL	Nereis belt	Sand	No	-0.039
Berelson_etal_2003	M_C	BC	Monterey Bay	CA	TS3	Mud	No	0.009
Berelson_etal_2003	M_C	BC	Monterey Bay	CA	TS4	Mud	No	-0.003
Berelson_etal_2003	M_C	BC	Monterey Bay	CA	CC2	Mud	No	-0.026
Berelson_etal_2003	M_C	BC	Monterey Bay	CA	CC3	Mud	No	-0.028
Berelson_etal_2003	M_C	BC	Monterey Bay	CA	CC1	Mud	No	-0.030
Berelson_etal_2003	M_C	BC	Monterey Bay	CA	TS1	Mud	No	-0.037
Berelson_etal_2003	M_C	BC	Monterey Bay	CA	TS2	Mud	No	-0.050
Bernard_etal_2015	M_C	SC_FT	Little Lagoon	AL	West	Sand	Yes	-0.095
Bernard_etal_2015	M_C	SC_FT	Little Lagoon	AL	Mouth	Sand	Yes	-0.103
Bernard_etal_2015	M_C	SC_FT	Little Lagoon	AL	East	Sand	Yes	-0.123
Binnerup_etal_1992	E	SC_FT	Norsminde Fjord	DENMARK	Station 4	Silt	No	-0.438
Callender_Hammond_1982	E	BC	Potomac River Estuary	MD	V_3	Mud	No	-0.049
Callender_Hammond_1982	E	BC	Potomac River Estuary	MD	V_PP	Mud	No	0.025
Callender_Hammond_1982	E	BC	Potomac River Estuary	MD	V_Q	Mud	No	-0.065
Callender_Hammond_1982	E	BC	Potomac River Estuary	MD	V_16	Mud	No	0.069
Callender_Hammond_1982	E	BC	Potomac River Estuary	MD	V_PC	Mud	No	-0.091
Callender_Hammond_1982	E	BC	Potomac River Estuary	MD	V_26	Mud	No	-0.015
Callender_Hammond_1982	E	BC	Potomac River Estuary	MD	V_PT	Mud	No	-0.026
Callender_Hammond_1982	E	BC	Potomac River Estuary	MD	V_14	Mud	No	0.023
Callender_Hammond_1982	E	BC	Potomac River Estuary	MD	V_SM	Mud	No	-0.094
Chau_2002	E	SC_S	Tolo Harbour	HONG KONG	SS1	Sand	No	0.001

Table A3.1 (cont'd)

Chau_2002	E	SC_S	Tolo Harbour	HONG KONG	SS2	Sand	No	0.001
Chau_2002	E	SC_S	Tolo Harbour	HONG KONG	SS3	Silt	No	0.001
Chau_2002	E	SC_S	Tolo Channel	HONG KONG	SS4	Silt	No	0.000
Chau_2002	E	SC_S	Tolo Channel	HONG KONG	SS5	Silt	No	0.001
Deek_etal_2012	M_O	SC_FT	North Frisian Wadden Sea	GERMANY	Busum_II	Sand	Yes	-0.163
Deek_etal_2012	M_O	SC_FT	North Frisian Wadden Sea	GERMANY	Sylt_II	Sand	Yes	-0.063
Deek_etal_2012	M_O	SC_FT	North Frisian Wadden Sea	GERMANY	Sylt_I	Sand	Yes	-0.139
Deek_etal_2012	M_O	SC_FT	North Frisian Wadden Sea	GERMANY	Busum_I	Sand	Yes	-0.329
Deek_etal_2012	M_O	SC_FT	North Frisian Wadden Sea	GERMANY	Sylt_I	Sand	No	-0.030
Deek_etal_2012	M_O	SC_FT	North Frisian Wadden Sea	GERMANY	Sylt_II	Sand	No	-0.074
Deek_etal_2012	M_O	SC_FT	North Frisian Wadden Sea	GERMANY	Busum_II	Sand	No	-0.140
Deek_etal_2012	M_O	SC_FT	North Frisian Wadden Sea	GERMANY	Busum_I	Sand	No	-0.259
Devol_Christensen_1993	M_O	BC	Pacific Ocean	WA	WE104B	Sand	No	-0.014
Devol_Christensen_1993	M_O	BC	Pacific Ocean	WA	NH07A	Sand	No	-0.024
Devol_Christensen_1993	M_O	BC	Pacific Ocean	WA	NH10A	Sand	No	-0.025
Devol_Christensen_1993	M_O	BC	Pacific Ocean	WA	NH12B	Sand	No	-0.027
Devol_Christensen_1993	M_O	BC	Pacific Ocean	WA	NH12A	Sand	No	-0.032
Devol_Christensen_1993	M_O	BC	Pacific Ocean	WA	WE105A	Sand	No	-0.032
Devol_Christensen_1993	M_O	BC	Pacific Ocean	WA	NH10B	Sand	No	-0.033
Devol_Christensen_1993	M_O	BC	Pacific Ocean	WA	NH07B	Sand	No	-0.036
Devol_Christensen_1993	M_O	BC	Pacific Ocean	WA	WE105B	Sand	No	-0.036
Devol_Christensen_1993	M_O	BC	Pacific Ocean	WA	NH02B	Sand	No	-0.043
Devol_Christensen_1993	M_O	BC	Pacific Ocean	WA	WE101A	Sand	No	-0.043
Devol_Christensen_1993	M_O	BC	Pacific Ocean	WA	NH03A	Sand	No	-0.047
Devol_Christensen_1993	M_O	BC	Pacific Ocean	WA	NH16A	Sand	No	-0.047
Devol_Christensen_1993	M_O	BC	Pacific Ocean	WA	NH16B	Sand	No	-0.047
Devol_Christensen_1993	M_O	BC	Pacific Ocean	WA	WE103A	Sand	No	-0.047
Devol_Christensen_1993	M_O	BC	Pacific Ocean	WA	NH01B	Sand	No	-0.050
Devol_Christensen_1993	M_O	BC	Pacific Ocean	WA	NH02A	Sand	No	-0.050
Devol_Christensen_1993	M_O	BC	Pacific Ocean	WA	NH18B	Sand	No	-0.050
Devol_Christensen_1993	M_O	BC	Pacific Ocean	WA	WE103B	Sand	No	-0.050

Table A3.1 (cont'd)

Devol_Christensen_1993	M_O	BC	Pacific Ocean	WA	NH17B	Sand	No	-0.054
Devol_Christensen_1993	M_O	BC	Pacific Ocean	WA	WE108A	Sand	No	-0.054
Devol_Christensen_1993	M_O	BC	Pacific Ocean	WA	WE108B	Sand	No	-0.054
Devol_Christensen_1993	M_O	BC	Pacific Ocean	WA	NH01A	Sand	No	-0.058
Devol_Christensen_1993	M_O	BC	Pacific Ocean	WA	NH06B	Sand	No	-0.058
Devol_Christensen_1993	M_O	BC	Pacific Ocean	WA	NH03B	Sand	No	-0.065
Devol_Christensen_1993	M_O	BC	Pacific Ocean	WA	NH19A	Sand	No	-0.065
Devol_Christensen_1993	M_O	BC	Pacific Ocean	WA	NH14A	Sand	No	-0.068
Devol_Christensen_1993	M_O	BC	Pacific Ocean	WA	WE107A	Sand	No	-0.068
Devol_Christensen_1993	M_O	BC	Pacific Ocean	WA	WE107B	Sand	No	-0.068
Devol_Christensen_1993	M_O	BC	Pacific Ocean	WA	NH18A	Sand	No	-0.072
Devol_Christensen_1993	M_O	BC	Pacific Ocean	WA	NH17A	Sand	No	-0.083
Devol_Christensen_1993	M_O	BC	Pacific Ocean	WA	WE104A	Sand	No	-0.086
Engelsen_etal_2008	M_C	SC_FT	Lindholmen Bay	SWEDEN	N/A	Sand	No	0.004
Engelsen_etal_2008	M_C	SC_FT	Bassholmen Bay	SWEDEN	N/A	Sand	No	-0.019
Engelsen_etal_2008	M_C	SC_FT	Bokevik Bay	SWEDEN	N/A	Sand	No	-0.031
Engelsen_etal_2008	M_C	SC_FT	Finsbo Bay	SWEDEN	N/A	Sand	No	-0.044
Engelsen_etal_2008	M_C	SC_FT	Fiskebackskil Bay	SWEDEN	N/A	Silt	No	0.002
Engelsen_etal_2008	M_C	SC_FT	Ragardsvik Bay	SWEDEN	N/A	Silt	No	-0.015
Gardner_etal_2001	L	SC_S	Lake Huron, Saginaw Bay	MI	Site 1	Sand	No	0.018
Gardner_etal_2001	L	SC_S	Lake Huron, Saginaw Bay	MI	Site 2	Sand	No	0.016
Henriksen_etal_1981	M_C	SC_S	Langelands Baelt	DENMARK	Station_III	Mud	No	0.650
Henriksen_etal_1981	M_C	SC_S	Hirtshals N	DENMARK	Station_XI	Mud	No	0.550
Henriksen_etal_1981	M_C	SC_S	Aarhus Bugt	DENMARK	Station_VIII	Mud	No	0.400
Henriksen_etal_1981	M_C	SC_S	Storebaelt	DENMARK	Station_II	Mud	No	0.350
Henriksen_etal_1981	M_C	SC_S	Anholt SE	DENMARK	Station_VI	Mud	No	0.300
Henriksen_etal_1981	M_C	SC_S	Laesso E	DENMARK	Station_IX	Mud	No	0.400
Henriksen_etal_1981	M_C	SC_S	Aalborg Bugt	DENMARK	Station_V	Sand	No	0.050
Henriksen_etal_1981	M_C	SC_S	Aalbaek Bugt	DENMARK	Station_XIII	Silt	No	0.550
Hopkinson_Wetzel_1982	M_C	BC	Georgia Bight	GA	N/A	Sand	No	0.005
Janssen_etal_2005	M_O	BC	North Sea	GERMANY	Coarse	Sand	No	0.041

Table A3.1 (cont'd)

Janssen_etal_2005	M_O	BC	North Sea	GERMANY	Medium	Sand	No	0.021
Janssen_etal_2005	M_O	BC	North Sea	GERMANY	Fine	Sand	No	0.011
Jensen_etal_1990	M_C	SC_S	Kattegat	DENMARK	Aarhus Bight	Sand	No	0.001
Laursen_Seitzinger_2002	M_O	BC	Mid-Atlantic	NJ	Station 9	Sand	No	0.005
Laursen_Seitzinger_2002	M_O	BC	Mid-Atlantic	NJ	Station C	Sand	No	0.005
Laursen_Seitzinger_2002	M_O	BC	Mid-Atlantic	NJ	Station C2	Sand	No	-0.028
Laursen_Seitzinger_2002	M_O	BC	Mid-Atlantic	NJ	Station 32	Silt	No	0.002
Li_Wang_2012	L	SC	Nansi Lake	CHINA	NSH1	Mud	No	0.023
Li_Wang_2012	L	SC	Nansi Lake	CHINA	NSH2	Mud	No	0.002
Li_Wang_2012	L	SC	Nansi Lake	CHINA	NSH3	Mud	No	-0.005
Li_Wang_2012	L	SC	Nansi Lake	CHINA	NSH4	Mud	No	0.012
Liikanen_etal_2002	L	SC_FT	Lake Kevaton	FINLAND	N/A	Mud	No	-0.008
Lim_etal_2011	L	SC	Lake Asan	SOUTH KOREA	Site B	Sand	No	-0.043
Lim_etal_2011	L	SC	Lake Asan	SOUTH KOREA	Site A	Silt	No	-0.067
Luijn_2012	L	SC	Lake Nuldernauw	NETHERLANDS	Muddy	Mud	Yes	-0.039
McCarthy_etal_2016_IAGLR	W	SC_FT	Kellogg Forest Pond	MI	N/A	Floc	Yes	-0.215
McCarthy_etal_2016_IAGLR	W	SC_FT	Kellogg Forest Pond	MI	N/A	Floc	No	-0.146
McCarthy_etal_2016_LO	L	SC_FT	Lake Champlain, Missisquoi Bay	QUEBEC	Central Basin	Mud	Yes	-0.024
McCarthy_etal_2016_LO	L	SC_FT	Lake Champlain, Missisquoi Bay	QUEBEC	Pike River Mouth	Sand	Yes	-0.415
Nedwell_Trimmer_1996	E	SC	Great Ouse	ENGLAND	Denver Sluice	Sand	No	-0.221
Nedwell_Trimmer_1996	E	SC	Great Ouse	ENGLAND	Magdalen Bridge	Sand	No	-0.267
Nedwell_Trimmer_1996	E	SC	Great Ouse	ENGLAND	Kings Lynn	Sand	No	-0.854
Nizzoli_etal_2010	L	SC_S	Lake Verde	ITALY	N/A	Mud	No	-0.068
Nizzoli_etal_2010	L	SC_S	Ca Stanga	ITALY	N/A	Mud	No	-0.198
Nowicki_Nixon_1985	M_C	BC	Potter Pond	RI	Segar Cove, Site 1	Mud	No	-0.004
Nowicki_Nixon_1985	M_C	BC	Potter Pond	RI	Whaleboat Pt, Site 2	Mud	No	0.007
Nowicki_Nixon_1985	M_C	BC	Potter Pond	RI	Wakamo, Site 3	Sand	No	-0.030
Obrien_etal_2012	W	ECO	Kellogg Forest Pond	MI	Cont. NH4 add.	Floc	Yes	-9.628
Ogilvie_etal_1997	E	SC_S	River Colne	TN	Wivenhoe, Site 3	Mud	No	-0.795

Table A3.1 (cont'd)

Ogilvie_etal_1997	E	SC_S	River Colne	TN	Hythe, Site 4	Mud	No	-0.908
Ogilvie_etal_1997	E	SC_S	River Colne	TN	Brightlingsea, Site 1	Sand	No	0.090
Ogilvie_etal_1997	E	SC_S	River Colne	TN	Alresford, Site 2	Silt	No	-0.443
Reay_etal_1995	E	BC	Cherrystone Inlet	VA	EV1_EV2	Sand	No	-0.004
Reay_etal_1995	E	BC	Cherrystone Inlet	VA	SC1_SC2	Silt	No	-0.005
Rizzo_Christian_1996	E	SC	Neuse River	NC	Site B	Sand	No	0.054
Rizzo_Christian_1996	E	SC	Neuse River	NC	Site C	Sand	No	0.032
Rizzo_Christian_1996	E	SC	Neuse River	NC	Site A	Sand	No	0.031
Rizzo_Christian_1996	E	SC	Neuse River	NC	Site E	Sand	No	0.007
Rizzo_Christian_1996	E	SC	Neuse River	NC	Site D	Sand	No	0.003
Sayama_2001	M_C	SC_S	Tokyo Bay	JAPAN	N/A	Mud	No	0.063
Shang_etal_2013	L	SC_FT	Lake Taihu	CHINA	N/A	Silt	Yes	-0.050
Small_etal_2014	L	SC	Lake Superior	USA	N/A	Silt	Yes	31.000
Small_etal_2014	L	SC	Lake Huron	USA	N/A	Silt	Yes	-38.000
Small_etal_2014	L	SC	Lake Erie	USA	N/A	Silt	Yes	-175.000
Soana_etal_2015	S	SC_S	Mincio River	ITALY	Macrophyte_meadow	Mud	No	-0.403
Svensson_etal_2001	L	SC_FT	Lake Ringsjon	SWEDEN	Low_nitrate	Floc	Yes	-0.144
Svensson_etal_2001	L	SC_FT	Lake Ringsjon	SWEDEN	High_nitrate	Floc	Yes	-0.199
Trimmer_etal_1998	E	SC	Great Ouse	ENGLAND	N/A	Silt	No	-0.238
Tyler_etal_2003	E	SC_S	Hog Island Bay	VA	Creek	Sand	No	-0.001
Tyler_etal_2003	E	SC_S	Hog Island Bay	VA	Willis Wharf	Sand	No	-0.006
Tyler_etal_2003	E	SC_S	Hog Island Bay	VA	Shoal	Sand	No	-0.002
Tyler_etal_2003	E	SC_S	Hog Island Bay	VA	Hog	Sand	No	-0.008
Zaman_etal_2008	W	ECO	Seepage wetland	NEW ZEALAND	N/A	Silt	Yes	-12.178

* ecosystem type: E = estuary, L = lake, M_C = coastal marine, M_O = open marine, S = stream, W = wetland

† experimental unit used to make NO_3^- flux measurement: BC = benthic chamber, ECO = whole ecosystem, SC = unstirred sediment core, SC_S = stirred sediment core, SC_FT = flow-through sediment core

‡ sediment type

§ whether NO_3^- flux measurement was made by enriching the overlying water with any amount of NO_3^- above ambient conditions

REFERENCES FOR TABLE A3.1

Anthony JL, Lewis WM (2012) Low boundary layer response and temperature dependence of nitrogen and phosphorus releases from oxic sediments of an oligotrophic lake. Aquat Sci 74:611–617. doi: 10.1007/s00027-012-0255-6

Asmus RM (2000) Nutrient fluxes in intertidal communities of a South European lagoon (Ria Formosa) – similarities and differences with a northern Wadden Sea bay (Sylt-Rømø Bay). Hydrobiologia 436:217–235. doi: 10.1023/A:1026542621512

Berelson W, McManus J, Coale K, et al (2003) A time series of benthic flux measurements from Monterey Bay, CA. Cont Shelf Res 23:457–481. doi: 10.1016/S0278-4343(03)00009-8

Bernard RJ, Mortazavi B, Kleinhuizen AA (2015) Dissimilatory nitrate reduction to ammonium (DNRA) seasonally dominates NO3- reduction pathways in an anthropogenically impacted sub-tropical coastal lagoon. Biogeochemistry 125:47–64. doi: 10.1007/s10533-015-0111-6

Binnerup SJ, Jensen K, Revsbech NP, et al (1992) Denitrification, dissimilatory reduction of nitrate to ammonium, and nitrification in a bioturbated estuarine sediment as measured with 15N and microsensor techniques. Appl Environ Microbiol 58:303–313.

Callender E, Hammond DE (1982) Nutrient exchange across the sediment-water interface in the Potomac River estuary. Est Coast Mar Sci 15:395–413. doi: 10.1016/0272-7714(82)90050-6

Chau KW (2002) Field measurements of SOD and sediment nutrient fluxes in a land-locked embayment in Hong Kong. Adv Environ Res 6:135–142. doi: 10.1016/S1093-0191(00)00075-7

Deek A, Emeis K, van Beusekom J (2012) Nitrogen removal in coastal sediments of the German Wadden Sea. Biogeochemistry 108:467–483. doi: 10.1007/s10533-011-9611-1

Devol AH, Christensen JP (1993) Benthic fluxes and nitrogen cycling in sediments of the continental margin of the eastern North Pacific. J Mar Res 51:345–372. doi: 10.1357/0022240933223765

Engelsen A, Hulth S, Pihl L, Sundbäck K (2008) Benthic trophic status and nutrient fluxes in shallow-water sediments. Est Coast Mar Sci 78:783–795. doi: 10.1016/j.ecss.2008.02.018

Gardner WS, Yang L, Cotner JB, et al (2001) Nitrogen dynamics in sandy freshwater sediments (Saginaw Bay, Lake Huron). J Great Lakes Res 27:84–97. doi: 10.1016/S0380-1330(01)70624-7

Henriksen K, Hansen JI, Blackburn TH (1981) Rates of nitrification, distribution of nitrifying bacteria, and nitrate fluxes in different types of sediment from Danish waters. Mar Biol 61:299–304. doi: 10.1007/BF00401569

Hopkinson CS, Wetzel RL (1982) In situ measurements of nutrient and oxygen fluxes in a coastal marine benthic community. Mar Ecol Prog Ser 10:23–35.

Janssen F, Huettel M, Witte U (2005) Pore-water advection and solute fluxes in permeable marine sediments (II): Benthic respiration at three sandy sites with different permeabilities (German Bight, North Sea). Limnol Oceangr 50:779–792. doi: 10.4319/lo.2005.50.3.0779

Jensen MH, Lomstein E, Sørensen J (1990) Benthic NH4+ and NO3- flux following sedimentation of a spring phytoplankton bloom in Aarhus Bight, Denmark. Mar Ecol Prog Ser 61:87–96. doi: 10.3354/meps061087

Laursen AE, Seitzinger SP (2002) The role of denitrification in nitrogen removal and carbon mineralization in Mid-Atlantic Bight sediments. Cont Shelf Res 22:1397–1416. doi: 10.1016/S0278-4343(02)00008-0

Li B, Wang ZQ (2012) Estimation of nitrogen and phosphorus release rates at sediment-water interface of Nansi Lake, China. Adv Mat Res 573-574:573–577. doi: 10.4028/www.scientific.net/AMR.573-574.573

Liikanen A, Tanskanen H, Murtoniemi T, Martikainen PJ (2002) A laboratory microcosm for simultaneous gas and nutrient flux measurements in sediments. Boreal Env Res 7:151–160.

Lim B, Ki B, Choi JH (2011) Evaluation of nutrient release from sediments of artificial lake. J Environ Eng 137:347–354. doi: 10.1061/(ASCE)EE.1943-7870.0000337

Luijn FV (2012) Nitrogen removal by denitrification in the sediments of a shallow lake (Thesis).

McCarthy MJ, Gardner WS, Lehmann MF, et al (2016a) Benthic nitrogen regeneration, fixation, and denitrification in a temperate, eutrophic lake: effects on the nitrogen budget and cyanobacteria blooms. Limnol Oceangr 61:1406–1423. doi: 10.1002/lno.10306

McCarthy MJ, Hamilton SK, Myers JA, Newell SE (2016b) Effects of nitrogen on phosphorus flux from wetland sediments: implications for nutrient management. International Association for Great Lakes Research, 59th Annual Conference on Great Lakes Research

Nedwell DB, Trimmer M (1996) Nitrogen fluxes through the upper estuary of the Great Ouse, England: the role of the bottom sediments. Mar Ecol Prog Ser 142:273–286. doi: 10.3354/meps142273

Nizzoli D, Carraro E, Nigro V, Viaroli P (2010) Effect of organic enrichment and thermal regime on denitrification and dissimilatory nitrate reduction to ammonium (DNRA) in hypolimnetic sediments of two lowland lakes. Water Res 44:2715–2724. doi: 10.1016/j.watres.2010.02.002

Nowicki BL, Nixon SW (1985) Benthic nutrient remineralization in a coastal lagoon ecosystem. Estuaries 8:182–9. doi: 10.2307/1352199

O'Brien JM, Hamilton SK, Kinsman-Costello LE, et al (2012) Nitrogen transformations in a through-flow wetland revealed using whole-ecosystem pulsed. Limnol Oceangr 57:221–234. doi: 10.4319/lo.2012.57.1.0221

Ogilvie B, Nedwell DB, Harrison RM, et al (1997) High nitrate, muddy estuaries as nitrogen sinks:the nitrogen budget of the River Colne estuary (United Kingdom). Mar Ecol Prog Ser 150:217–228. doi: 10.3354/meps150217

Reay WG, Gallagher DL, Simmons GM Jr (1995) Sediment-water column oxygen and nutrient fluxes in nearshore environments of the lower Delmarva Peninsula, USA. Mar Ecol Prog Ser 118:215–227. doi: 10.3354/meps118215

Rizzo WM, Christian RR (1996) Significance of subtidal sediments to heterotrophically-mediated oxygen and nutrient dynamics in a temperate estuary. Estuaries 19:475–13. doi: 10.2307/1352464

Sayama M (2001) Presence of nitrate-sccumulating sulfur bacteria and their influence on nitrogen cycling in a shallow coastal marine sediment. Appl Environ Microbiol 67:3481–3487. doi: 10.1128/AEM.67.8.3481-3487.2001

Shang J, Zhang L, Shi C, Fan C (2013) Influence of Chironomid larvae on oxygen and nitrogen fluxes across the sediment-water interface (Lake Taihu, China). J Environ Sci 25:978–985. doi: 10.1016/S1001-0742(12)60116-8

Small GE, Cotner JB, Finlay JC, et al (2014) Nitrogen transformations at the sediment–water interface across redox gradients in the Laurentian Great Lakes. Hydrobiologia 731:95–108. doi: 10.1007/s10750-013-1569-7

Soana E, Naldi M, Bonaglia S, et al (2015) Benthic nitrogen metabolism in a macrophyte meadow (Vallisneria spiralis L.) under increasing sedimentary organic matter loads. Biogeochemistry 124:387–404. doi: 10.1007/s10533-015-0104-5

Svensson JM, Enrich-Prast A, Leonardson L (2001) Nitrification and dentrification in a eutrophic lake sediment bioturbated by oligochaetes. Aquat Microb Ecol 23:177–186. doi: 10.3354/ame023177

Trimmer M, Nedwell DB, Sivyer DB, Malcolm SJ (1998) Nitrogen fluxes through the lower estuary of the river Great Ouse, England: the role of the bottom sediments. Mar Ecol Prog Ser 163:109–124. doi: 10.3354/meps163109

Tyler AC, McGlathery KJ, Anderson IC (2003) Benthic algae control sediment-water column fluxes of organic and inorganic nitrogen compounds in a temperate lagoon. Limnol Oceangr 48:2125–2137. doi: 10.4319/lo.2003.48.6.2125

Zaman M, Nguyen ML, Gold AJ, et al (2008) Nitrous oxide generation, denitrification, and nitrate removal in a seepage wetland intercepting surface and subsurface flows from a grazed dairy catchment. Aust J Soil Res 46:565–13. doi: 10.1071/SR07217

Table A3.2. Response of NH_4^+, SO_4^{2-}, and SRP to nitrate enrichment in the overlying water columns. Slopes represent the slope of the linear relationship between log transformed solute to bromide (Br^-) ratios and time lapsed (days). Negative fluxes indicate movement of the solute from the water column to the sediment.

		NH_4^- : Br^-		SO_4^{2-} : Br^-		SRP : Br^-		Resulting flux (mmol m^{-2} h^{-1})		
Site	Year	Slope	*p*	Slope	*p*	Slope	*p*	NH_4^-	SO_4^{2-}	SRP
Eagle	2016	0.42	0.11	-0.04	0.56	-0.02	0.77	--	--	--
Gull	2016	**0.41**	<0.001	0.01	0.74	-0.02	0.72	0.02	--	--
KRFP	2016	-0.04	0.19	-0.01	0.42	-0.05	0.22	--	--	--
Loosestrife	2016	-0.10	0.58	-0.11	0.26	-0.40	0.47	--	--	--
LTER	2016	0.08	0.61	-0.41	0.19	0.03	0.71	--	--	--
Ransom	2016	**0.11**	0.02	0.03	0.20	0.00	0.98	0.02	--	--
Sheriffs	2016	0.06	0.23	0.31	0.19	-0.07	0.85	--	--	--
Three	2016	0.09	0.10	0.00	0.90	-0.06	0.22	--	--	--
Turkey	2016	0.27	0.10	**-0.19**	0.03	-0.12	0.24	--	-0.03	--
Windmill	2016	**-0.15**	0.01	-0.01	0.67	-0.07	0.11	-0.07	--	--
Wintergreen	2016	**1.04**	<0.001	**0.69**	<0.001	0.23	0.21	0.10	0.85	--
Wintergreen Out	2016	**0.82**	<0.001	**0.36**	<0.001	-0.15	0.25	0.01	0.61	--

Table A3.3. Results of Kruskal-Wallis rank sum tests and post-hoc pairwise comparisons using Dunn's test to test for differences in nitrate removal rates among sediment types without and with consideration of nitrate enrichment.

	Kruskal-Wallis			Dunn's test	
Comparison[*]	χ^2	d.f.[†]	*p*	*Dunn's z*	Bonferroni *p*[‡]
Comparing nitrate removal rate without consideration of nitrate enrichment					
Floc vs. sand	38.65	3	<0.001	-5.24	<0.001
Floc vs. silt	38.65	3	<0.001	-3.63	<0.001
Floc vs. mud	38.65	3	<0.001	-6.14	<0.001
Comparing nitrate removal rate with consideration of nitrate enrichment					
$Floc_{yes}$ vs. $Floc_{no}$	51.39	7	<0.001	0.34	1.00
$Floc_{yes}$ vs. $sand_{no}$	51.39	7	<0.001	-5.55	<0.001
$Floc_{yes}$ vs. $sand_{yes}$	51.39	7	<0.001	-0.89	1.00
$Floc_{yes}$ vs. $silt_{no}$	51.39	7	<0.001	-4.02	<0.001
$Floc_{yes}$ vs. $silt_{yes}$	51.39	7	<0.001	-1.21	1.00
$Floc_{yes}$ vs. mud_{no}	51.39	7	<0.001	-6.08	<0.001
$Floc_{yes}$ vs. mud_{yes}	51.39	7	<0.001	-2.03	0.59

[*] Comparison of sediment type and then sediment type + enrichment level; Subscript $_{yes}$ = measurement was made by enriching overlying water column nitrate with nitrate above ambient levels; Subscript $_{no}$ = measurement was made at ambient nitrate levels

[†] degrees of freedom

[‡] *p*-value adjusted using a Bonferroni correction

LITERATURE CITED

LITERATURE CITED

Alexander RB, Smith RA, Schwarz GE (2000) Effect of stream channel size on the delivery of nitrogen to the Gulf of Mexico. Nature 403:758–761. doi: 10.1038/35001562

Alexander RB, Smith RA, Schwarz GE, et al (2008) Differences in phosphorus and nitrogen delivery to the Gulf of Mexico from the Mississippi River Basin. Environ Sci Technol 42:822–830. doi: 10.1021/es0716103

Aminot A, Kirkwood DS, Kérouel R (1997) Determination of ammonia in seawater by the indophenol-blue method: Evaluation of the ICES NUTS I/C 5 questionnaire. Mar Chem 56:59–75. doi: 10.1016/S0304-4203(96)00080-1

Anthony JL, Lewis WM (2012) Low boundary layer response and temperature dependence of nitrogen and phosphorus releases from oxic sediments of an oligotrophic lake. Aquat Sci 74:611–617. doi: 10.1007/s00027-012-0255-6

Baron JS, Hall EK, Nolan BT, et al (2012) The interactive effects of excess reactive nitrogen and climate change on aquatic ecosystems and water resources of the United States. Biogeochemistry 114:71–92. doi: 10.1007/s10533-012-9788-y

Bastviken SK, Eriksson PG, Premrov A, Tonderski K (2005) Potential denitrification in wetland sediments with different plant species detritus. Ecol Eng 25:183–190. doi: 10.1016/j.ecoleng.2005.04.013

Bernhardt ES, Blaszczak JR, Ficken CD, et al (2017) Control points in ecosystems: moving beyond the hot spot hot moment concept. Ecosystems 20:665–682. doi: 10.1007/s10021-016-0103-y

Beutel MW, Newton CD, Brouillard ES, Watts RJ (2009) Nitrate removal in surface-flow constructed wetlands treating dilute agricultural runoff in the lower Yakima Basin, Washington. Ecol Eng 35:1538–1546. doi: 10.1016/j.ecoleng.2009.07.005

Boesch DF, Brinsfield RB, Magnien RE (2001) Chesapeake Bay eutrophication: scientific understanding, ecosystem restoration, and challenges for agriculture. J Environ Qual 30:303–18. doi: 10.2134/jeq2001.302303x

Camargo JA, Alonso Á (2006) Ecological and toxicological effects of inorganic nitrogen pollution in aquatic ecosystems: a global assessment. Environ Int 32:831–849. doi: 10.1016/j.envint.2006.05.002

Caraco NF, Lampman G, Cole JJ, et al (1998) Microbial assimilation of DIN in a nitrogen rich estuary: implications for food quality and isotope studies. Mar Ecol Prog Ser 167:59–71. doi: 10.3354/meps167059

Chang J-J, Wu S-Q, Dai Y-R, et al (2013) Nitrogen removal from nitrate-laden wastewater by

integrated vertical-flow constructed wetland systems. Ecol Eng 58:192–201. doi: 10.1016/j.ecoleng.2013.06.039

Cheng FY, Basu NB (2017) Biogeochemical hotspots: role of small water bodies in landscape nutrient processing. Water Resour Res 53:5038–5056. doi: 10.1002/2016WR020102

Dillon PJ, Molot LA (1990) The role of ammonium and nitrate retention in the acidification of lakes and forested catchments. Biogeochemistry 11:23–43. doi: 10.1007/BF00000850

Dinno A (2017) dunn.test: Dunn's test of multiple comparisons using rank sums. R Package version 1.3.5. Retrieved from: https://CRAN.R-project.org/package=dunn.test

Dunn C, Jones TG, Girard A, Freeman C (2014) Methodologies for extracellular enzyme assays from wetland soils. Wetlands 34:9–17. doi: 10.1007/s13157-013-0475-0

El-Habr H, Golterman HL (1990) *In vitro* and *in situ* studies on nitrate disappearance in water-sediment systems of the Camargue (southern France). Hydrobiologia 192:223–232. doi: 10.1007/BF00006017

Farías L, Graco M, Ulloa O (2004) Temporal variability of nitrogen cycling in continental-shelf sediments of the upwelling ecosystem off central Chile. Deep Sea Res Part II 51:2491–2505. doi: 10.1016/j.dsr2.2004.07.029

Finlay JC, Small GE, Sterner RW (2013) Human influences on nitrogen removal in lakes. Science 342:247–250. doi: 10.1126/science.1242575

Galloway JN, Aber JD, Erisman JW, et al (2003) The nitrogen cascade. BioScience 53:341–356. doi: 10.1641/0006-3568(2003)053[0341:TNC]2.0.CO;2

Galloway JN, Dentener FJ, Capone DG, et al (2004) Nitrogen cycles: past, present, and future. Biogeochemistry 70:153–226. doi: 10.1007/s10533-004-0370-0

Galloway JN, Townsend AR, Erisman JW, et al (2008) Transformation of the nitrogen cycle: recent trends, questions, and potential solutions. Science 320:889–892. doi: 10.1126/science.1136674

Gardner WS, McCarthy MJ (2009) Nitrogen dynamics at the sediment–water interface in shallow, sub-tropical Florida Bay: why denitrification efficiency may decrease with increased eutrophication. Biogeochemistry 95:185–198. doi: 10.1007/s10533-009-9329-5

Gersberg R, Elkins B, Goldman C (1983) Nitrogen removal in artificial wetlands. Water Res 17:1009–1014. doi: 10.1016/0043-1354(83)90041-6

Golterman HL (2000) Denitrification and a numerical modelling approach for shallow waters. Hydrobiologia 431:93–104. doi: 10.1023/A:1004062607313

Gruber N, Galloway JN (2008) An Earth-system perspective of the global nitrogen cycle. Nature 451:293–296. doi: 10.1038/nature06592

Han H, Lu X, Burger DF, et al (2014) Nitrogen dynamics at the sediment–water interface in a tropical reservoir. Ecol Eng 73:146–153. doi: 10.1016/j.ecoleng.2014.09.016

Harrison JA, Maranger RJ, Alexander RB, et al (2009) The regional and global significance of nitrogen removal in lakes and reservoirs. Biogeochemistry 93:143–157. doi: 10.1007/s10533-008-9272-x

Howarth RW, Billen G, Swaney D, et al (1996) Regional nitrogen budgets and riverine N & P fluxes for the drainages to the North Atlantic Ocean: natural and human influences. In: Nitrogen Cycling in the North Atlantic Ocean and its Watersheds. Springer Netherlands, Dordrecht, pp 75–139

Ingersoll TL, Baker LA (1998) Nitrate removal in wetland microcosms. Water Res 32:677–684. doi: 10.1016/S0043-1354(97)00254-6

Jordan SJ, Stoffer J, Nestlerode JA (2011) Wetlands as sinks for reactive nitrogen at continental and global scales: a meta-analysis. Ecosystems 14:144–155. doi: 10.1007/s10021-010-9400-z

Kelly CA, Rudd JWM, Hesslein RH, et al (1987) Prediction of biological acid neutralization in acid-sensitive lakes. Biogeochemistry 3:129–140. doi: 10.1007/BF02185189

Klein JJM, Overbeek CC, Jørgensen CJ, Veraart AJ (2017) Effect of temperature on oxygen profiles and denitrification rates in freshwater sediments. Wetlands 37:975–983. doi: 10.1007/s13157-017-0933-1

Kozub DD, Liehr SK (1999) Assessing denitrification rate limiting factors in a constructed wetland receiving landfill leachate. Water Sci Technol 40:75–82. doi: 10.1016/S0273-1223(99)00459-X

Liikanen A, Murtoniemi T, Tanskanen H, et al (2002) Effects of temperature and oxygen availability on greenhouse gas and nutrient dynamics in sediment of a eutrophic mid-boreal lake. Biogeochemistry 59:269–286. doi: 10.1023/A:1016015526712

Loecke TD, Burgin AJ, Riveros-Iregui DA, et al (2017) Weather whiplash in agricultural regions drives deterioration of water quality. Biogeochemistry 133:7–15. doi: 10.1007/s10533-017-0315-z

Lohse L, Malschaert JFP, Slomp CP, et al (1993) Nitrogen cycling in North Sea sediments: interaction of denitrification and nitrification in offshore and coastal areas. Mar Ecol Prog Ser 101:283–296.

McCarthy MJ, Hamilton SK, Myers JA, Newell SE (2016) Effects of nitrogen on phosphorus flux from wetland sediments: implications for nutrient management. International Association for Great Lakes Research, 59th Annual Conference on Great Lakes Research

McClain ME, Boyer EW, Dent CL, et al (2003) Biogeochemical hot spots and hot moments at the interface of terrestrial and aquatic ecosystems. Ecosystems 6:301–312. doi:

10.1007/s10021-003-0161-9

Misiti TM, Hajaya MG, Pavlostathis SG (2011) Nitrate reduction in a simulated free-water surface wetland system. Water Res 45:5587–5598. doi: 10.1016/j.watres.2011.08.019

Molot LA, Dillon PJ (1993) Nitrogen mass balances and denitrification rates in central Ontario lakes. Biogeochemistry 20:195–212. doi: 10.1007/BF00000787

Mulholland PJ, Helton AM, Poole GC, et al (2008) Stream denitrification across biomes and its response to anthropogenic nitrate loading. Nature 452:202–205. doi: 10.1038/nature06686

Murphy J, Riley JP (1962) A modified single solution method for the determination of phosphate in natural waters. Analytica Chimica Acta 27:31–36. doi: 10.1016/S0003-2670(00)88444-5

O'Brien JM, Dodds WK (2010) Saturation of NO_3^- uptake in prairie streams as a function of acute and chronic N exposure. J N Am Benthol Soc 29:627–635. doi: 10.1899/09-021.1

O'Brien JM, Hamilton SK, Kinsman-Costello LE, et al (2012a) Nitrogen transformations in a through-flow wetland revealed using whole-ecosystem pulsed. Limnol Oceangr 57:221–234. doi: 10.4319/lo.2012.57.1.0221

O'Brien JM, Hamilton SK, Podzikowski L, Ostrom N (2012b) The fate of assimilated nitrogen in streams: an in situ benthic chamber study. Freshwater Biol 57:1113–1125. doi: 10.1111/j.1365-2427.2012.02770.x

Peterson BJ, Wollheim WM, Mulholland PJ, et al (2001) Control of nitrogen export from watersheds by headwater streams. Science 292:86–90. doi: 10.1126/science.1056874

Puckett LJ, Tesoriero AJ, Dubrovsky NM (2011) Nitrogen contamination of surficial aquifers—a growing legacy. Environ Sci Technol 45:839–844. doi: 10.1021/es1038358

R Core Team (2017) R: A language and environment for statistical computing. Vienna: R Foundation for Statistical Computing. Available online at: https://www.R-project.org/

Rabalais NN, Turner RE, Wiseman WJ (2001) Hypoxia in the Gulf of Mexico. J Environ Qual 30:320–10. doi: 10.2134/jeq2001.302320x

Reay DS, Nedwell DB, Priddle J, Ellis-Evans JC (1999) Temperature dependence of inorganic nitrogen uptake: reduced affinity for nitrate at suboptimal temperatures in both algae and bacteria. Appl Environ Microbiol 65:2577–2584.

Risgaard-Petersen N (2003) Coupled nitrification-denitrification in autotrophic and heterotrophic estuarine sediments: On the influence of benthic microalgae. Limnol Oceangr 48:93–105. doi: 10.4319/lo.2003.48.1.0093

Risgaard-Petersen N, Rysgaard S, Nielsen LP, Revsbech NP (2003) Diurnal variation of denitrification and nitrification in sediments colonized by benthic microphytes. Limnol Oceangr 39:573–579. doi: 10.4319/lo.1994.39.3.0573

RStudio Team (2017) RStudio: Integrated development for R. Boston, MA: RStudio Inc.

Rupert MG (2008) Decadal-scale changes of nitrate in ground water of the United States, 1988–2004. J Environ Qual 37:S–240–9. doi: 10.2134/jeq2007.0055

Rysgaard S, Risgaard-Petersen N, Niels Peter S, et al (2003) Oxygen regulation of nitrification and denitrification in sediments. Limnol Oceangr 39:1643–1652. doi: 10.4319/lo.1994.39.7.1643

Saunders DL, Kalff J (2001) Denitrification rates in the sediments of Lake Memphremagog, Canada–USA. Water Res 35:1897–1904. doi: 10.1016/S0043-1354(00)00479-6

Seitzinger S, Harrison JA, Böhlke JK, et al (2006) Denitrification across landscapes and waterscapes: a synthesis. Ecol Appl 16:2064–2090. doi: 10.1890/1051-0761(2006)016[2064:DALAWA]2.0.CO;2

Seitzinger SP, Mayorga E, Bouwman AF, et al (2010) Global river nutrient export: a scenario analysis of past and future trends. Global Biogeochem Cycles. doi: 10.1029/2009GB003587

Seitzinger SP, Styles RV, Boyer EW, et al (2002) Nitrogen retention in rivers: model development and application to watersheds in the northeastern U.S.A. Biogeochemistry 57/58:199–237.

Small GE, Cotner JB, Finlay JC, et al (2014) Nitrogen transformations at the sediment–water interface across redox gradients in the Laurentian Great Lakes. Hydrobiologia 731:95–108. doi: 10.1007/s10750-013-1569-7

Smith RA, Schwarz GE, Alexander RB (1997) Regional interpretation of water-quality monitoring data. Water Resour Res 33:2781–2798. doi: 10.1029/97WR02171

Smith VH, Tilman GD, Nekola JC (1999) Eutrophication: impacts of excess nutrient inputs on freshwater, marine, and terrestrial ecosystems. Environ Pollut 100:179–196. doi: 10.1016/S0269-7491(99)00091-3

Strokal M, Yang H, Zhang Y, et al (2014) Increasing eutrophication in the coastal seas of China from 1970 to 2050. Mar Pollut Bull 85:123–140. doi: 10.1016/j.marpolbul.2014.06.011

Svensson JM, Enrich-Prast A, Leonardson L (2001) Nitrification and dentrification in a eutrophic lake sediment bioturbated by oligochaetes. Aquat Microb Ecol 23:177–186. doi: 10.3354/ame023177

Townsend AR, Howarth RW, Bazzaz FA, et al (2003) Human health effects of a changing global nitrogen cycle. Front Ecol Environ 1:240–246. doi: 10.1890/1540-9295(2003)001[0240:HHEOAC]2.0.CO;2

Vitousek PM, Mooney HA, Lubchenco J, Melillo JM (1997) Human domination of Earth's ecosystems. Science 277:494–499. doi: 10.1126/science.277.5325.494

Walker RR, Snodgrass WJ (1986) Model for sediment oxygen demand in lakes. J Environ Eng 112:25–43. doi: 10.1061/(ASCE)0733-9372(1986)112:1(25)

Wetzel RG (2001) Limnology: Lake and River Ecosystems, 3rd edn. Academic Press, San Diego

Windolf JR, Jeppesen E, Jensen J, Kristensen P (1996) Modelling of seasonal variation in nitrogen retention and in-lake concentration: a four-year mass balance study in 16 shallow Danish lakes. Biogeochemistry 33:1–20. doi: 10.1007/BF00000968

Wollheim WM, Vörösmarty CJ, Bouwman AF, et al (2008) Global N removal by freshwater aquatic systems using a spatially distributed, within-basin approach. Global Biogeochem Cycles. doi: 10.1029/2007GB002963

Yan W, Mayorga E, Li X, et al (2010) Increasing anthropogenic nitrogen inputs and riverine DIN exports from the Changjiang River basin under changing human pressures. Global Biogeochem Cycles. doi: 10.1029/2009GB003575

Yasin JA, Kroeze C, Mayorga E (2010) Nutrients export by rivers to the coastal waters of Africa: past and future trends. Global Biogeochem Cycles. doi: 10.1029/2009GB003568

CHAPTER 4

TRANSPORT MECHANISMS DRIVING EXCHANGE BETWEEN FLOCCULENT SEDIMENT AND OVERLYING WATER IN SHALLOW FRESHWATERS

ABSTRACT

Biogeochemical processes in shallow aquatic ecosystems are strongly influenced by sediment-water interactions. In waterbodies lacking significant flow, the movement of heat, nutrients, and oxygen across the sediment-water interface is typically dominated by molecular diffusion, a relatively slow process, though other processes such as bioturbation, wind-induced resuspension of sediments, and ebullition pay important roles as well. More recently, buoyancy-induced flow (also known as natural convection)—fluid flow induced by thermal gradients—has been recognized as a potentially important exchange mechanism in shallow freshwaters. This transport phenomenon can result from rapid nocturnal cooling of overlying waters or temperature differences between sediments and overlying water during seasonal cooling. In this chapter, I present multiple lines of evidence that demonstrate that thermal gradients drive buoyancy-induced flow in loosely consolidated layers of flocculent sediment—a rarely investigated, though common sediment type—in shallow waterbodies. Supporting evidence includes direct observation of fluid movement with a high-resolution acoustic Doppler profiler and results from hydrodynamic models that make use of temperature time series measured in floc sediments and overlying waters. Consequently, I suggest that buoyancy flow is likely an important transport mechanism driving the exchange of heat and solute mass across the sediment-water interface in shallow waterbodies.

INTRODUCTION

Although often small in area, shallow aquatic ecosystems are recognized as being abundant in many landscapes, and their cumulative roles in global biogeochemical cycles (including carbon sequestration and nitrogen retention) are increasingly appreciated (Downing et al. 2008; Harrison et al. 2009; Tranvik et al. 2009; Cheng and Basu 2017). However, shallow waterbodies have been far less studied than larger lakes and rivers (Smith et al. 2002; Harrison et al. 2009; Downing 2010; Raymond et al. 2013). To understand how these ecosystems regulate biogeochemical fluxes and how they might respond to global change drivers, we need to further investigate the controls on biogeochemical rates and transport processes in shallow waters.

In all but the deepest waterbodies, sediment-water interactions strongly influence biogeochemical processes (McClain et al. 2003; Abbott et al. 2016; Bernhardt et al. 2017), including aquatic ecosystem metabolism and productivity, fluxes of nutrients to downstream ecosystems, and atmospheric greenhouse gas exchanges (Grimm and Fisher 1984; Golterman 2004; Megonigal et al. 2004). The influence of the sediment-water interface (SWI) is especially great in shallow waters, which often have high watershed inputs of groundwater, nutrients and organic matter and tend to be very productive (Wetzel 1992; Alexander et al. 2000; Beaulieu et al. 2011; Helton et al. 2011).

In shallow waterbodies that are continuously inundated, flocculent sediments, or floc—loosely consolidated organic deposits with dry bulk densities frequently <0.1 g cm^{-3} and water contents frequently >90%—often occur as thick layers (>10 cm; Kincaid, Chapter 1). This loosely structured layer represents a potentially reactive SWI that can be considered an ecotone between the water column and the sediment porewater and deeper groundwater. As with other organic sediments, nutrients and gases such as ammonium, phosphorus, and methane tend to

accumulate in floc at concentrations that frequently surpass those in overlying waters by more than 1-2 orders of magnitude (Kincaid, Chapter 1). Therefore, floc accumulations, like other better-studied SWIs (e.g., deep lake benthic, riparian, and river hyporheic zones), may play an important role in the biogeochemical cycles of freshwater ecosystems.

The relative importance of the floc-water interface to biogeochemical cycles in these waterbodies is in part controlled by the transport mechanisms driving solute exchange across the SWI. In lentic (non-flowing) waters, the movement of heat, nutrients, and oxygen across the SWI is slow because transport within the sediments is typically dominated by molecular diffusion (Mortimer 1971; Berner 1980; Wetzel 2001). However, there are mechanisms that can enhance transport rates in certain cases, including bioturbation (Krantzberg 1985; Svensson and Leonardson 1996; Van Rees et al. 1996; Nogaro and Burgin 2014; Hölker et al. 2015), wind-induced sediment resuspension (Simon 1989; Longhi et al. 2013; Kleeberg and Herzog 2014; Plach et al. 2014), and ebullition (release of methane-rich bubbles) (Liikanen et al. 2003; Canário et al. 2009; Flury et al. 2015). Similarly, there are times when buoyancy-induced flow (also known as natural convection), which includes both molecular diffusion and advective transport (transport via fluid flow), may accelerate the transfer of heat and mass within the sediment and across the SWI. Convective mixing occurs as a result of gravitational instability when water overlying the sediment becomes cooler and denser than fluid in the sediment matrix. If the thermal and resulting density gradient is great enough, the cooler water sinks and the warmer water rises, producing buoyancy-induced flow and interfacial transfer of heat and mass.

Multiple studies have demonstrated that buoyancy-induced flow occurs in sediments of a variety of lentic water bodies under different conditions. In large lakes convective mixing and the subsequent transfer of heat and mass across the SWI occurs when internal seiches (internal

waves) replace water above the sediment with colder water (Kirillin et al. 2009; Bernhardt et al. 2014). In shallow lakes and ponds, this exchange mechanism can occur during seasonal cooling of water overlying warmer sediments in autumn (Lappalainen 1982; Golosov and Ignatieva 1999) and spring (Lappalainen 1982; Tarasiuk et al. 2010). In an attempt to understand solute transport mechanisms in a shallow mire, researchers demonstrated that nocturnal cooling of overlying water could induce buoyancy flow in saturated peat moss (Rappoldt et al. 2011). In all of these examples, thermal gradients resulted in buoyancy-induced flows that drove exchanges between overlying water and sediments with high porosities. Floc sediments are an even more loosely consolidated and highly porous medium, and thus I predicted that fluid movement will drive exchange between floc porewaters and overlying water if there are substantial thermal gradients at this interface that produce buoyancy-induced flows.

Given that shallow water columns often experience diel temperature oscillations of several degrees with diurnal thermal stratification and nocturnal mixing (Condie and Webster 2001; Ford et al. 2002; MacIntyre 2006; Poindexter et al. 2016) and that flocculent sediments may present less resistance to convective flow than denser sediments, I hypothesized that buoyancy-induced flow is an important solute exchange mechanism for floc layers in shallow lentic water bodies. In this chapter, I present multiple lines of evidence to demonstrate that buoyancy flow is an important transport mechanism in flocculent sediments. I employ both heat transport modeling and direct observations of flow in shallow waterbodies to demonstrate that buoyancy-induced flow drives the transfer of heat across the floc-water interface, at least episodically.

METHODS

Site selection

The LTER Kettle Pond (Figure 4.1) is a small pond (surface area <0.01 km^2; maximum water depth of approximately 1 m) located in Kalamazoo County, MI, USA near the Kellogg Biological Station. The pond occupies a small glacial depression (kettle) surrounded by a mature northern, mixed hardwood forest. There are no fish in the pond, and algae and duckweed (primarily *Wolffia* sp.) dominate primary production. The bottom consists of a flocculent organic sediment layer, ranging in thickness from 5 to 50 cm, overlying a consolidated clay mixture. I chose this site because groundwater inputs are minimal and it is relatively protected from the influences of wind.

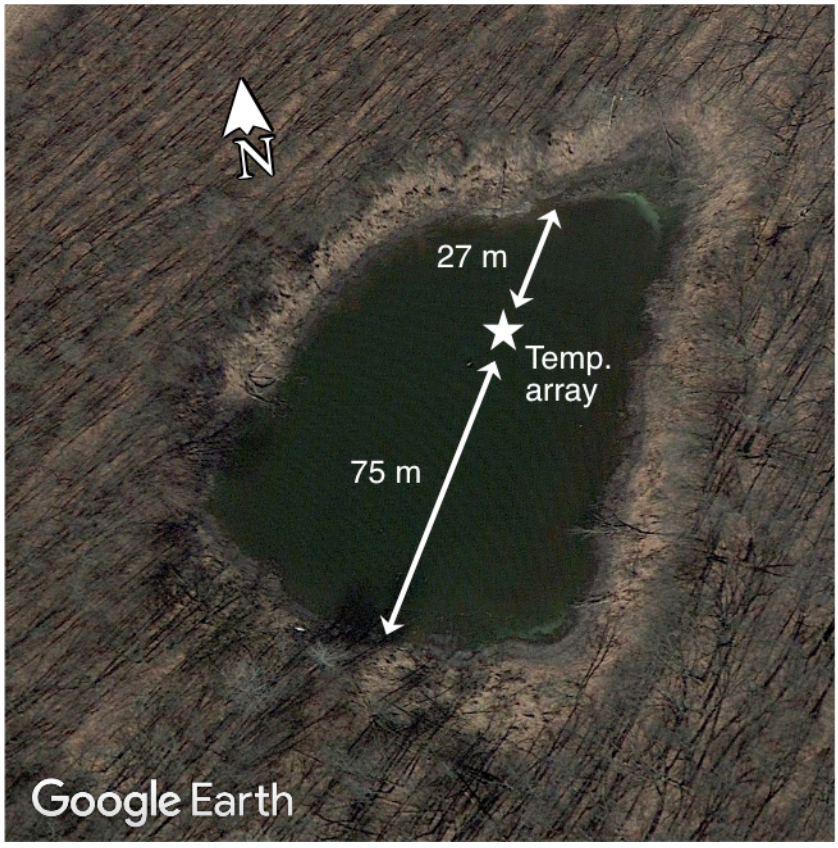

Figure 4.1. Aerial photo of the LTER Kettle Pond. The star denotes the location of the vertical temperature array (temp. array).

Measuring temperature profiles

I measured temperature continuously within and above the flocculent sediment in the pond in October 2016 at a location 27 m from the northern wetted edge (Figure 4.1). At this location, the depth of the water column was 0.66 m and the floc layer was 0.18 m thick. The temperature logging setup consisted of a vertical array of Thermocron® iButton temperature loggers (model DS1922L, Maxim Integrated, San Jose, CA; ± 0.5°C accuracy; 0.0625°C resolution). The loggers were set into predrilled holes (16.67 mm diameter) in a strip of rigid polypropylene plastic (5 cm width, 1.22 m length) the same thickness as the iButtons (4.77 mm). The array was inserted vertically into the floc layer and secured to a metal fence post such that loggers were located at 0.54 and 0.02 m above and 0.00, 0.02, 0.04, 0.06, 0.08, 0.10, 0.14, and 0.18 m below the floc-water interface. Temperatures were logged every 10 minutes.

Measuring high-resolution water current velocity profiles

I measured high-resolution water current velocity profiles continuously within the overlying water column and the upper layers of the flocculent sediment for a 24-hour period (October 23-24, 2016). To do this, I mounted a Nortek 2-MHz Aquadopp® High Resolution Acoustic Doppler Current Profiler (ADCP; Nortek AS, Rud, Norway) to a stand with the sensors facing the sediment layer (downward-looking) and the top of the ADCP just under the surface of the water. The instrument measured 3D velocity profiles every second at a vertical resolution of 1 cm.

Sediment sampling and analyses

Following thermal data collection, I collected a sediment core at the location of the vertical temperature array to analyze sediment samples for water and organic matter content, dry bulk density, and porosity. Using a plastic coring tube (7.2 internal diameter), I sampled the entire floc layer and then transported the core to the lab for processing. The core was sectioned into 1-5 cm depth intervals by extruding the sediment out of the top of the core. If the water content of the floc was too high, I scooped the section out of the core. I determined the water content (% of wet weight) by drying homogenized subsamples in the oven at 60°C. After weighing the dried subsamples, I determined organic matter content (% of dry weight) by loss on ignition upon combusting the subsamples at 550°C for two hours. I calculated the dry bulk density and porosity of each depth layer assuming a sediment particle density of 1.25 and 2.65 g cm^{-3} for organic and inorganic particles, respectively (Avnimelech et al. 2001).

During a previous sampling event in a nearby pond, I measured thermal properties of saturated flocculent sediment, including thermal diffusivity and volumetric specific heat capacity of flocculent sediment, using a KD2 Pro Thermal Properties Analyzer (Decagon Devices, Inc., Pullman, WA, USA). To do this, I collected several intact cores of flocculent sediment from the pond. In the laboratory, I inserted the dual-needle sensor into the core at known depths via pre-drilled holes in the core tube covered with vinyl tape. All measurements were made between 21-23°C.

Nomenclature for heat transport modeling

C	Forchheimer constant, Eqs. (7, 8)
c_P	specific heat capacity at constant pressure
Da	Darcy number, Eqs. (12, 13)
Fo_f	flow Fourier number, Eqs. (12, 13)
Fo_t	thermal Fourier number, Eqs. (13, 14)
g	gravitational acceleration
H	height of floc layer
k	thermal conductivity of water
K	permeability of the floc layer
p	pressure
Ra	Rayleigh number, Eq. (13)
T	temperature
t	time
u, v	horizontal and vertical velocity components
$\lvert\vec{V}\rvert$	$\sqrt{u^2 + v^2}$
x, y	horizontal and vertical Cartesian coordinates

Greek symbols

α	thermal diffusivity
β	coefficient of thermal expansion
ε	porosity of the floc layer
μ	coefficient of dynamic viscosity
ν	kinematic viscosity
ρ	density
τ	dimensionless time
θ	dimensionless temperature

Suffixes

C	relatively cold surface
e	effective property for the floc layer
f	property of fluid portion of floc matrix
H	relatively hot surface
s	property of solid portion of floc matrix
w	property of overlying water
∞	ambient conditions

Two-dimensional heat transport modeling

Model domain and governing equations—I simulated buoyancy-induced flows in the water column and the flocculent sediment layer in the LTER Kettle Pond for a period of 8 days from 18 October to 26 October 2016; the first 4 days were used for model spin-up and the last 4 days were used for comparisons and presentation of results. Our modeling domain considered a cross-section of the floc and overlying water in the pond that extends 600 cm in the x-direction and 72 cm in the y-direction (Figure 4.2). Previous research examined buoyancy-induced flows in sediment layers in a different wetland (e.g., Rappoldt et al. 2011); however, in the high-porosity floc layers considered in this work, the interface between floc and the overlying water may be highly dynamic, allowing free exchange of heat, solute mass, and momentum. A novel aspect of

the present work is the integrated modeling of the floc and the overlying water as a single connected system. The governing equations in this approach change smoothly from those for a porous medium to the equations for a pure fluid while obeying continuity of fluxes at the interface. To allow for non-Darcy effects, I used a Brinkman-extended Forchheimer flow model for the porous medium; for the overlying water its equations reduce to the well-known Navier-Stokes equations for flow in viscous fluids. The switch from one domain to the other was achieved using a binary flag δ as defined in subsequent text.

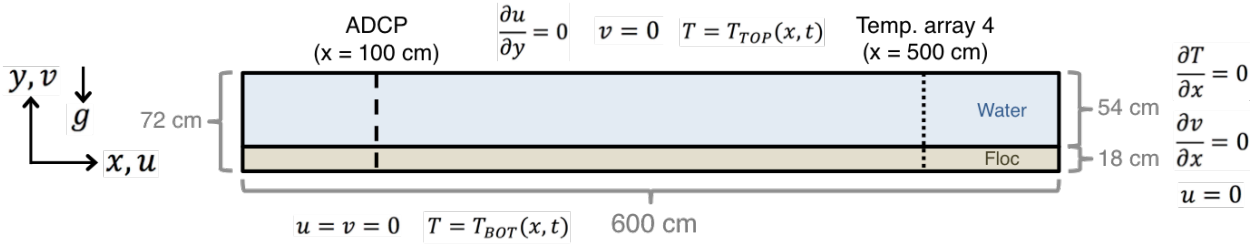

Figure 4.2. Modeling domain for buoyancy-induced flow simulations in the LTER Kettle Pond. The vertical dashed lines indicate the locations of the acoustic Doppler current profiler (ADCP) and the vertical temperature array.

The flow analysis was governed by the following two-dimensional equations expressing the conservation of mass, momentum, and energy. In the equations below, u and v denote the longitudinal (East-West) and vertical (up-down) components of velocity in the x and y coordinate directions as shown in Figure 4.2. Variables shown with a prime (e.g., u', v', T', x', y') denote dimensional quantities with units while their non-dimensional counterparts do not have primes. The subscript w in the equations denotes properties of "water" while e denotes effective properties for the porous medium.

Continuity and momentum in the water column:

$$\frac{\partial u}{\partial x} + \frac{\partial v}{\partial y} = 0 \tag{2}$$

$$\rho_w \left(\frac{\partial u}{\partial t} + u\frac{\partial u}{\partial x} + v\frac{\partial u}{\partial y}\right) = -\frac{\partial p}{\partial x} + \mu\nabla^2 u \tag{3}$$

$$\rho_w \left(\frac{\partial v}{\partial t} + u\frac{\partial v}{\partial x} + v\frac{\partial v}{\partial y}\left(u\frac{\partial v}{\partial x} + v\frac{\partial v}{\partial y}\right)\right) = -\frac{\partial p}{\partial y} + \mu\nabla^2 v + \rho_w g\beta(T - T_\infty) \tag{4}$$

Energy in the water column:

$$\rho_w c \left(\frac{\partial T}{\partial t} + u\frac{\partial T}{\partial x} + v\frac{\partial T}{\partial y}\right) = k\nabla^2 T \tag{5}$$

The two-dimensional governing equations for the non-Darcy model were derived using well-known volume averaging procedures for flow through a porous medium (Whitaker 1999; Prosperetti and Tryggvason 2007; Gray and Miller 2013):

Continuity and momentum for the floc layer:

$$\frac{\partial u'}{\partial x'} + \frac{\partial v'}{\partial y'} = 0, \tag{6}$$

$$\frac{\rho}{\varepsilon}\cdot\frac{\partial u'}{\partial t'} + \frac{\rho}{\varepsilon^2}\left(u'\frac{\partial u'}{\partial x'} + v'\frac{\partial u'}{\partial y'}\right) = -\frac{\partial p'}{\partial x'} + \frac{\mu'}{\varepsilon}\nabla^2 u' - \frac{\mu'}{K}u' - \frac{C}{\sqrt{K}}\rho|\overrightarrow{V'}|u' \tag{7}$$

$$\frac{\rho}{\varepsilon}\cdot\frac{\partial v'}{\partial t'} + \frac{\rho}{\varepsilon^2}\left(u'\frac{\partial v'}{\partial x'} + v'\frac{\partial v'}{\partial y'}\right) = -\frac{\partial p'}{\partial y'} + \rho_w g\beta(T - T_\infty) + \frac{\mu'}{\varepsilon}\nabla^2 v' - \frac{\mu'}{K}v' - \frac{C}{\sqrt{K}}\rho|\overrightarrow{V'}|v' \tag{8}$$

Energy for the floc layer:

$$\zeta\frac{\partial T}{\partial t'} + u'\frac{\partial T}{\partial x'} + v'\frac{\partial T}{\partial y'} = \frac{\partial}{\partial x'}\left(\alpha_e\frac{\partial T}{\partial x'}\right) + \frac{\partial}{\partial y'}\left(\alpha_e\frac{\partial T}{\partial y'}\right) \tag{9}$$

In Eqs. (7) and (8), the last three terms on the right hand side of the equations are (from left to right) the Brinkman (or friction) term, the Darcy term, and the Forchheimer (or inertia) term, respectively. As fluid flows past the porous medium matrix, two types of drag forces are important: frictional or viscous drag that arises from the friction between the fluid and the solid

matrix and pressure or form drag that results from eddy shedding behind the solid matrix. The Darcy term accounts for the frictional drag while the Forchheimer term accounts for the form drag. The parameter C (called the Forchheimer constant) represents the form drag and values of C for floc material are unknown. However, C can be calculated using empirical relations based on the experimental data of Ergun (1952) who determined drag coefficients for gas flow in packed beds of spheres:

$$C = \frac{1.75}{\sqrt{150}}\left(\frac{1}{\varepsilon^{3/2}}\right)$$

where ε denotes porosity. For $\varepsilon = 0.95$ used in this work, C is equal to 1.544.

In the energy equations (9 and 13), ζ denotes the heat capacity ratio of the porous medium to that of water:

$$\zeta = \left(\frac{\varepsilon\rho_f c_{pf} + (1-\varepsilon)\rho_s c_s}{\rho_f c_{pf}}\right) \tag{10}$$

Boundary and initial conditions are needed to solve the above system of equations. For the momentum equations, I used the no-slip boundary condition ($u = v = 0$) at the bottom of the domain at $y = 0$ (Figure 4.2). This condition represents the flow physics accurately as long as vertical groundwater upwelling (downwelling) into (out of) the domain can be neglected. For the top surface, I used the following boundary condition: $v = 0, \frac{\partial u}{\partial y} = 0$ (Figure 4.2), which is based on the assumption that water does not leave the domain at the top boundary. Since there is no obvious choice for the horizontal extent of the domain, I considered a 6 m long domain of the floc layer and the overlying water column in which ADCP and temperature sensors were deployed (Figure 4.2). To minimize "boundary effects" that could potentially affect flow physics close to boundaries, I used symmetry boundary conditions on the left and right boundaries as shown in Figure 4.2. For the energy equation, I used the observed time-dependent temperatures

at the top of the water column and the bottom of the floc layer to drive the flow. Lateral boundaries were assumed to be adiabatic (no heat transfer at these boundaries). Initial conditions were based on the assumption that the fluid was isothermal and at rest ($u = v = T = 0$).

The governing equations for the overlying water and floc layer were solved using a one-domain approach. This approach is advantageous because it automatically satisfies the interfacial conditions (continuity of pressure, temperature, and velocities) without requiring complicated inner iteration loops for values at the interface (Martins-Costa and Saldanha de Gama 1994). To combine the two sets of equations for the two regions into a single set of equations, I used a binary flag δ as described in a later section.

Dimensionless equations—The governing equations can be made dimensionless using a variety of length and time scales, and characteristic variables such as velocity or pressure can be derived from the length and time scales. The choice of these scales and variables depends on the processes of interest. In this model, the diurnal cycles of heating and cooling and their effect on flow are of interest; therefore, I chose $t_0 = 43,200$ seconds (12 hours) as a fundamental time scale. The thickness of the floc layer H measured at the site was used as the characteristic length scale although other choices were possible (e.g., depth of thermal propagation of the diurnal cycle). I made the above equations dimensionless using the following scales and dimensionless terms:

$$x = \frac{x'}{H}\,, \qquad u = \frac{u'}{U_c}\,, \qquad U_c = \frac{H}{t_0}\,, \qquad p = \frac{p' {t_0}^2}{\rho H^2} = \frac{p'}{\rho {U_c}^2}\,,$$

$$y = \frac{y'}{H}\,, \qquad v = \frac{v'}{U_c}\,, \qquad \tau = \frac{t}{t_0}\,,$$

$$Fo_f = \frac{\nu t_0}{H^2}\ , \quad Fo_t = \frac{\alpha t_0}{H^2}\ , \qquad Fo_{t,e} = \frac{\alpha_e t_0}{H^2}\ , \quad Ra(t) = \frac{g\beta T(t) H^3}{\nu\alpha}\ ,$$

$$Da = \frac{K}{H^2} \tag{11}$$

Above, the Rayleigh number (Ra) denotes the strength of buoyant convection. In most similar studies, ΔT is treated as a constant, and thus the Rayleigh number is also a constant. In our analysis, temperature at the top and bottom and bottom surfaces of the computational domain changed with time; however, the average bottom temperature was higher than the average top temperature, and therefore the mathematical problem is a variant of the classical bottom heating case, although, as shown in Figure 4.4, the nature of heating changes from bottom-heating to top-heating and vice versa. This transition introduces additional complexity to the analysis. To address this complexity, I defined the dimensionless temperature based on the average bottom temperature $\overline{T_H}$ (where the suffix H denotes a relatively hot surface) and the average surface temperature $\overline{T_C}$ (where the suffix C denotes a relatively cold surface):

$$\theta = \left(\frac{T - \overline{T_C}}{\overline{T_H} - \overline{T_C}}\right), \qquad \Delta T(t) = |\overline{T_H} - \overline{T_C}|$$

The absolute value of the temperature difference was used to make the Rayleigh number positive while the temperature boundary conditions at the top and bottom surfaces control the direction of flow. The Fourier number Fo_t is a dimensionless number associated with the degree of thermal penetration in diffusion problems. In addition to this classic Fourier number based on thermal diffusivity, I also included a viscous Fourier number Fo_f based on the kinematic viscosity of water (ν). The resulting dimensionless equations are shown below (see Appendix for derivation of each term):

Momentum equations for the floc layer and the overlying water column:

$$\varepsilon\frac{\partial u}{\partial \tau}+\left(u\frac{\partial u}{\partial x}+v\frac{\partial u}{\partial y}\right)=-\varepsilon^2\frac{\partial p}{\partial x}+Fo_f\nabla^2 u-\frac{\delta Fo_f}{Da}\varepsilon u-\frac{\delta C}{\sqrt{\frac{Da}{\varepsilon}}}\sqrt{u^2+v^2}\cdot u \tag{12}$$

$$\varepsilon\frac{\partial v}{\partial \tau}+\left(u\frac{\partial v}{\partial x}+v\frac{\partial v}{\partial y}\right)$$

$$=-\varepsilon^2\frac{\partial p}{\partial y}+Fo_f\nabla^2 v-\frac{\delta Fo_f}{Da}\varepsilon v-\frac{\delta C}{\sqrt{\frac{Da}{\varepsilon}}}\sqrt{u^2+v^2}\cdot v+\ Ra\cdot Fo_f\cdot Fo_{t,e}$$

$$\cdot\varepsilon^2\theta \tag{13}$$

Energy equation for the floc layer and the water column:

$$\zeta\frac{\partial \theta}{\partial \tau}+\left(u\frac{\partial \theta}{\partial x}+v\frac{\partial \theta}{\partial y}\right)=\left[(1-\delta)Fo_t+\delta Fo_{t,e}\right]\nabla^2\nabla^2\theta \tag{14}$$

In the above equations, I use the binary flag δ to switch between the two domains as such:

$$\delta=\begin{cases}1 & \text{inside floc layer}\\ 0 & \text{outside the layer}\end{cases}$$

The governing equations with the boundary and initial conditions were solved using the SIMPLE (Semi-Implicit Method for Pressure Linked Equations) method (Patankar 1980). A uniform Cartesian grid of 718 (x) x 86 (y) points was used for the computations. Observed temperatures were linearly interpolated to model times and used as boundary conditions at the top and bottom boundaries. A list of dimensional parameters is included in Table 4.1 and values of the dimensionless parameters are available in the Appendix.

Diffusion-only solution—To confirm that buoyancy-induced flow was necessary to reproduce the observed temperature patterns in the pond, I also simulated temperatures in the LTER Kettle Pond assuming that diffusion was the only driver of two-dimensional heat exchange in the

system. To do this, I used the same model as before, but I set the Rayleigh number to zero in Equation 13. This approach eliminates buoyant convection as a driver of fluid flow in the system.

Table 4.1. Parameter values for the buoyancy-induced flow model.

Parameter	Value	Unit	Remark
ΔT	0.349	Kelvin	Temperature difference between the mean temperature at the top of the water column and the mean temperature at the bottom of the floc layer for the 8 day period
t_0	43,200	Second	Half a day
H	0.18	Meter	Thickness of the floc layer
ε	0.95	Unitless	Average porosity of the floc layer
ν	1.12×10^{-6}	$m^2 \cdot s^{-1}$	Kinematic viscosity of water at 15°C
K	1.7×10^{-5}	$m \cdot s^{-1}$	Maximum hydraulic conductivity reported for fine organic sediments in a small lake bed*
α	1.41×10^{-7}	$m^2 \cdot s^{-1}$	Thermal diffusivity of water at 15°C
α_e	1.81×10^{-7}	$m^2 \cdot s^{-1}$	Measured thermal diffusivity of saturated floc at ~22°C
β	0.16×10^{-3}	$Kelvin^{-1}$	Coefficient of thermal expansion for water at 15°C
$\varepsilon\rho_f c_{pf} + (1-\varepsilon)\rho_s c_s$	3.7448×10^6	$J \cdot m^{-3} \cdot K^{-1}$	Measured volumetric specific heat capacity of saturated floc at ~22°C
ρ_f	999.1	$kg \cdot m^{-3}$	Density of water at 15°C
c_{pf}	4.186×10^3	$J \cdot kg^{-1} \cdot K^{-1}$	Specific heat at constant pressure of water at 15°C
C	0.1544	Unitless	Empirically derived
g	9.81	$m\ s^{-2}$	Gravitational acceleration

* (Rudnick et al. 2014)

RESULTS AND DISCUSSION

ADCP: direct observations of fluid movement

Direct measurements of fluid movement using the ADCP indicate that fluid flow occurs within floc layers. During the 24-hour deployment, I observed multi-directional flow in the floc layer and overlying water. Flow velocities in all directions ranged from 0 to 0.90 m s^{-1} in the floc layer and 0 to 0.53 m s^{-1} in the water column. Vertical velocities measured at the surface of the floc layer ranged from -0.15 to 0.14 m s^{-1} (negative velocities indicate downward movement

of fluid), indicating that convective exchanges across the floc-water interface occurred in both directions.

Vertical profiles of fluid movement measured as speed (velocity magnitude) exhibited patterns that seem to correlate with periods of rapid heating or cooling of the overlying water and periods when the overlying water temperature was considerably lower than the temperature at the bottom of the floc layer (Figure 4.3). The ADCP observations clearly showed that the flow is three-dimensional in nature and that the highest values of velocity generally occurred at the interface between the floc layer and the overlying water. Typical values of the velocity magnitude were of the order of 0.02 m/s (see plot 1, plot 2 and plot 4 in Figure 4.3) although significantly larger values were found at times that coincide with large temperature differences in the system (plot 3 in Figure 4.3).

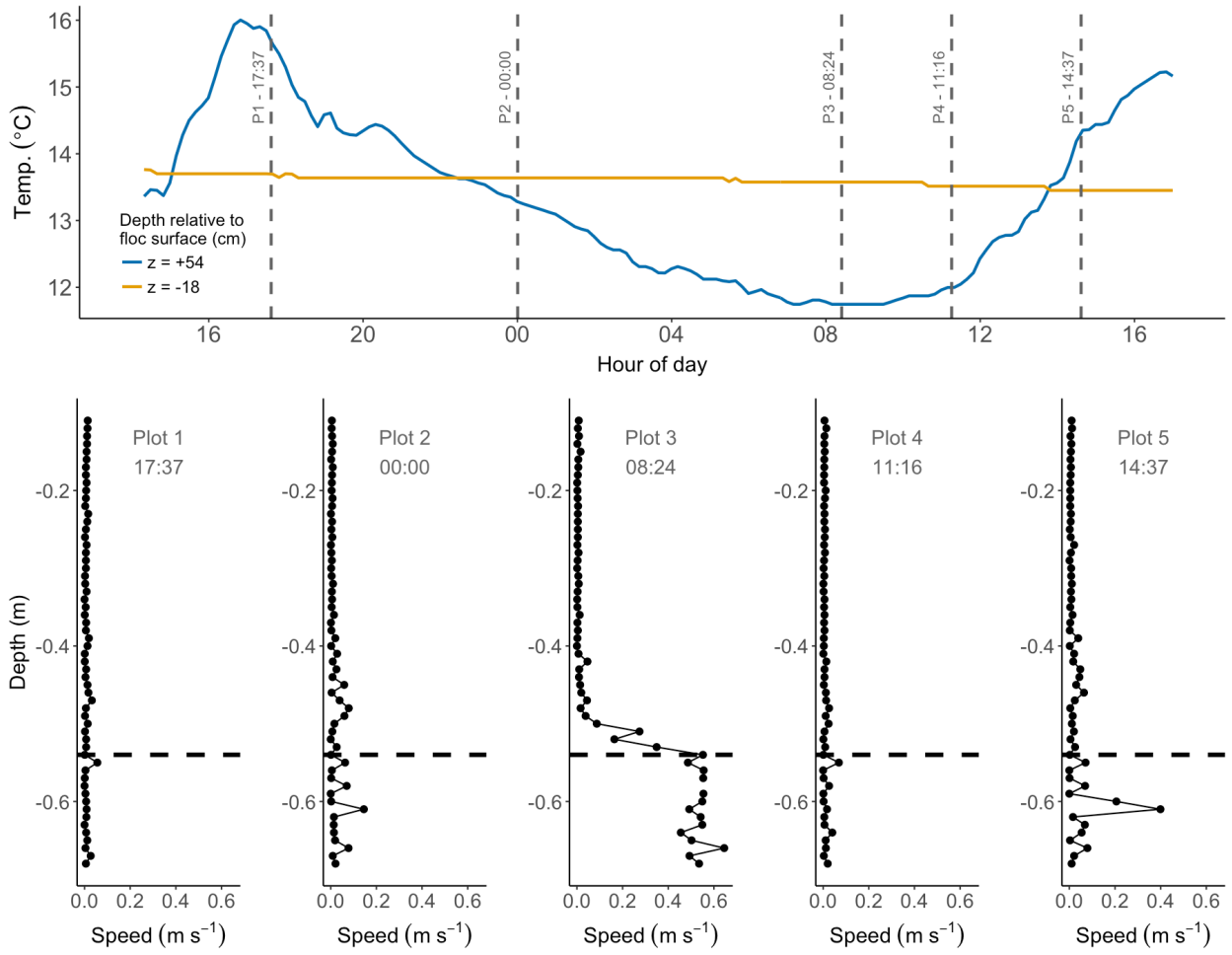

Figure 4.3. (Upper) Temperature times series measured 54 cm above and 18 cm below the floc surface during the 24-hour deployment of the HR-ADCP in the LTER Kettle Pond. (Lower) vertical profiles of the velocity magnitude (speed) of fluid flow at various times throughout the measurement period. The dashed vertical gray lines in the upper plot show at what time point each vertical profile was captured.

Two-dimensional heat transport modeling

Temperature time series—In general, the mean temperature at the bottom of the floc layer for the 8-day modeling period was 0.349°C warmer than the mean temperature at the top of the water column (Figure 4.4). This means that the system was generally heated from the bottom during the modeling period. This scenario can result in buoyancy-induced mixing of the sediment

porewaters which may result in exchanges across the sediment-water interface if the temperature differential between the two layers is large enough (Gebhart et al. 1988; Tritton 1988). However, there were also periods when the water column cooled rapidly (evening), which can induce buoyancy flows in the water column that may lead to exchange across the sediment-water interface if the resulting convective mixing cells penetrate the sediment-layer (Gebhart et al. 1988).

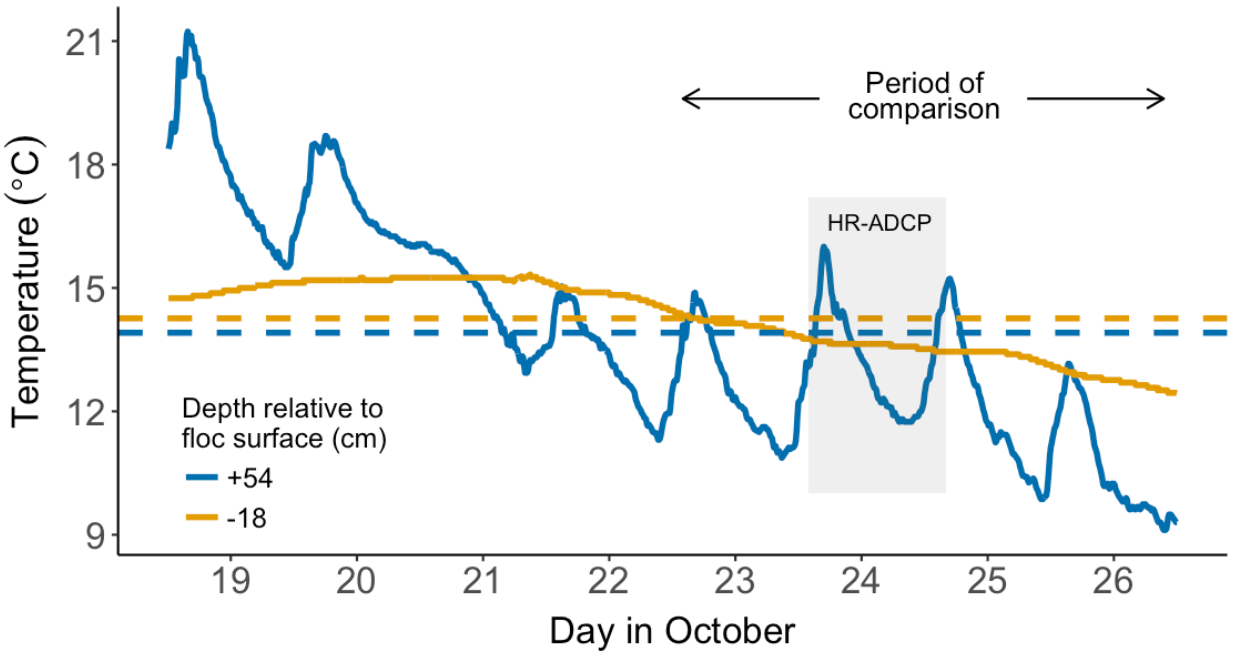

Figure 4.4. Temperature time series from the LTER Kettle Pond during the 8-day modeling period. Observed temperatures are plotted for 54 cm above (solid blue line) and 18 cm below (solid brown line) the floc surface. Eight-day temperature means for those depths are plotted as dashed lines. The first 4 days of temperatures were used for the unsteady or transient solution for the buoyancy-induced flow model, but I only use results from the final 4 days of this temperature series for comparisons. Also shown is the period when the HR-ADCP was deployed in the pond (gray rectangle).

Buoyancy-induced flow model—The temperature time series simulated using the buoyancy-induced flow model (Figure 4.5b) captured the main heating and cooling patterns I observed in the pond (Figure 4.5a), though there were a few notable differences. First, the model failed to

reproduce the elevated bottom temperatures I observed at the site. Second, there were differences in the depths of penetration of the heating and cooling cycles into the water column. Both of these differences could driven by groundwater inflows at the pond that were not measured or specified in the model. Groundwater inflows would represent a flux boundary condition, but the model uses observed bottom temperatures with no associated inflows. The groundwater inflow hypothesis would help explain why the model produced thermal waves that originate from the top boundary and extended all the way to the bottom of the floc layer (most obvious during cooling periods), a pattern that is absent in the observed temperature time series. If relatively warmer groundwater inflows were present, they would limit the depths that these thermal waves would penetrate, especially during cooling periods.

Comparisons of observed and simulated temperatures at selected depths in Figure 4.6 show that while the trends are similar in the top layers, the comparison between observed temperatures and those simulated with the buoyancy-induced flow model becomes progressively worse with depth in the floc layer. In fact, the diffusion-only model seems to match observed temperatures better in deeper floc layers (Figure 4.6). The poor performance of the buoyancy-induced flow model is partially due to a crude grid size and time step used in this version of the model. Future model runs will refine both of these. Further, a flux boundary condition that allows water to enter the domain from the subsurface with a temperature corresponding to the groundwater temperature may improve model performance.

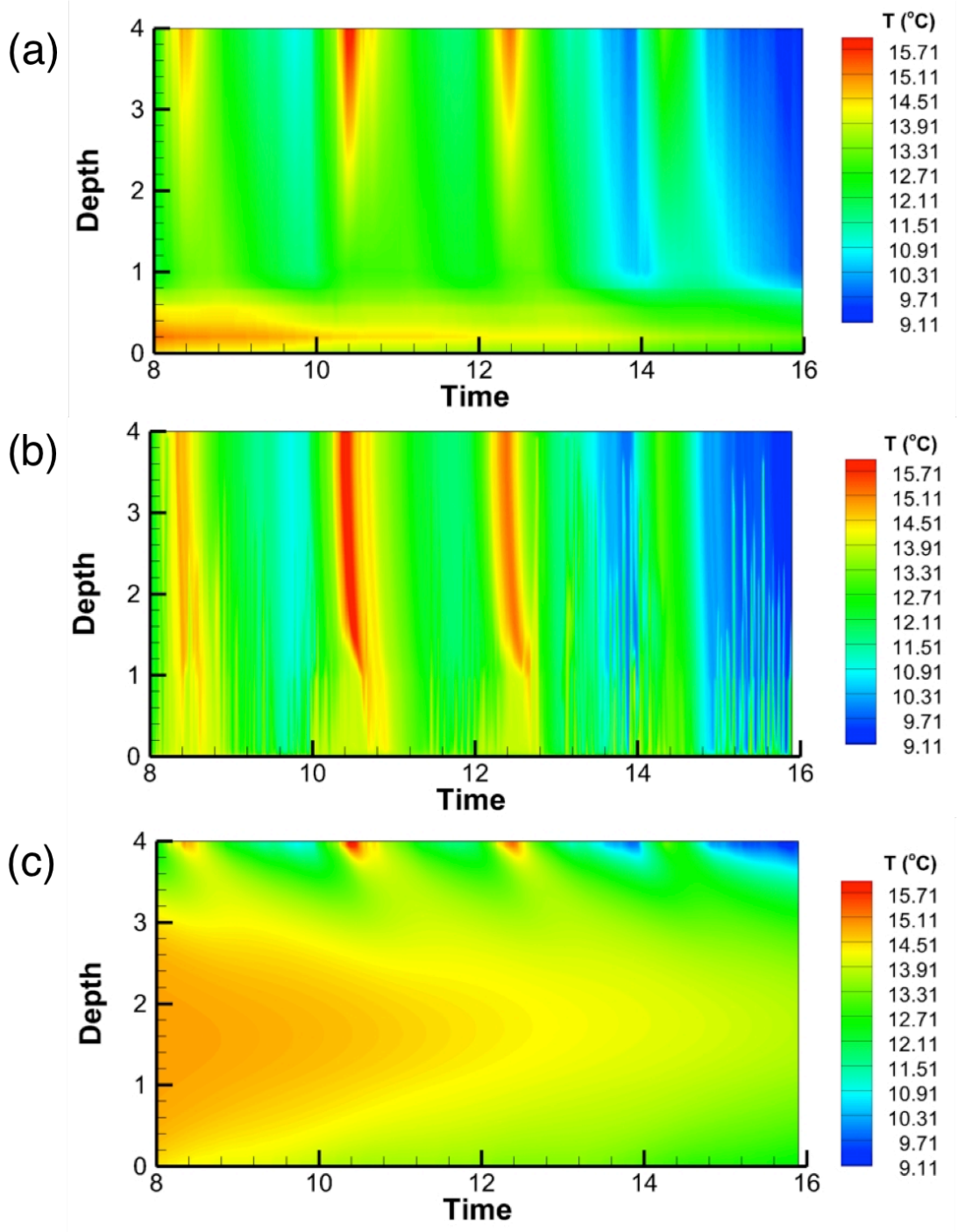

Figure 4.5. Time series of (**a**) observed temperatures, (**b**) simulated temperatures with buoyancy-induced flow, and (**c**) simulated temperatures with diffusion only in the water column and within the floc layer for the 4-day period of comparison shown in Figure 4.4. The y-axis represents the vertical distance between the top and bottom of the model domain (0.72 m) normalized by the thickness of the floc layer (0.18 m). Consequently, the surface of the floc layer is at a depth of 1. Because time was normalized by a characteristic time scale of a half day in the model, the dimensionless time τ (x-axis) for the 4-day period is 8.

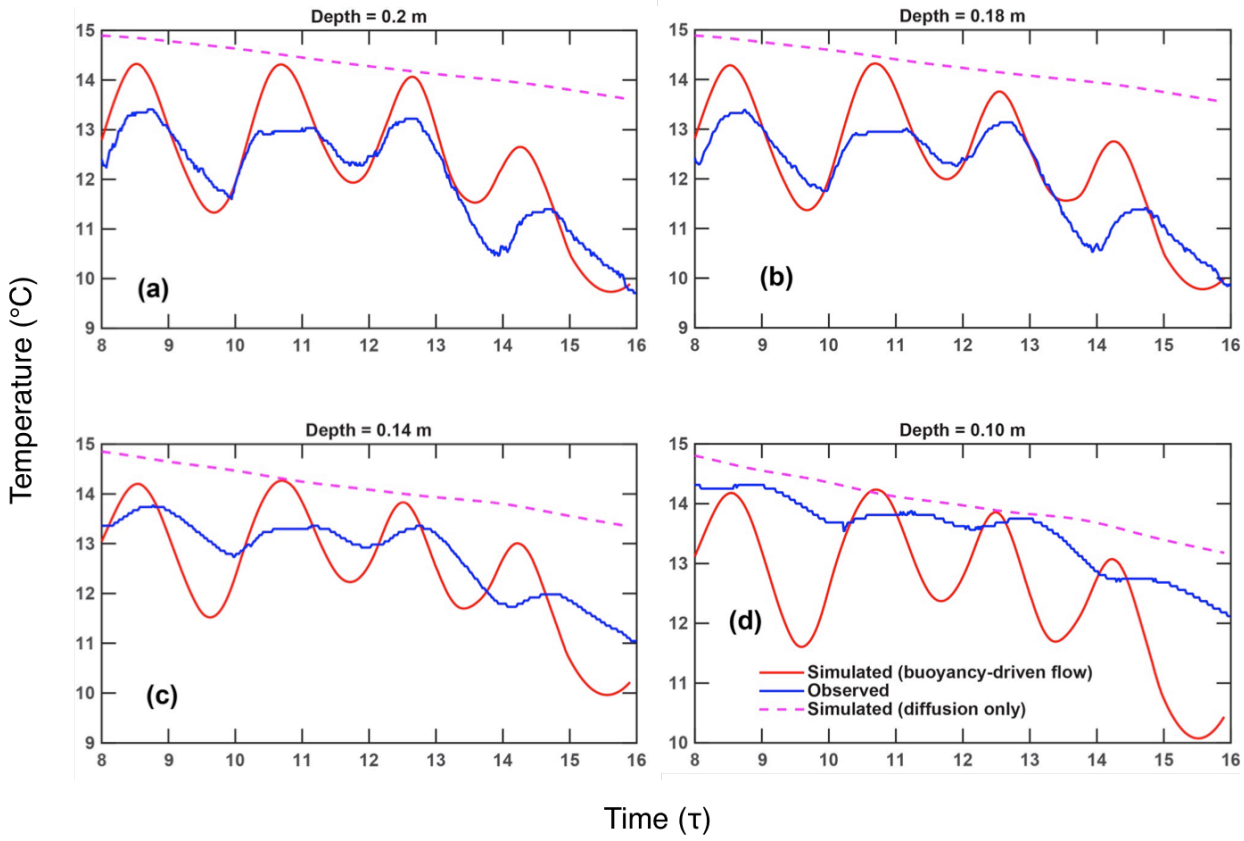

Figure 4.6. Comparison of observed temperatures and simulated temperatures at selected depths, including (**a**) 0.02 m above the floc surface, (**b**) at the floc-water interface, and (**c**) 0.04 m and (**d**) 0.08 m below the floc surface. Depths shown above subplots are relative to the bottom of the floc layer and model domain. Depth = 0.18 m is at the floc-water interface. Time on the y-axis is model time and represents the 4-day period of comparison shown in Figure 4.4.

Despite the differences between observed and simulated temperatures, it is clear that buoyancy-induced flow drives the main temperature patterns observed in the pond. The diffusion-only solution (Figure 4.5c), which eliminates buoyant convection as a driver of fluid flow in the system, poorly replicates temperatures in the pond, especially the penetration of thermal pulses into the water column. This confirms that vertical convection cells created by buoyancy-induced flow are responsible for the deeper penetration of surface heating and cooling signals.

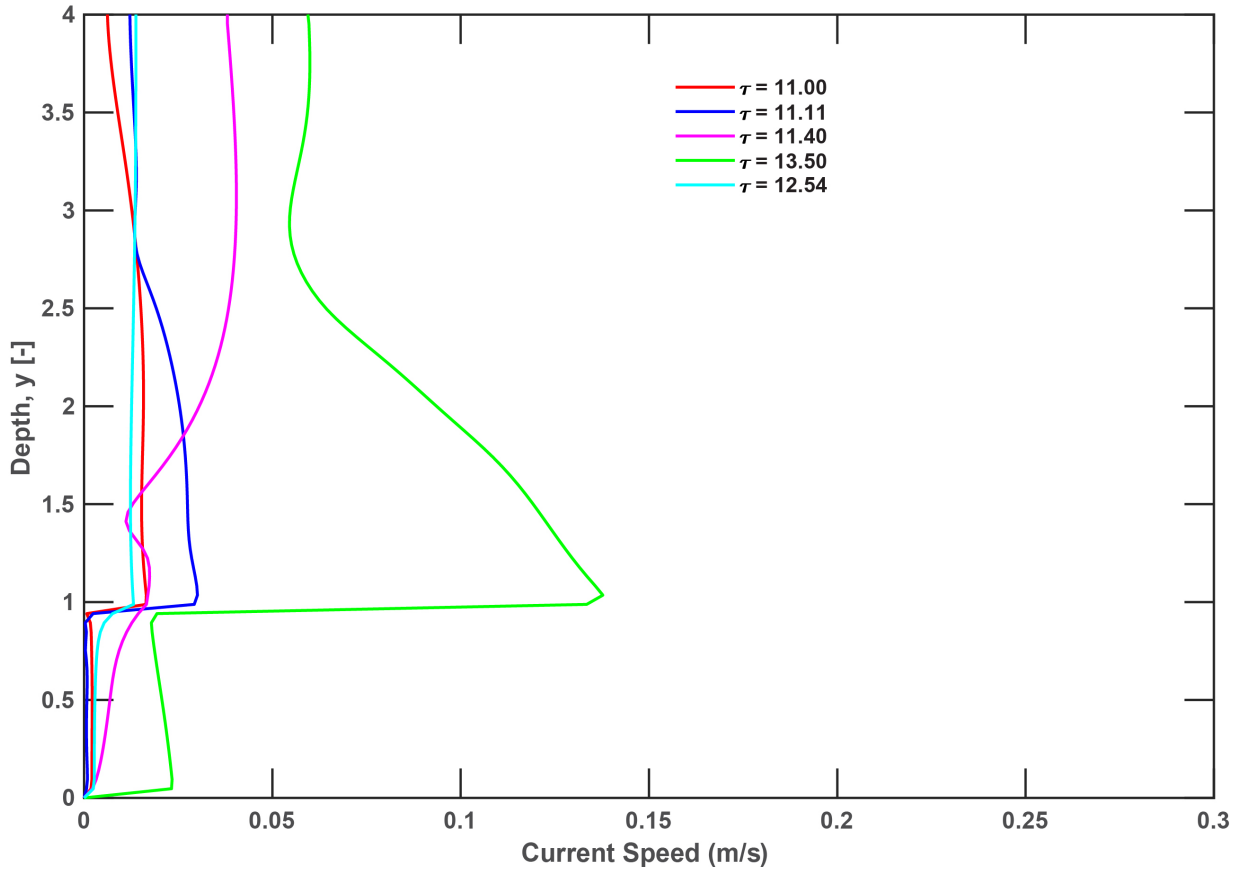

Figure 4.7. Simulated velocity profiles in the floc layer and the overlying water column at selected times. The y-axis represents the vertical distance between the top and bottom of the model domain (0.72 m) normalized by the thickness of the floc layer (0.18 m). Consequently, the surface of the floc layer is at a depth of 1. High velocities were generally associated with large temperature differences in the system and occurred at the interface between the floc layer and the overlying water, a feature also noted in our ADCP observations.

The model simulated velocities that agreed with general patterns we observed with the ADCP. High velocities were generally associated with large temperature differences in the system and occurred at the interface between the floc layer and the overlying water (Figure 4.7), a feature also noted in our ADCP observations (Figure 4.3). The velocity magnitudes (around 0.02 m/s) are comparable to the values observed at the field site although the model did not produce the largest values (~ 0.6 m/s) observed at the field site.

CONCLUSIONS

This study confirmed my hypothesis that buoyancy-driven convective flow in addition to diffusion is likely an important mechanism for exchange of solutes between flocculent sediments and overlying water in shallow waterbodies. Time-dependent, three-dimensional fluid movement in flocculent sediments in a shallow pond was demonstrated using a high resolution ADCP. The novel two-dimensional non-Darcy hydrodynamic model used to simulate buoyancy-induced flows demonstrated that these flows are likely driven by thermal gradients between the overlying water and flocculent sediments, which result in buoyancy-driven convective flow. Flow was temporally variable, but the greatest fluid flow velocities occurred at the floc-overlying water interface when temperature differentials were greatest (e.g., when warm surface waters cooled at night and when sediment temperatures were greater than temperatures in the overlying water before daytime warming events). While the model can be improved, results suggest that buoyancy-driven flow resulting from both diel and seasonal heating and cooling cycles is a potentially important transport mechanism for heat and solute mass across the sediment-water interface in shallow waters.

APPENDIX

Deriving dimensionless terms for the buoyancy-induced flow model

Dimensionless term	Notes
$\tau_{max} = \frac{t_{max}}{t_0} = \frac{4\ d \times 24\ h \times 3600\ s}{43,200\ s} = 8$	For simulations using 4 days of temperature; recall that $t_0 = 0.5\ days\ or\ 43{,}200\ sec$
$\tau_{max} = \frac{t_{max}}{t_0} = \frac{8\ d \times 24\ h \times 3600\ s}{43,200\ s} = 16$	For simulations using 8 days of temperature; recall that $t_0 = 0.5\ days\ or\ 43{,}200\ sec$
$\varepsilon = 0.95$	Average measured porosity for upper 20 cm of floc layer
$Fo_f = \frac{\nu t_0}{H^2} = \frac{(1.12 \times 10^{-6}\ \frac{m^2}{s})(43{,}200\ s)}{(0.18\ m)^2} = 1.493$	ν is the kinematic viscosity for water @ 15°C; H is currently the depth of the floc layer; do not need different Fo_f for floc and water
$Da = \frac{K}{H^2} = \frac{1.7 \times 10^{-5}\ m/s}{(0.18\ m)^2} = 5.2469 \times 10^{-4}$	K here is the maximum hydraulic conductivity reported by Rudnick et al. (2015) for Small Lake Gollinsee bed sediments (fine organic sediments); estimates for K found in the literature for lake sediments range 1.7 x 10^{-5} to 6.9 x 10^{-9}; H is the depth of the floc layer
$C = \frac{1.75}{\sqrt{150}}\left(\frac{1}{\varepsilon^{3/2}}\right) = \frac{1.75}{\sqrt{150}}\left(\frac{1}{(0.95)^{3/2}}\right) = 0.1544$	ε here is the average measured porosity for the upper 20 cm of the floc layer
$Pr = \frac{\nu}{\alpha} = \frac{(1.12 \times 10^{-6}\ \frac{m^2}{s})}{(1.41 \times 10^{-7}\ \frac{m^2}{s})} = 7.94$	ν is the kinematic viscosity for water @ 15°C; α is thermal diffusivity for water @ 15°C
$Ra_{8days} = \frac{g\beta\Delta T H^3}{\nu\alpha} = \frac{(9.81\ \frac{m}{s^2})(0.16 \times 10^{-3}/°K)(0.34949)(0.18\ m)^3}{(1.12 \times 10^{-6}\ \frac{m^2}{s})(1.41 \times 10^{-7}\ \frac{m^2}{s})} = 2.03 \times 10^7$	Ra for 8-day period; β=coef. of thermal expansion for water at 15°C; ΔT = 0.34949 is difference between mean temperature at top boundary condition (12 cm below surface of water column) and mean temp at bottom of floc layer (84 cm) for the 8-day period; ν is the kinematic viscosity for water @ 15°C; α = thermal diffusivity for water @ 15°C
$Fo_f = \frac{\nu t_0}{H^2} = \frac{(1.12 \times 10^{-6}\ \frac{m^2}{s})(43{,}200\ s)}{(0.18\ m)^2} = 1.493$	Fo_f is the flow Fourier #; ν is the kinematic viscosity for water @ 15°C
$\zeta = \left(\frac{\varepsilon\rho_f c_{pf} + (1-\varepsilon)\rho_s c_{ps}}{\rho_f c_{pf}}\right) = \frac{3.7448 \times 10^6\ \frac{J}{m^3 \cdot K}}{\left(999.1\ \frac{kg}{m^3}\right)\left(4.186 \times 10^3\ \frac{J}{kg \cdot K}\right)} = 0.8954$	For the numerator I used the mean volumetric heat capacity that I measured on cores of saturated floc from KFP site using the KD2 Pro Thermal Analyzer
$Fo_{t_{water}} = \frac{\alpha t_0}{H^2} = \frac{(1.41 \times 10^{-7}\ \frac{m^2}{s})(43{,}200\ s)}{(0.18\ m)^2} = 0.188$	$Fo_{t_{water}}$ is the thermal Fourier # for the water column

$Fo_{t,e_{floc}} = \frac{\alpha_e t_0}{H^2} = \frac{(1.81 \times 10^{-7}\ \frac{m^2}{s})(43{,}200\ s)}{(0.18\ m)^2} = 0.2413$	Thermal Fourier # for the floc layer; α_e for floc was measured on a saturated floc core from Kelfor Pond using an KD2 Pro Thermal Analyzer @ ~ 22°C

LITERATURE CITED

LITERATURE CITED

Abbott BW, Baranov V, Mendoza-Lera C, et al (2016) Using multi-tracer inference to move beyond single-catchment ecohydrology. Earth-Sci Rev 160:19–42. doi: 10.1016/j.earscirev.2016.06.014

Alexander RB, Smith RA, Schwarz GE (2000) Effect of stream channel size on the delivery of nitrogen to the Gulf of Mexico. Nature 403:758–761. doi: 10.1038/35001562

Avnimelech Y, Ritvo G, Meijer LE, Kochba M (2001) Water content, organic carbon and dry bulk density in flooded sediments. Aquacult Eng 25:25–33. doi: 10.1016/S0144-8609(01)00068-1

Beaulieu JJ, Tank JL, Hamilton SK, et al (2011) Nitrous oxide emission from denitrification in stream and river networks. PNAS 108:214–219. doi: 10.1073/pnas.1011464108

Berner RA (1980) Early Diagenesis: A Theoretical Approach. Princeton University Press

Bernhardt ES, Blaszczak JR, Ficken CD, et al (2017) Control points in ecosystems: moving beyond the hot spot hot moment concept. Ecosystems 20:665–682. doi: 10.1007/s10021-016-0103-y

Bernhardt J, Kirillin G, Hupfer M (2014) Periodic convection within littoral lake sediments on the background of seiche-driven oxygen fluctuations. Limnol Oceanogr 4:17–33. doi: 10.1215/21573689-2683238

Briggs MA, Lautz LK, McKenzie JM, et al (2012) Using high-resolution distributed temperature sensing to quantify spatial and temporal variability in vertical hyporheic flux. Water Resour Res. doi: 10.1029/2011WR011227

Canário J, Poissant L, OŁDriscoll N, et al (2009) Sediment processes and mercury transport in a frozen freshwater fluvial lake (Lake St. Louis, QC, Canada). Environ Pollut 157:1294–1300. doi: 10.1016/j.envpol.2008.11.042

Cheng FY, Basu NB (2017) Biogeochemical hotspots: role of small water bodies in landscape nutrient processing. Water Resour Res 53:5038–5056. doi: 10.1002/2016WR020102

Condie SA, Webster IT (2001) Estimating stratification in shallow water bodies from mean meteorological conditions. J Hydraul Eng 127:286–292. doi: 10.1061/(ASCE)0733-9429(2001)127:4(286)

Downing J (2010) Emerging global role of small lakes and ponds: little things mean a lot. Limnetica 29:9–24.

Downing JA, Cole JJ, Middelburg JJ, et al (2008) Sediment organic carbon burial in agriculturally eutrophic impoundments over the last century. Global Biogeochem Cycles.

doi: 10.1029/2006GB002854

Ergun S (1952) Fluid flow through packed columns. Chem Eng Prog 48:89–94.

Flury S, Glud RN, Premke K, McGinnis DF (2015) Effect of sediment gas voids and ebullition on benthic solute exchange. Environ Sci Technol 49:10413–10420. doi: 10.1021/acs.est.5b01967

Ford PW, Boon PI, Lee K (2002) Methane and oxygen dynamics in a shallow floodplain lake: the significance of periodic stratification. Hydrobiologia 485:97–110. doi: 10.1023/A:1021379532665

Gebhart B, Jaluria Y, Mahajan RL, Sammakia B (1988) Buoyancy-Induced Flows and Transport. CRC Press

Golosov SD, Ignatieva NV (1999) Hydrothermodynamic features of mass exchange across the sediment-water interface in shallow lakes. In: Walz N, Nixdorf B (eds) Shallow Lakes '98: Trophic Interactions in Shallow Freshwater and Brackish Waterbodies. Springer Netherlands, Dordrecht, pp 153–157

Golterman HL (2004) The chemistry of phosphate and nitrogen compounds in sediments. Kluwer Academic Publishers, Dordrecht

Gray WG, Miller CT (2013) A generalization of averaging theorems for porous medium analysis. Advances in Water Resources 62:227–237. doi: 10.1016/j.advwatres.2013.06.006

Grimm NB, Fisher SG (1984) Exchange between interstitial and surface water: Implications for stream metabolism and nutrient cycling. Hydrobiologia 111:219–228. doi: 10.1007/BF00007202

Harrison JA, Maranger RJ, Alexander RB, et al (2009) The regional and global significance of nitrogen removal in lakes and reservoirs. Biogeochemistry 93:143–157. doi: 10.1007/s10533-008-9272-x

Helton AM, Poole GC, Meyer JL, et al (2011) Thinking outside the channel: modeling nitrogen cycling in networked river ecosystems. Front Ecol Environ 9:229–238. doi: 10.1890/080211

Hölker F, Vanni MJ, Kuiper JJ, et al (2015) Tube-dwelling invertebrates: tiny ecosystem engineers have large effects in lake ecosystems. Ecol Monogr 85:333–351. doi: 10.1890/14-1160.1

Kirillin G, Engelhardt C, Golosov S (2009) Transient convection in upper lake sediments produced by internal seiching. Geophys Res Lett 36:L18601–5. doi: 10.1029/2009GL040064

Kleeberg A, Herzog C (2014) Sediment microstructure and resuspension behavior depend on each other. Biogeochemistry 119:199–213. doi: 10.1007/s10533-014-9959-0

Krantzberg G (1985) The influence of bioturbation on physical, chemical and biological

parameters in aquatic environments: A review. Environ Pollut A 39:99–122. doi: 10.1016/0143-1471(85)90009-1

Lappalainen KM (1982) Convection in bottom sediments and its role in material exchange between water and sediments. Hydrobiologia 86:105–108. doi: 10.1007/BF00005795

Liikanen A, Huttunen JT, Murtoniemi T, et al (2003) Spatial and seasonal variation in greenhouse gas and nutrient dynamics and their interactions in the sediments of a boreal eutrophic lake. Biogeochemistry 65:83–103. doi: 10.1023/A:1026070209387

Longhi D, Bartoli M, Nizzoli D, Viaroli P (2013) Benthic processes in fresh water fluffy sediments undergoing resuspension. J Limnol 72:1–12. doi: 10.4081/jlimnol.2013.e1

MacIntyre S (2006) Vertical mixing in a shallow, eutrophic lake: possible consequences for the light climate of phytoplankton. Limnol Oceangr 38:798–817.

Martins-Costa ML, Saldanha de Gama RM (1994) A local model for the heat transfer process in two distinct flow regions. Int J Heat Fluid Flow 15:477–485. doi: 10.1016/0142-727X(94)90007-8

McClain ME, Boyer EW, Dent CL, et al (2003) Biogeochemical hot spots and hot moments at the interface of terrestrial and aquatic ecosystems. Ecosystems 6:301–312. doi: 10.1007/s10021-003-0161-9

Megonigal JP, Hines ME, Visscher PT (2004) Anaerobic metabolism: Linkages to trace gases and aerobic processes. In: Schlesinger WH (ed) Biogeochemistry. Oxford, U.K, pp 317–424

Mortimer CH (1971) Chemical exchanges between sediments and water in the Great Lakes-speculations on probable regulatory mechanisms. Limnol Oceangr 16:387–404. doi: 10.4319/lo.1971.16.2.0387

Nogaro G, Burgin AJ (2014) Influence of bioturbation on denitrification and dissimilatory nitrate reduction to ammonium (DNRA) in freshwater sediments. Biogeochemistry 120:279–294. doi: 10.1007/s10533-014-9995-9

Patankar SV (1980) Numerical Heat Transfer and Fluid Flow. Hemisphere Pub. Corp., Washington

Plach JM, Lin S, Droppo IG, Warren LA (2014) Iron cycling in a littoral freshwater beach: Implications for floc trace metal dynamics. J Great Lakes Res 40:47–57. doi: 10.1016/j.jglr.2014.01.002

Poindexter CM, Baldocchi DD, Matthes JH, et al (2016) The contribution of an overlooked transport process to a wetland's methane emissions. Geophys Res Lett 43:6276–6284. doi: 10.1002/2016GL068782

Press WH, Teukolsky SA, Vetterling WT, Flannery BP (2007) Numerical Recipes: The Art of Scientific Computing, 3rd edn. Cambridge University Press, New York

Prosperetti A, Tryggvason G (2007) Computational Methods for Multiphase Flow. Cambridge University Press, Cambridge

Rappoldt C, Pieters GJJM, Adema EB, et al (2011) Buoyancy-driven flow in a peat moss layer as a mechanism for solute transport. PNAS 100:14937–14942. doi: 10.1073/pnas.1936122100

Raymond PA, Hartmann J, Lauerwald R, et al (2013) Global carbon dioxide emissions from inland waters. Nature 503:355–359. doi: 10.1038/nature12760

Rudnick S, Lewandowski J, Nützmann G (2014) Investigating groundwater-lake interactions by hydraulic heads and a water balance. Groundwater 53:227–237. doi: 10.1111/gwat.12208

Simon NS (1989) Nitrogen cycling between sediment and the shallow-water column in the transition zone of the Potomac River and Estuary. II. The role of wind-driven resuspension and adsorbed ammonium. Est Coast Mar Sci 28:531–547. doi: 10.1016/0272-7714(89)90028-0

Smith SV, Renwick WH, Bartley JD, Buddemeier RW (2002) Distribution and significance of small, artificial water bodies across the United States landscape. Sci Total Environ 299:21–36. doi: 10.1016/S0048-9697(02)00222-X

Svensson J, Leonardson L (1996) Effects of bioturbation by tube‐dwelling chironomid larvae on oxygen uptake and denitrification in eutrophic lake sediments. Freshwater Biol 35:289–300. doi: 10.1046/j.1365-2427.1996.00500.x

Tarasiuk N, Moisejenkova A, Koviazina E (2010) On the mechanism of the enrichment in radiocesium of near-bottom water in Lake Juodis, Lithuania. J Environ Radioact 101:883–894. doi: 10.1016/j.jenvrad.2010.06.001

Tranvik LJ, Downing JA, Cotner JB, et al (2009) Lakes and reservoirs as regulators of carbon cycling and climate. Limnol Oceangr 54:2298–2314. doi: 10.4319/lo.2009.54.6_part_2.2298

Tritton DJ (1988) Physical Fluid Dynamics, 2nd edn. Oxford University Press, Oxford, UK

Van Rees KCJ, Reddy KR, Rao PSC (1996) Influence of benthic organisms on solute transport in lake sediments. Hydrobiologia 317:31–40. doi: 10.1007/BF00013723

Wetzel RG (2001) Limnology: Lake and River Ecosystems, 3rd edn. Academic Press, San Diego

Wetzel RG (1992) Gradient-dominated ecosystems: sources and regulatory functions of dissolved organic matter in freshwater ecosystems. Hydrobiologia 229:181–198. doi: 10.1007/BF00007000

Whitaker S (1999) The Method of Volume Averaging. Kluwer Academic Publishers, Dordrecth, The Netherlands